AD_____

Award Number: DAMD17-01-1-0689

TITLE: The BESCT Lung Cancer Program (Biology, Education, Screening, Chemoprevention, and Treatment)

PRINCIPAL INVESTIGATOR: Waun K. Hong, M.D.

CONTRACTING ORGANIZATION: The University of Texas
M.D. Anderson Cancer Center
Houston, Texas 77030

REPORT DATE: March 2004

TYPE OF REPORT: Annual

PREPARED FOR: U.S. Army Medical Research and Materiel Command
Fort Detrick, Maryland 21702-5012

DISTRIBUTION STATEMENT: Approved for Public Release;
Distribution Unlimited

REPORT DOCUMENTATION PAGE

Public reporting burden for this collection of information is estimated to average 1 hour per response, including the time for reviewing instructions, searching existing data sources, gathering and maintaining the data needed, and completing and reviewing this collection of information. Send comments regarding this burden estimate or any other aspect of this collection of information, including suggestions for reducing this burden to Washington Headquarters Services, Directorate for Information Operations and Reports, 1215 Jefferson Davis Highway, Suite 1204, Arlington, VA 22202-4302, and to the Office of Management and Budget, Paperwork Reduction Project (0704-0188), Washington, DC 20503

1. AGENCY USE ONLY (Leave blank)	2. REPORT DATE March 2004	3. REPORT TYPE AND DATES COVERED Annual (16 Feb 2003 – 15 Feb 2004)

4. TITLE AND SUBTITLE

The BESCT Lung Cancer Program (Biology, Education, Screening, Chemoprevention, and Treatment)

5. FUNDING NUMBERS

DAMD17-01-1-0689

6. AUTHOR(S)

Waun K. Hong, M.D.

7. PERFORMING ORGANIZATION NAME(S) AND ADDRESS(ES)

The University of Texas
M.D. Anderson Cancer Center
Houston, TX 77030

E-Mail: whong@mdanderson.org

8. PERFORMING ORGANIZATION REPORT NUMBER

9. SPONSORING / MONITORING AGENCY NAME(S) AND ADDRESS(ES)

U.S. Army Medical Research and Materiel Command
Fort Detrick, Maryland 21702-5012

10. SPONSORING / MONITORING AGENCY REPORT NUMBER

11. SUPPLEMENTARY NOTES

12a. DISTRIBUTION / AVAILABILITY STATEMENT
Approved for Public Release; Distribution Unlimited

12b. DISTRIBUTION CODE

13. ABSTRACT (Maximum 200 Words)

Our long-term objectives are to define the molecular processes contributing to lung cancer development and progression in order to recognize genetic and phenotypic changes early enough to be reversed with molecularly-targeted therapy and to develop innovative therapeutic approaches to lung cancer. Therefore, the specific goals of this program are to understand molecular alterations in lung cancer, develop lung cancer prevention strategies, and implement experimental molecular approaches to lung cancer. We report herein that enolase-α down-regulation is common in NSCLC and associated with a poor clinical outcome; IL-10 expression is lost in a subset of NSCLC and such loss predicts a poor clinical outcome in patients with stage I NSCLC; the combination of the COX-2 inhibitor Celecoxib and the retinoid 4HPR results in more effective growth inhibition than each agent alone; lack of PTEN expression in NSCLC may be related to promoter methylation and is of prognostic importance in stage I NSCLC; Farnesyl Transferase Inhibitors down-regulate phosphorylated RAF and AKT and induce the ubiquitination of AKT protein.

14. SUBJECT TERMS

Lung cancer, genetic alterations, chemoprevention, molecular therapy

15. NUMBER OF PAGES
78

16. PRICE CODE

17. SECURITY CLASSIFICATION OF REPORT Unclassified	18. SECURITY CLASSIFICATION OF THIS PAGE Unclassified	19. SECURITY CLASSIFICATION OF ABSTRACT Unclassified	20. LIMITATION OF ABSTRACT Unlimited

NSN 7540-01-280-5500

20040902 081

TABLE OF CONTENTS

INTRODUCTION

Lung cancer is a devastating worldwide public health hazard, with a total of 1,500,000 new cases anticipated in the year 2000 (1). Advances in the surgery, radiation therapy, and chemotherapy of non-small cell lung cancer have led to an improvement in five-year survival from 7% in 1970 to 15.8% IN 1994 (2). To reduce lung cancer incidence and mortality, it is imperative to develop effective therapeutic and preventive strategies targeting smokers and lung cancer patients. Our long-term objectives are to define the molecular processes contributing to lung cancer development and progression in order to recognize genetic and phenotypic changes early enough to be reversed with molecularly-targeted therapy and to develop innovative therapeutic approaches to lung cancer. The objectives can be met only by understanding the biology of lung cancer through molecular studies and preclinical experimental molecular therapeutic research. Therefore, the specific goals of this program are to understand molecular alterations in lung cancer, develop lung cancer prevention strategies, and implement experimental molecular approaches to lung cancer.

PROGRESS REPORT

Project 1   Mechanisms of Molecular Alterations in Lung Cancer

The following progress has been made in the past fiscal year, including those studies continued from previous year.

1.   Alternative RNA processing of tumor suppressor gene *CEACAM1* is correlated with over-expression of polypyrimidine tract-binding protein (PTB) in lung cancers

CEACAM1 is part of a large family of Ig-related cellular adhesion molecules that function in maintaining normal cellular growth. Down-regulated expression or aberrant alternative RNA splicing of this gene has been associated with malignant progression. We have previously demonstrated that *CEACAM1* exon 7 is aberrantly skipped (S-form) in a majority of lung cancers. The exclusion of this exon results in the production of a protein lacking the intracellular domain and the tumor suppressive activity possessed by L-form. To address the mechanism responsible for the aberrant skipping of exon 7 in lung cancers, we have looked for tumor cell-specific changes in regulators of RNA splicing. Exon skipping is primarily mediated through the binding of various hnRNP classes of repressor proteins. PTB, an hnRNP protein with known roles in exon skipping, was found overexpressed in most of the primary lung cancers as well as in several lung cancer cell lines. To determine a potential role for PTB in the regulation of *CEACAM1* splicing, we examined protein binding to a conserved region (a 16-nt sequence within *CEACAM1* exon 7) that appears to be an important determinate of splicing. We found that this sequence strongly bound to PTB. Fractionation and gel shift studies also support that the specific nuclear binding of PTB to this sequence may be associated with the exon 7 skipping. To provide additional evidence to support the notion, we co-transfected a PTB expression plasmid with a mini-gene reporter construct containing *CEACAM1* exon 7 into lung cancer cell lines and found that overexpression of PTB enhanced expression of the S-from *CEACAM1*. Our results clearly demonstrate that the splicing repressor protein PTB is frequently overexpressed in human lung cancers. Although PTB is known to alter the splicing of several genes, *CEACAM1* may be an important target in lung tumorigenesis. A novel outcome of our findings is that PTB may regulate exon 7 exclusion through the binding of exon sequence. It is significant because most of the studies in other genes have shown that the binding of PTB to intronic splicing silencer sequences is the primary mechanism for regulation of exon skipping. (Abstract for AACR 2004 annual meeting)

2. Identified an association of a functional tandem repeats downstream of human telomerase gene and lung cancer

Chemoprevention has been widely explored as a promising strategy for controlling incidence of lung cancer, the leading cause of cancer-related death. To maximize the benefit of lung cancer chemoprevention, it is important to identify individuals at high risk for the disease. The genetic background has been shown to play an important role in one's risk of developing lung cancer. We report here the identification of a polymorphic tandem repeats minisatellite (termed MNS16A) in the downstream region of the human telomerase gene. This minisatellite is located upstream of an antisense transcript from the human telomerase gene locus and was demonstrated to have promoter activity. The promoter activity was significantly lower in the construct containing the shorter repeats, suggesting the MNS16A variant may have a relevance of functionality. To explore the role of this novel polymorphism in lung cancer, we conducted a pilot hospital-based case-control study by identifying the MNS16A genotype with genomic DNA from 53 lung cancer patients and 72 cancer-free controls. We found four different alleles and classified as shorter (S) or longer (L) on the functional basis of the length of the repeats in the controls. The MNS16A genotype distributions of the SS, SL and LL genotypes were 11%, 32%, and 57% respectively in the cases, and 14%, 40%, and 46% respectively, in the controls . Compared with the SS+SL genotype, the LL genotype was associated with greater than 2-fold increased risk of lung cancer (odds ratio=2.18; 95% confidence interval=0.92, 5.20) after adjustment for age, sex, ethnicity, and smoking status, suggesting a potential role of MNS16A in lung cancer susceptibility. Larger studies are needed to verify our findings. (Oncogene, 22:7123-7129, 2003)

3. Enolase-alpha is frequently down-regulated in non-small cell lung cancer and predicts aggressive biological behavior

Enolase-α is a cytoplasmic glycolytic enzyme important in the formation of phosphoenolpyruvate. Enolase-α and c-myc binding protein (MBP-1) originate from a single gene through alternative use of translational starting sites. Both enolase-α and MBP-1 can bind to the P2 element in the c-myc promoter and compete with TATA-box binding protein (TBP) to suppress transcription of c-myc. Using a proteomic approach, we revealed that enolase-α is down-regulated in cell lines derived from metastases. To determine a potential role of enolase-α in vivo, we analyzed enolase-α expression in non-small cell lung cancer (NSCLC) tissues from 46 patients by Western blotting and immunohistochemical analysis. Twelve (26%) of the 46 tumors showed a significantly reduced enolase-α expression. Although no statistically significant association was observed between the down-regulation of enolase-α and pathologic stage, tumor histology, or differentiation, the patients whose tumors showed reduced endolase-α expression had a significantly poorer overall survival compared to those without down-regulation of this molecule (P = 0.0398). Our results indicate down-regulation of enolase-α is common in NSCLC and may play an important role in lung tumorigenesis. (Clinical Cancer Research, 9:3641-3644, 2003)

4. Lack of interleukin-10 expression could predict poor outcome in patients with stage I non-small cell lung cancer

Interleukin-10 (IL-10) may play an important role in controlling tumor growth and metastasis. Some reports have shown that IL-10 can be a potent inhibitor of tumor growth, but others suggest that IL-10 expression by the tumor is an adverse prognostic factor. Since normal bronchial epithelial cells constitutively produce IL-10, we decided to test the prognostic value of

IL-10 in a well-defined population of patients with stage I non-small cell lung cancer (NSCLC) treated in a single institution. Using immunohistochemical analysis, we retrospectively analyzed IL-10 expression in specimens from 138 patients with completely resected clinical/radiographic stage I NSCLC for whom clinical follow-up data were available. IL-10 expression was retained (IL-10 labeling index $\geq$ 10%) in 94 patients (68.1%) and lost in 44 patients (31.9%). The duration of overall survival, disease-specific survival and disease-free survival in the 44 patients lacking IL-10 expression was worse than in the 94 patients with IL-10 expression (P = 0.08; 0.02; and 0.05, respectively; log-rank test). Interestingly, IL-10 expression was observed more frequently in tumors with squamous cell histology than in tumors of other histological subtypes (P = 0.04; chi-square test). Multivariate analysis confirmed the independent prognostic value of IL-10 expression for disease-specific survival (P = 0.04). Lack of IL-10 expression by the tumor was associated with a significantly worse outcome of early-stage NSCLC. The mechanisms underlying this clinically and biologically important finding need to be explored further. (Clinical Cancer Research, 9:1785-1891, 2003)

5. **Distinct value of $p16^{INK4a}$ and RASSF1A promoter hypermethylation in prognosis of patients with resectable non-small cell lung cancer[1]**

$p16^{INK4a}$ and RASSF1A are tumor suppressors frequently inactivated by de novo promoter hypermethylation in non-small cell lung cancer (NSCLC). We studied 119 patients with NSCLC (70 stage I/II and 49 stage IIIA) who had undergone surgery with curative intent. Promoter hypermethylation status of $p16^{INK4a}$ and RASSF1A was determined by methylation-specific PCR. Statistical analyses, all two-sided, were performed to determine the prognostic effect of hypermethylation on various clinical parameters. Hypermethylation of $p16^{INK4a}$ and RASSF1A was found in 58 (49%) and 46 (39%) of the tumors respectively, while 36 (30%) tumors exhibited hypermethylation of both genes. In patients with stage I/II tumors, only hypermethylation of $p16^{INK4a}$ was associated with poor overall survival (P = 0.002). In patients with stage IIIA disease, however, hypermethylation of RASSF1A strongly predicted a poor overall survival (P < 0.0001), which was more profound than $p16^{INK4a}$ promoter hypermethylation. Among 49 stage IIIA patients, 16 (89%) of the 18 patients whose tumors showed hypermethylation of RASSF1A died within 3 years after surgery, while only 12 (39%) of the 31 patients whose tumors had no RASSF1A hypermethylation did so (P < 0.0001). Multivariate analysis indicated that hypermethylation of RASSF1A is the strongest independent predictor for survival in patients with locally advanced NSCLC. Our results indicate that $p16^{INK4a}$ promoter hypermethylation predicts poor survival for patients with resectable NSCLC, particularly early stage tumors, while RASSF1A promoter hypermethylation is a profound prognostic predictor for patients with locally advanced NSCLC, suggesting an important role of RASSF1A in NSCLC progression. (manuscript in preparation)

6. **Expression of ΔDNMT3B is strongly associated with promoter methylation of p16INK4a and RASSF1A tumor suppressor genes in non-small cell lung cancer**

DNMT3B is important in de novo DNA methylation and often overexpressed in human cancers. However, the overexpression does not correlate with overall promoter DNA methylation status in cancers. We have recently identified a new DNMT3B subfamily, termed ΔDNMT3B (DNMT3B6 in our previous progress report), initiated through a novel promotor located at intron 4 and exon 5 of DNMT3B1. ΔDNMT3B consists of at least 7 isoforms through alternative RNA splicing. We hypothesize that expression patterns of ΔDNMT3B variants (ΔDNMT3B1-7) play an important role in determining methylation of specific promoters. To test this hypothesis, we designed 14 pairs of primers specific for each variant of DNMT3Bs and ΔDNMT3Bs to examine

expression patterns of DNMT3Bs and ΔDNMT3Bs in 109 primary NSCLC tumor specimens and their corresponding non-malignant lung tissues. Promoter methylation status of the P16INK4a and RASSF1A was also determined in these specimens by a methylation-specific PCR. We found that ΔDNMT3Bs were the predominantly expressed forms in both NSCLC and non-malignant lung tissues, and were detected in 87 (80%) of the 109 NSCLC tumors, but only 22 (20%) of the corresponding non-malignant lung tissues ($P < 0.0001$). Three major expression patterns of ΔDNMT3B variants were observed in the NSCLC tissues. ΔDNMT3B1, ΔDNMT3B2 and ΔDNMT3B3 were the most frequently detected transcripts in the tumor tissues (61%, 74%, and 45% respectively). Promoter methylation of P16INK4a and RASSF1A was detected in 55 (50%) and 42 (39%) of the tumor tissues respectively, while only 7 (6%) and 5 (5%) in the corresponding non-malignant lung tissues. We found that the methylation status of P16INK4a and RASSF1A was strongly correlated with ΔDNMT3B expression patterns in the tumors. Promoter methylation was detected in 50 (57%) for P16INK4a and 42 (48%) for RASSF1A among 87 tumors with detectable ΔDNMT3B(s), while only 5 (25%) and 0 (0%) respectively, among the 22 tumors without detectable ΔDNMT3Bs. We have also found a strong correlation between ΔDNMT3B2 expression and methylation of P16INK4a (64% in tumors expressed ΔDNMT3B2 compared to 30% in tumors without [$P < 0.001$]). Likewise, the expression of ΔDNMT3B4 was strongly correlated with promoter methylation of RASSF1A. Among 42 tumors with expression of ΔDNMT3B4, 38 (91%) exhibited RASSF1A promoter methylation. In contrast, among 67 tumors without expression of the variant, only 3 (7%) showed RASSF1A promoter methylation ($P < 0.0001$). Our data provide evidence to support the involvement of ΔDNMT3B in differential promoter methylation in lung tumorigenesis. (AACR 2004 abstract)

Project 2   Novel Strategies for Lung Cancer Chemoprevention

Specific Aim 2.1   *Evaluate the effects of aerosolized 13cRA delivered to former smokers by inhalation alone or in combination with Celecoxib*

This clinical trial will not be conducted due to excessive toxicity with aerosolized delivery. We plan another clinical trial, a phase I/II study of the combination of bexarotene/celecoxib in solid tumors, which will be submitted imminently.

Specific Aim 2.2   *Evaluate the effects of NSAIDS and 13cRA as single agents and in combinations on growth, apoptosis and carcinogenesis using an in vitro cell system and an animal model*

Tobacco-related cancers including those that develop in the head and neck and lungs are a major cause of cancer morbidity and mortality. Despite advances in chemotherapy, radiotherapy and surgery alone or in combination, the survival rates for lung cancer are still under 15% and those for head and neck cancers are under 50%. Therefore, there is an urgent need to develop new approaches to the prevention of cancers of the upper airways. The purpose of this specific aim is to evaluate effects of NSAIDs and retinoic acid as single agents and in combinations on lung cancer growth, apoptosis and carcinogenesis using an in vitro cell system and an animal model. In the second year of funding, we determined the relationships among the expression of various arachidonic acid and linoleic acid metabolizing enzymes, modulation of the metabolism of arachidonic adic, and growth and apoptosis in head and neck cancer by the COX-2 inhibitor celecoxib.

Eicosanoid metabolism through cyclooxygenases (COXs) and lipoxygenases (LOXs) generates various lipids that play a role in carcinogenesis. We used pairs of head and neck squamous cell carcinoma (HNSCC) cell lines derived from primary or metastatic tumors of the same patient to analyze different eicosanoids by LC/MS/MS and COX/LOX enzymes by western immunoblotting. The effects of celexocib, a selective COX-2 inhibitor, on eicosanoid synthesis and HNSCC cell growth were examined. Prostaglandin E_2 (PGE_2) was the major metabolite in 3 of 6 cell lines. COX-2 was detected in 3 cell lines (2 from metastases), which markedly produced PGE_2. We found low expression of COX-1 at similar intensities for each pair of cell lines. 5-LOX was detected in all cells. Some expressed 12-LOX, 15-LOX-1 and 15-LOX-2, but there was no correlation with their products. Exogenous arachidonic acid did not change the pattern of eicosanoid production. Low doses of celecoxib inhibited the PGE_2 levels in UMSCC-14A cells by 84% as early as 6 h. In contrast, 5-HETE, 12-HETE, and 15-HETE levels were increased by approximately 40-, 5- and 3-fold, respectively with a decline to baseline levels within 24 h. However, high-dose celecoxib increased the 12-HETE level 2.3-fold after 3-days incubation. Celecoxib inhibited growth of all HNSCC cell lines in a dose-dependent manner after 72 h regardless of COX expression (IC_{50} values: 33 to 62 μM). Our findings provide new insights into the significance of individual eicosanoids produced by HNSCC cells and their differential regulation by celecoxib.

Specific Aim 2.3   Investigate whether genetic approaches to inhibit PI3K activity decrease lung tumor size and number in K-ras mutant mice

In this aim, we proposed to administer adenoviral vectors to the lungs of k-ras mutant mice, which develop lung adenocarcinoma due to expression of mutant k-ras, by aerosolized delivery via jet nebulizer. The adenoviral vectors express the PTEN lipid phosphastase (ad-PTEN) or a dominant negative mutant p85 alpha regulatory subunit of P13K (ad-delta p85), which inhibit P13K activation by receptor tyrosine kinase pathways.

Over the past two years, we have sought to optimize the delivery system to attain consistent adenoviral expression in the lungs of mice with repeated delivery and long-term blockade of P13K pathways. However, we have been unable to convincingly demonstrate that this approach will achieve this objective.

To optimize the system, we have modified the delivery conditions, including variations in the concentration of calcium phosphate in the adenoviral mixture, which is meant to stabilize adenovirus in the nebulization process and to enhance transfection efficiency in cells, and modifications in the adenovirus incubation time in calcium phosphate, which determines the size of calcium phosphate crystals and, we thought, may affect passage of the crystals through the nebulizer. In addition, we have made new preparations of adenovirus for the purpose of optimizing the viability of the adenovirus particle, have modified the dose of adenovirus delivered to the animals, and have optimized our ability to detect biologic effects on the tumor by developing immunohistochemical assays for apoptosis, cellular proliferation, and P13K pathway activity. Despite these changes, we have observed significant inter-mouse variability in adenovirus expression and extent of P13K pathway blockade.

Based on these findings, we have decided that the adenoviral vector delivery system is not optimal for the purposes of this study, and we have decided to discontinue its use. We will instead move to the systemic delivery of small molecules that inhibit specific components of the P13K pathway, to which we have gained access through collaborations with pharmaceutical companies, and these experiments will be performed through out Lung Cancer SPORE grant. Thus, at this point, we will discontinue our involvement in the BESCT Program.

Project 3   Experimental Molecular Therapeutic Approaches to Lung Cancer

Specific Aim 3.1   *Develop a relatively faithful murine model of lung cancer by crossing the k-ras mutant mouse (T. Jacks) with our p53 mutant missense mouse (G. Lozano) such that we can study the evolution of non-small cell lung cancer in primary lung tumor model with metastatic potential, as well as the effectiveness of these molecularly targeted strategies in that model.*

We proposed to develop a mouse model with mutations in genes commonly occurring in human lung cancer (ras and p53) to use as a model for lung therapies. The first phase of the study has been completed. Mice inheriting a common *p53* mutation (*p53R172H□g/+*) that also inherit a certain probability of generating a *ras* mutation somatically (*K-rasLA1/+*) in the lung have been made and monitored for tumor formation. At one year of age, about 90% of double heterozygous mice had died, while only 60% of *K-rasLA1/+* or 20% of *p53R172H□g/+* control mice have died (figure 1). Double heterozygous mice had significantly reduced life spans and all developed lung carcinomas. The median age of death for double heterozygous mice is 8.5 months, while that of *K-rasLA1/+* is 12 months. During this time frame very few *p53R172H□g/+* have died. Metastases from primary lung carcinomas were observed in 33% of the double heterozygous mice by histopathological evaluation. To confirm pathological findings, sections were stained with surfactant protein C, a marker of lung epithelial cells. The expression of surfactant protein C was clearly visible in many of the metastatic lesions. Surprisingly, metastasis to the adrenal gland was common as occurs in human metastatic lung cancer (figure 2). Metastases to the liver and lymph nodes were also seen.

Subsequent studies will include treatment of mice with IRESSA and FTI to determine efficacy in this animal model with known mutations in p53 and ras.
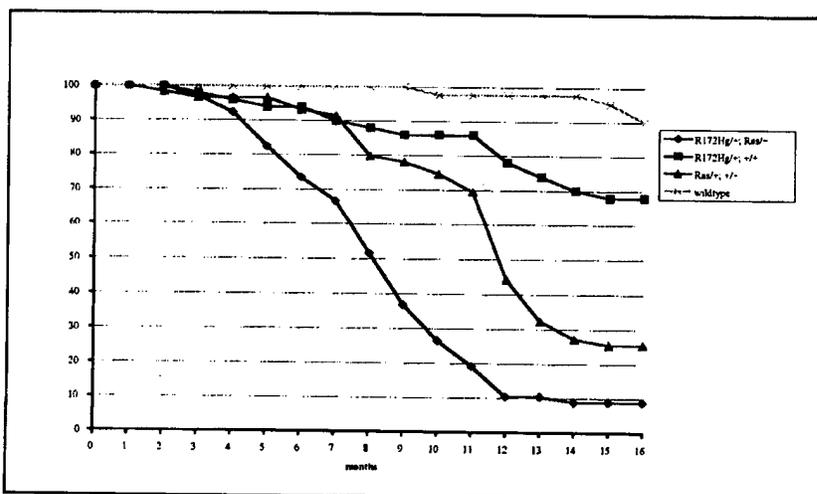

Figure 1. Survival curve of mice with the indicated genetic defects.

Figure 2. Surfactant protein C staining of a metastatic lesion on the adrenal gland that arose from a primary lung carcinoma

Specific Aim 3.2   *Evaluate novel signal transduction inhibitors, both alone and in combination with one another and with cytotoxic agents, in the treatment of these mouse lung cancer models and, ultimately, in the treatment of human lung cancers.*

Ras gene mutations are among the first described oncogenic changes in human cancer. Broadly, much work has been undertaken in the last two decades to better comprehend the functions of the various isoforms of *ras*, h-, n-, k-, and r-*ras*. A recent collaboration by the laboratories of Adrienne Cox (University of North Carolina) and Mark Phillips (New York University) has begun to elucidate the specific functions of various isotypes, by better defining their specific membrane localization. Added to the extensive work studying the *ras* gene mutations in the hematologic and oncologic malignancies, the functional significance of this crucial family of G-proteins/GTPases is becoming increasingly clear.

The major focus of our laboratory is on targeting post-translational modifications of the *ras* genes as a therapeutic target. Since Brown and Goldstein first elucidated the importance of isoprenylation of *ras* genes as a critical step in the maintenance oncogenic *ras* signaling, an academic and pharmaceutical race has been initiated to develop and license the first "*ras*-targeting" agents in man. Several clinical trials of farnesyl transferase inhibitors (FTIs), both alone and in combination with cytotoxic agents have shown promise, but not yet definitive efficacy in patients with hematological and solid tumor malignancies. To date, we have led or been involved in both single agent and combination trials of the three FTIs currently in phase II/III clinical trials, and have contributed to the understanding of how these agents down-regulate *ras*-dependent signaling in aerodigestive tract cancers. A major focus of our laboratory has been to understand how FTIs down-regulate phosphorylated raf and phosphorylated akt, and induce the degradation/ubiquitination of AKT/PKB proteins in lung cancers and head and neck squamous cell cancers (HNSCC).

We have studied the effects of FTIs on *raf* and *akt* activity in lung and head and neck cancers in preparation for combining them with Iressa. We have shown that in head and neck cancers and cell lines, the FTI lonafarnib induces downregulation of phosphorylated raf and phosphorylated akt, and induce the degradation/ubiquitination of AKT/PKB proteins. We have also continued our fruitful collaborations with Dr. Li Mao, PI of project 1, on the development of a molecular prognostic model of lung cancer, so that we can differentiate between those individuals with early stage(Stage I) Non-Small Cell Lung Cancer(NSCLC) who will do well postoperatively and those individuals whose prognosis is more guarded. Our collaborations have expanded to the study of the promoter methylation patterns in the PTEN/akt signaling pathway, whose downregulation we have shown to be vital to the effect of lonafarnib in NSCLC and HNSCC, and the prognostic expression of the vital telomeric regulatory component, hTERT, whose expression has been shown by Hahn and Weinberg to be necessary for ras dependent transformation of mammalian cell lines. Our continued prognostic understanding of these various critical signaling proteins in ras dependent transformation and progression, is the underpinning for our subsequent development of targeted, individualized therapies for high risk lung cancer patients.

Farnesyltransferase inhibitors (FTIs), including Lonafarnib, represent a novel class of anticancer agents that show promise in suppressing the growth of tumors both in preclinical studies and in clinical trials. Although FTIs were originally designed to target Ras activation, many studies indicate that they may inhibit cell growth and induce apoptosis independent of Ras mutation. Alternatively, the PI3 kinase/Akt pathway has been proposed as a potential target for the FTI's actions. In this study, we found that Lonafarnib was effective in inhibiting the growth of 11 non-small cell lung cancer

(NSCLC) cell lines, particularly after a 5-day treatment, regardless of Ras mutational status. The $IC_{50}s$ for a 5-day treatment ranged from 0.14 to 3.12 μM. Lonafarnib arrested cells growth at G1 or G2/M phase in the majority tested cell lines under normal culture condition (5% serum). However it induced rapid apoptosis when cells were cultured in a low serum (0.1%) medium. The majority of NSCLC cell lines used in our study expressed undetectable level of phosphorylated Akt (p-Akt). Lonafarnib at up to 10 μM did not decrease either total Akt level or p-Akt level in any of the tested cell lines, even after a 48 h treatment. Unexpectedly, Lonafarnib increased p-Akt level in one cell line, which, however, was as sensitive as other cell lines to Lonafarnib treatment and underwent G2/M arrest. The PI3 kinase inhibitor LY294002 enhanced Lonafarnib's effect on apoptosis induction but this effect was not associated with a suppression of Akt activation. Moreover, bovine serum albumin (BSA) completely rescued cells from Lonafarnib-induced apoptosis in low serum medium, indicating that proteins rather than cytokines or growth factors in serum masks Lonafarnib's pro-apoptotic effect. These results together indicate that Akt is unlikely to be a target for Lonafarnib's effect on growth arrest or apoptosis induction in human NSCLC cells.

Farnesyl transferase inhibitors (FTIs) are anti-cancer agents developed to specifically target oncogenic Ras proteins by inhibiting Ras farnesylation. FTIs are known to synergize with taxanes; however the mechanistic basis underlying this synergistic interaction remains elusive. Here we show that lonafarnib-treated cells displayed microtubule bundles, increased tubulin acetylation and polymerization, and decreased microtubule dynamics. Importantly, the combination of lonafarnib with taxanes dramatically enhanced tubulin acetylation as compared to either drug alone. This effect was accompanied by a synergistic increase in mitotic arrest and cell death, suggesting that tubulin acetylation underlies its synergism with taxol. Furthermore, *in vitro* analyses show that lonafarnib alone (at high doses), as well as the combination of low doses of lonafarnib and taxol, inhibit the function of the tubulin deacetylase, HDAC6. Lastly, analysis of tumors resected from patients who received lonafarnib treatment revealed differential levels of tubulin acetylation that correlate with response. Thus, our results identify interphase microtubules as a target for lonafarnib and provide a mechanistic explanation for the synergy between lonafarnib and taxol.

Specific Aim 3.3   *Produce and test a liposomal gene-therapeutic strategy targeted to a novel tumor suppressor gene located on chromosome 3p, both in the mouse model and in human patients with advanced non-small cell lung cancer*

Suppression of Tumor Growth by Systemic Delivery of FUS1-lipoplex. Since the main aim of the present proposal is to develop and deliver therapeutic genes via the systemic route, we tested the therapeutic effect of FUS1 gene on experimental lung metastasis and animal survival. Preliminary studies were conducted in a nude mouse model bearing experimental A549 lung metastasis. Treatment with DOTAP:Chol-FUS1 resulted in a significant inhibition (P = 0.01) of tumor metastasis as indicated by the reduction in number of tumor nodules in the lungs. Animals treated with PBS, DOTAP:Chol.liposome alone, plasmid DNA alone, and DOTAP:Chol-CAT complex served as controls in these experiments. Correlating with these observations was the prolonged survival of lung tumor bearing animals (mean = 80 days; P = 0.01) treated with DOTAP:Chol-FUS1 complex compared to animals treated with PBS (mean =47.8 days), treated with DOTAP:Chol. liposome (mean= 47.2 days), treated plasmid DNA (mean = 51.6 days), and treated with DOTAP:Chol-CAT complex (mean = 47.8 days). These results demonstrate the feasibility of using these vectors for systemic therapy. However, further analyses using other xenograft models as well toxicity studies are warranted prior to testing these vectors and genes in the clinic.

<u>Toxicity in Mice.</u> The objective of this study was to determine the single-dose toxicology of DOTAP:Chol-*FUS1* in preparation for Phase I studies. The nontoxic dose and dose-limiting toxicity for C3H/HeNCR mice were determined. The study contained three control groups: D5W (vehicle), 4 mM DOTAP:Chol (highest dose of lipid), and 70 μg DNA (highest dose of *fus1* plasmid).The study also contained three experimental groups: 70 μg DNA, DOTAP:Chol, 40 μg DNA, DOTAP:Chol, and 10 μg DNA, DOTAP:Chol. Each group contained 15 mice (8 female and 7 male). Acute (0-72 h), subacute (14 days) and chronic (6 weeks) toxicity were evaluated. At 3 and 14 days and at 6 weeks, five mice per group were euthanized. For each mouse, an attempt was made to collect urine for analysis for CBC and serum chemistries. Necropsies were performed, and histopathological analysis was done on all mice, including those that died during the study. This study was conducted in an AAALAC accredited facility (2000). All mice in the three control groups (D5W, 4mM DOTAP:Chol, and 70 □g DNA alone) and in the experimental group receiving 10 □g DNA, DOTAP:Chol were observed to be normal at all observation time points. Mice in the experimental group receiving 40 □g DNA, DOTAP:Chol appeared normal at the end of the 4 h post-injection observation period. When observed later that day at approximately 7 h post injection 14/15 mice were squinting and appeared to be lethargic. One female mouse was euthanized and sent to necropsy at that time. All mice were thereafter normal at all observation time points. In summary, one female mouse became moribund on day 0 and was euthanized. Mice in the experimental group receiving 70 □g DNA, DOTAP:Chol appeared normal at the end of the 4 h post-injection observation period. On day 1 PI, one female mouse died. Three male mice and one female mouse were found to be moribund and were euthanized and necropsied. On day 2, a female mouse was found to be moribund and was euthanized and necropsied. Another female mouse was found dead on day 2. The remaining mice had decreased or slightly decreased activity levels and some were squinting. On day 3, 2/8 remaining mice appeared normal, while 6/8 still had decreased activity levels and abnormal general appearance. From day 4 on, all mice appeared normal at all observation time points. In summary, two female mice died. Three male and two female mice were found moribund and were killed. In conclusion 10 μg DNA, DOTAP:Chol was a well-tolerated non-lethal dose.

Non-human primate toxicology. Ten cynomolgus monkeys (Macaca fascicularis) were used in Protocol No. 10-01-10681, titled "GLP Study Prior to Phase I Clinical Trials for DOTAP: Cholesterol-Fus 1 Liposome Complex (DOTAP: Chol-Fus 1) Relevant Safety Study". Six experimental animals (three male and three female) were injected with DOTAP:Chol-Fus 1 complex on Day 1 and Day 21 of the study. Four control animals (two male and two female) were injected with DOTAP:Cholesterol alone on Day 1 and Day 21 of the study. At days 46-52 the animals were necropsied, blood was collected for hematology and blood chemistry assays, and organs were collected for histopathological analysis. Significant gross and microscopic lesions were found in one of the 10 monkeys on protocol. This animal received 1 dose of 0.6 mg/kg DNA, DOTAP: Chol (high dose) and died within 18-20 h. Lesions in this monkey were most likely treatment related. A second monkey that received the high dose of DNA, DOTAP: Chol had changes in a lymph node. The significance of these minimal changes is not known. Equivocal lesions were found in the femoral bone marrow of two low dose (0.2 mg/kg DNA, DOTAP: Chol) monkeys. The latter may be incidental findings, but were not seen in other protocol animals. No significant gross or microscopic lesions were found in the remaining six animals that received either DOTAP: Chol only or 0.2 mg/kg DNA, DOTAP: Chol.

Phase I clinical trial to evaluate anticancer activity and toxicity of the *FUS1* TSG delivered systemically using a DOTAP:Chol lipoplex as the first in a series of translational clinical trials. Based on these pre-clinical studies, A Phase I clinic trial (Human Gene Transfer Protocol

#0201-513) is under taking in later stage lung cancer patients in M.D. Anderson Cancer Center. Patients are treated by systemic administration of the DOTAP:cholesterol complexed FUS1-expression plasmid DNA.

Specific Aim 3.4   ***Develop specific vascularly targeted strategies to the vascular epithelium of lung cancer cells in order to decrease the toxicity to normal cells and enhance the therapeutic index.***

Angiogenesis is essential for tumor growth, invasion and metastasis, thus the inhibition of angiogenesis is a promising strategy for cancer treatment. The PI3K/Akt signaling pathway can contribute to angiogenesis by regulating expression of angiogenic factors. We found that SCH66336, a farnesyltransferase inhibitor (FTI), inhibits the level and activity of Akt in human lung and head and neck cancer (HNSCC) cells. It has been demonstrated that PI3K/Akt is constitutively active in most NSCLC cells. Therefore, we postulated that SCH66336 inhibits angiogenesis in the aerodigestive tract cancer, including NSCLC and HNSCC. Recently, we found several lines of evidence showing that SCH66336 has antiangiogenic activity in aerodigestive tract cancer. Antiangiogenic activity of SCH66336 was evaluated *in vitro* by analyzing the effects of SCH66336 on the proliferation and/or tube formation of human endothelial cells and on the cell sprouts from chick aorta ring and *in vivo* by performing the chick chorioallantoic membrane and Matrigel plug assays. We found that treatment of SCH66336 leads to a decrease in human umbilical vein endothelial cell proliferation. SCH66336 also effectively inhibited neovascularization as assessed by the chick embryo chorioallantoic membrane assay and the mouse matrigel plug assay. Furthermore, we show that treatment of SCH66336 leads to a decrease in the ability of NSCLC cells in stimulating endothelial cell proliferation by suppressing the secretion of angiogeneic factors from NSCLC cells. Our findings provide the preclinical rationale for the use of SCH66336 as a novel treatment strategy targeting angiogenesis in aerodigestive cancer. We are now investigating the mechanisms that mediate the antiangiogenic activities of SCH66336 in NSCLC and HNSCC cells.

KEY RESEARCH ACCOMPLISHMENTS

- HNSCC cells that express COX-2 synthesize PGE2 from arachidonic acid.
- Celecoxib suppresses the generation of PGE2 from arachidonic acid, however, this inhibition does not appear to be the cause for result growth inhibition of HNSCC cells because cells that do not possess COX-2 and do not generate Pge2 are equally sensitive to celecoxib as those that possess COX-2.
- HNSCC cells contain various arachidonic acid and linoleic acid metabolizing enzymes, however, most of these enzymes appear to be inactive because they do not generate the expected metabolites.
- Evaluated the therapeutic efficacy of systemic administration of DOTAP:Cholesterol: FUS1 DNA (FUS1-lipoplex) on development of human lung metastases and animal survival, nd found that treatment with FUS1-lipoplex resulted in significant inhibition of tumor metastases
- Evaluated the toxicity of systemic administration of FUS1-lipoplex in mice and non-human primates in an AAALAC-accredited GLP-grade facility and no signs of toxicity at therapeutic dose levels were shown in those animal models.

- Based on the pre-clinical efficacy and toxicity study, a Phase I clinical trial with systemic administration of FUS1-lipoplex is being undertaken in later stage lung cancer patients at M. D. Anderson Cancer Center.
- Clinical synergy was seen in a phase I trial of the farnesyl transferase inhibitor, lonafarnib, with paclitaxel in patients with non-small cell lung cancer. The molecular mechanism of synergy between FTIs and taxanes may depend on upregulation of acetylated α-tubulin.

REPORTABLE OUTCOMES

Chang YS, Wu W, Walsh G, Hong WK, Mao L. Enolase-α is frequently down-regulated in non-small cell lung cancer and predicts aggressive biological behavior. *Clinical Cancer Research* 9: 3641-3644, 2003.

Soria JC, Moon C, Kemp BL, Liu D, Feng L, Tang X, Chang YS, Mao L, Khuri FR. Lack of interleukin-10 expression could predict poor outcome in patients with stage I non-small cell lung cancer. *Clinical Cancer Research* 9: 1785-1791.

Wang L, Soria JC, Chang YS, Lee HY, Wei Q, Mao L. Association of a functional tandem repeats in the downstream of human telomerase gene and lung cancer. *Oncogene* 22: 7123-7129, 2003.

Ren H, Tang X, Feng L, Lee JJ, Everett AD, Mao L. Frequent overexpression of hepatoma-derived growth factor in early stage non-small cell lung cancer. *Proc AACR* 44: #371, 2003.
Ito I, Saeki T, Mohuiddin I, Saito Y, Branch CD, Vaporciyan A, Roth JA, Ramesh R. *Molecular Therapy* 9: 318-327, 2004.

Carboni GL, Gao B, Nishizaki M, Xu K, Minna JD, Roth JA, and Ji L. CACNA2D2-mediated apoptosis in NSCLC cells is associated with alterations of the intracellular calcium signaling and disruption of mitochondria membrane integrity. *Oncogene* 22:615-626, 2003.

Futoshi U, Sasaki J, Nishizaki M, Carboni G, Xu K, Gao B, Kondo M, Atkinson EN, Lerman MI, Minna JD, Roth JA, Ji L. Myristoylation of Fus1 protein is required for tumor suppression in lung cancer. *Cancer Research* 2004 (in press).

Ji L, Nishizaki M, Gao B, Burbee D, Toyooka S, Kamibayashi G, Xu K, Yen N, Fang B, Lerman MI, Roth JA, and Minna JD. Expression of several genes in the human chromosome 3p21.3 homozygous deletion region by an adenovirus vector results in tumor suppressor activities in vitro and in vivo. *Cancer Research* 62: 2715-2720, 2002.

Ito I, Saeki T, Mohuiddin I, Saito Y, Branch CD, Vaporciyan A, Roth J, Ramesh R. Persistent transgene expression following intravenous administration of a liposomal complex: Role of interleukin-10-mediated immune suppression. *Molecular Therapy* 9: 318-327, 2004.

Khuri FR, Glisson BS, Kim ES, Statkevich P, Thall PF, Meyers ML, Herbst RS, Munden RF, Zaknoen S, Tendler C, Zhu Y, Bangert S, Thompson E, Lu C, Wang X-M, Shin DM, Kies MS, Papadimitrakopoulou V, Fossella FV, Kirschmeier P, Bishop WR, Hong WK. Phase I study of farnesyl transferase inhibitor (FTI) SCH66336 with paclitaxel in solid tumors. *Clinical Cancer Research* in press, May 2004.

Abstracts and Presentations (2003)

Ji L, Xu K, Sasaki J, Nishizaki M, Carboni G, Girard L, Garner H, Minna JD, and Roth JA. Discovery of specific cellular regulatory pathway mediated by the tumor gene FHIT in NSCLC cells by mRNA microarray and protein chip expression profiling. National Cancer Institute Winter Lung SPORE Meeting, Santa Monica, California, February 15-16, 2003, pp. #10, 2003. (presentation)

Began G, Ji L, Ito I, Saito Y, Branch C, Xu K, Stephens C, Minna JD, Roth JA. and Ramesh R. The anti-inflammatory drug naproxen protects mice from lipoplex-mediated toxicity. National Cancer Institute, Winter Lung Cancer SPORE Meeting, Santa Monica, California, February 15-16, 2003, pp. # 41, 2003.

Carboni GL, Shao J, Xu K, Gao B, Nishizaki M, Schmid RA, Minna JD, Roth JA, and Ji L. Synergistic inhibition of tumor cell growth by CACNA2D2 and p53 via activation of DAPK pathway in lung cancer. American Association for Cancer Research (AACR), 94th Annual Meeting, Toronto, Ontario, Canada, April 5-9, 2003. Proc. Am. Assoc. Cancer Res., 44:241-242, 2003.

Gopalan B, Ji L, Ito I. Saito Y, Branch CD. Xu K, Stephens C, Minna JD, Roth JA, and Ramesh R. Protection of mice from liposome-DNA complex induced toxicity by anti-inflammatory drugs. Annual Trainee Recognition Day, M. D. Anderson Cancer Center, Houston, TX April 25, 2003

Nishizaki M, Sasaki J. Carboni G, Roth JA. and Ji L. Overexpression of FHIT inhibits tumor cell invasion and metastases via inactivation of the Rho-PKC-Ezrin signaling pathway in human pancreatic cancer. American Association for Cancer Research (AACR) 94th Annual Meeting, Washington, District of Columbia, July 11-14, 2003. Proc. Am. Assoc. Cancer Res., 44:1178, 2003.

Uno F, Sasaki J, Nishizaki M. Carboni G, Xu K, Minna JD. Roth JA. and Ji L. Myristoylation of Fus1 protein is required for Fus1-mediated tumor suppressing activities in human lung cancer. American Association for Cancer Research (AACR), 94th Annual Meeting, Washington, District of Columbia, July 11-14, 2003. Proc. Am. Assoc. Cancer Res., 44:75, 2003.

Gopalan B, Ji L. Ito I. Saito Y, Branch CD, Xu K, Stephens C, Minna JD, Roth JA, and Ramesh R. The anti-inflammatory drug naproxen protects mice from lipoplex-mediated toxicity. American Association for Cancer Research (AACR), 94th Annual Meeting, Washington, District of Columbia, July 11-14, 2003. Proc. Am. Assoc Cancer Res., 44:923, 2003.

Ji L, Xu K, Nishizaki M, Sasaki J. Uno F, Girard L. Garner H, Minna JD, and Roth JA. Discovery of specific cellular regulatory pathway medicated by the tumor suppressor gene FHIT in NSCLC cells by gene and protein expression profiling. American Association for Cancer Research (AACR), 94th Annual Meeting, Washington, District of Columbia, July 11-14, 2003. Proc. Am. Assoc. Cancer Res., 44:243, 2003. (presentation)

Chang YS, Khuri FR, Hassan KA, Wiehle SA, Ji L, Lotan R. Chun K. Hong WK, Cristiano R, and Lee H. IGFBP-3 and the farnesyl transferase inhibitor SCH66336 act synergistically to induce apoptosis in non-small cell lung cancer (NSCLC) cells. American Association for Cancer Research (AACR), 94th Annual Meeting, Washington, District of Columbia, July 11-14, 2003. Proc. Am. Assoc. Cancer Res., 44:1234, 2003.

Project Generated Resources

NIH U01 (Mouse Models of Human Cancers Consortium)
(Baylor College of Medicine
 and U.T. M.D. Anderson Cancer Center)   4/1/2004-3/31/2009
Modeling Airway Lung Cancer and the Role of Inflammation
Role: Project (2, and 5) Leader (Lin Ji)

Patent:

Ji L, Roth JA, Minna JD, and Lerman MI. Chromosome 3p21.3 genes as tumor suppressors.
     U.S. Patent pending NO. 60/217, 112; International Patent Application No. PCT/US01/2178;
     European Patent Application Based on PCT/US01/21781;

CONCLUSIONS

The sensitivity of HNSCC cells to celecoxib is independent of COX-2 expression and PGE2
production.
The detection of arachidonic acid and linoleic acid metabolizing enzymes by western blotting
does not mean that these enzymes are active. One should examine the presence of metabolites
to complement western blotting data.
We have successfully conducted preclinical evaluation of therapeutic efficacy and toxicity of
DOTAP:Chol-FUS1 and initiated a phase I human clinical trial in lung cancer patients.
The biologic underpinnings of synergy beween signal transduction inhibitors and cytotoxics are
highly dependent on the sequences and concentrations of the compounds, as well as on the
successful induction of vital molecular modifications, as demonstrated by both our clinical and
preclinical studies combining lonafarnib and taxanes.

APPENDIX

Enolase-α Is Frequently Down-Regulated in Non-Small Cell Lung Cancer and Predicts Aggressive Biological Behavior[1]

Yoon Soo Chang, Weiguo Wu, Garrett Walsh, Waun Ki Hong, and Li Mao[2]

Molecular Biology Laboratory, Department of Thoracic/Head and Neck Medical Oncology [Y. S. C., W. W., W. K. H., L. M.] and Department of Thoracic and Cardiovascular Surgery [G. W.], The University of Texas M. D. Anderson Cancer Center, Houston, Texas, 77030

ABSTRACT

Purpose: Enolase-α is a cytoplasmic glycolytic enzyme important in the formation of phosphoenolpyruvate. Enolase-α and *c-myc* binding protein (MBP-1) originate from a single gene through alternative use of translational starting sites. Both enolase-α and MBP-1 can bind to the P2 element in the *c-myc* promoter and compete with TATA-box binding protein (TBP) to suppress transcription of *c-myc*.

Experimental Design: To determine a potential role of enolase-α *in vivo*, we analyzed enolase-α expression in non-small cell lung cancer (NSCLC) tissues from 46 patients by Western blotting and immunohistochemical analysis.

Results: Twelve (26%) of the 46 tumors showed a significantly reduced enolase-α expression. Although no statistically significant association was observed between the down-regulation of enolase-α and pathological stage, tumor histology, or differentiation, the patients whose tumors showed reduced enolase-α expression had a significantly poorer overall survival compared with those without down-regulation of this molecule (*P* = 0.0398).

Conclusions: Our results indicate down-regulation of enolase-α is common in NSCLC and may play an important role in lung tumorigenesis.

INTRODUCTION

Lung cancer is the leading cause of cancer-related death in the United States. More than 157,000 patients will die of the disease this year alone. Development of lung cancer is the result of an accumulation of molecular abnormalities that activate

oncogenes and inactive tumor suppressor genes. Understanding the biology of the disease is critical to developing novel strategies for early detection, prevention, classification, and treatment. The *c-myc* proto-oncogene is a critical factor in controlling both cell proliferation and apoptosis (1–4). The *c-myc* oncogene is important in tumor progression in multiple tumor types, including NSCLC[3] (2, 3). Several distinct mechanisms have been suggested as regulating *c-myc* expression (5). Because *c-myc* has multiple promoters, termed P0, P1, P2, and P3, regulation of its gene expression is complicated. Yet in normal and transformed cells, the majority of *c-myc* transcripts are initiated through the P2 promoter (3, 4).

MBP-1 is a M_r 37,000–38,000 protein that can bind just 5′ to the P2 TATA motif and decrease *c-myc* promoter activity in both human and mouse models (6–8). Both MBP-1 and TBP can bind to the minor groove of the *c-myc* P2 promoter, suggesting that MBP-1 may negatively regulate *c-myc* transcription by preventing transformation of a transcriptional initiation complex (8, 9). MBP-1 mRNA is identical to enolase-α mRNA, which encodes a polypeptide of about M_r 48,000 using an alternative translation site (GenBank accession nos.: M14328 and M55914). *In vitro* transcription and translation experiments show that the enolase-α transcript encodes 2 proteins, M_r 48,000 and 37,000, both of which have the ability to down-regulate *c-myc* expression (10, 11). To determine a role of enolase-α in lung tumorigenesis, we analyzed enolase-α protein expression in 46 primary NSCLC. We found that enolase-α was down-regulated in 26% of the primary NSCLC and that such down-regulation was associated with a poor clinical outcome, suggesting that enolase-α plays an important role in NSCLC.

MATERIALS AND METHODS

Study Population. Surgically resected primary tumors and corresponding normal lung tissues were obtained from the Department of Pathology at The University of Texas M. D. Anderson Cancer Center after patients' consent. These specimens were collected between 1995 and 1998, and follow-up information was obtained from the Tumor Registry at the M. D. Anderson Cancer Center. All of the patients were treated by surgery at the time of diagnosis. The primary tumor specimens consisted of 20 adenocarcinomas, 19 squamous cell carcinomas, and 7 samples of other cell types. The study population consisted of 24 males and 22 females, with a mean age of 64.1 ± 10.83 years. Other clinical characteristics are shown in Table 1.

Protein Extraction. The samples consisted of 46 paired normal/tumor tissues from patients with lung cancer. Briefly, samples were weighed and diced into small pieces with a clean

Table 1 Analysis of the patients with NSCLC according to the expression status of enolase-α

	Normal expression	Down-Regulation	P
Age	64.3 ± 10.07	63.6 ± 13.24	0.394
Gender			
Male	18	6	
Female	16	6	1.000
Diameter of tumor	4.83 ± 2.72	8.32 ± 8.58	0.193
Tumor stage			
I, II	21	6	
III, IV	13	6	0.298
Tumor histology			
Adenocarcinoma	13	7	
Squamous carcinoma	15	4	
Large cell carcinoma	2	1	
Others	4	0	0.463
Differentiation			
Well differentiated	4	2	
Moderately differentiated	10	4	
Poorly differentiated	18	6	
Unclassified	2	0	0.911
Smoking status: n (%)			
Current; pack-year	17; 40.4 ± 22.98	2; 29.0 ± 25.52	0.183
Ex-smoker	12	7	
Nonsmoker	3	2	
Unknown	2	1	0.130
Median survival, mo (95% CI)			
Overall survival	43 (8.1–77.7)	6 (0–19.9)	0.040

Fig. 1 Western blot of normal (*N*)-tumor (*T*) paired samples revealed that enolase-α is frequently down-regulated in primary NSCLC. β-actin was used as an internal control of protein loading.

razor blade and then were disrupted with a dunce homogenizer in ice-cold radioimmunoprecipitation buffer containing a protease inhibitor cocktail (Boehringer Mannheim, Indianapolis, IN). Phenylmethanesulfonyl fluoride (Sigma Chemical Co., St. Louis, MO) stock solution was added, and the lysates were incubated on ice for 30 min, followed by centrifugation twice at 10,000 × g for 10 min at 4°C. The supernatant was taken and stored for protein analysis.

Western Blot Analysis. Twenty μg of protein extract were loaded into each well and were separated in 10% SDS-PAGE gel under reducing conditions. Separated proteins on the gel were electrotransferred onto Hybond-polyvinylidene difluoride membranes (Amersham Pharmacia Biotechnology, Arlington Heights, IL). Membranes were blocked with 5% nonfat dry milk to reduce background.

The membrane was incubated at 4°C overnight with anti-enolase-α monoclonal antibody (9C12) at a dilution of 1:50. This antibody, donated by Dr. E. F. Plow, does not cross-react with enolase-β and γ. β-actin was detected with a monoclonal anti-β-actin antibody AC-15 (Sigma) at a dilution of 1:1000. Then the blots were incubated with a sheep antimouse secondary antibody conjugated to horseradish peroxidase. Signals were detected by enhanced chemiluminescence on Hyperfilm ECL films (Amersham Pharmacia Biotechnology). Each signal was scanned and measured using the Scion Image program (Scion Corp., Frederick, MD). β-actin was used as an internal control. The level of enolase-α expression was calculated by dividing the signal of normal tissue by that of tumor tissue. Patient tissues were classified into two groups according to the level of enolase-α expression. One group included cases that did not show down-regulation of enolase-α (ratio, <2.0), and the other was
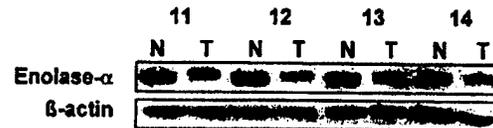
composed of cases that did show down-regulation of enolase-α (ratio, ≥2.0).

Immunohistochemistry. IHC was performed in a conventional manner. Briefly, paraffin sections on slides were deparaffinized and rehydrated in serial graded ethanol. Antigen retrieval was skipped. Endogenous peroxidase activity was blocked in methanol containing 3% hydrogen peroxide. The blocking was performed by incubation in 5% horse serum, followed by overnight incubation with 1:100 anti-enolase-α antibody. After the sections were incubated with secondary antibody, the ABC complex and 3,3'-diaminobenzidine (Vector Laboratories, Inc., Burlingame, CA) solutions were used serially, and the slides were counterstained with hematoxylin.

Statistical Analysis. In univariate analysis, independent sample *t* tests and χ^2 tests were used for continuous and categorical variables, respectively. Kaplan-Meier analysis was performed to estimate a survival function over time for individual covariates. The log-rank test was used to compare patient survival time between groups. All of the statistical tests were two-sided. $P < 0.05$ was considered to be statistically significant.

RESULTS

Enolase-α Is Frequently Down-Regulated in NSCLC. We analyzed the expression level of enolase-α from 46 normal/cancer pairs from patients with NSCLC through Western blotting. Although 42 (91.3%) of 46 of the tumors showed some degree of reduced enolase-α expression, we used a more stringent cutoff (a 2-fold reduction) to offset experimental variations (Fig. 1). Twelve (26.1%) of the tumors were assigned to the down-regulation group according to this criterion. We performed further IHC to determine enolase-α expression status at the cellular level. In normal lung tissues, IHC showed a ubiquitous cytoplasmic and membranous staining, including staining of the bronchial epithelium and alveolar wall (Fig. 2*A*). Nuclear staining also was observed in bronchial epithelial cells, type I and type II alveolar cells, and endothelial cells, consistent with a recent report (10). Endothelial cells showed a strong cytoplasmic and nuclear staining with the anti-enolase-α antibody. Lymphocytes, however, were barely stained with this antibody. In contrast, tumors exhibiting down-regulation of enolase-α exhibited lack of antibody staining, consistent with Western blotting analysis (Fig. 2, *B* and *C*).

Enolase-α Expression and Clinical/Pathological Parameters. We analyzed clinical and pathological parameters according to enolase-α expression status. In univariate analysis, we found no age and gender differences among patients with down-regulation and those without down-regulation. In addition, no significant associations were found between down-

Fig. 2 IHC of normal lung tissue with enolase-α showed ubiquitous staining, including bronchial epithelium and alveolar structure (*A*). IHC of squamous lung cancer showed down-regulation of enolase-α that was consistent with the Western blot (*B*). Bronchioalveolar carcinoma, which generally has an excellent prognosis, showed a staining pattern similar to that of normal bronchial epithelium (*C*).

A **B** **C**
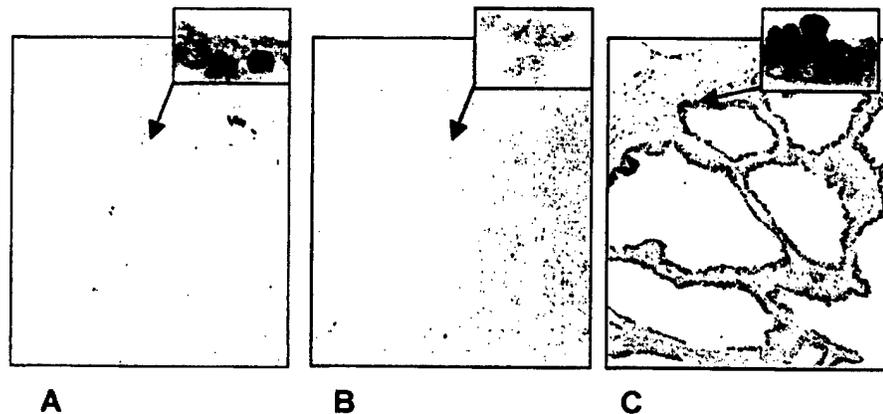
regulation of enolase-α and pathological stage, tumor histology, or the degree of differentiation. Although the difference was not statistically significant, patients whose tumors showed down-regulation of enolase-α bore larger tumors at the time of surgery (8.3 ± 8.58 cm) than did patients without down-regulation (4.8 ± 2.72 cm; Table 1).

Down-Regulation of Enolase-α and Clinical Outcome. At last follow-up, 29 of the 46 patients had died, and 17 were still alive. Among the living patients, the median follow-up duration was 5.7 years. During the same follow-up period, 9 (75.0%) of the 12 patients whose tumors showed loss of enolase-α expression died, compared with 20 (59%) of the 34 patients whose tumors retained enolase-α expression.

Kaplan-Meier estimates were used to examine the relationship between down-regulation of enolase-α and patients' overall survival. The median survival of patients whose tumors showed down-regulation of enolase-α was only 6 months (95% CI, 0.00–19.9 months), whereas the median survival of those whose tumors showed no down-regulation was 43 months (95% CI, 8.1–77.7 months; P = 0.0398 by log-rank test; Fig. 3).

Fig. 3 Survival analysis demonstrated that patients whose tumors showed down-regulation of enolase-α had poorer overall survival compared with those whose tumors had normal expression levels of enolase-α.

DISCUSSION

Enolases have been characterized as highly conserved cytoplasmic glycolytic enzymes that catalyze the formation of phosphoenolpyruvate from 2-phosphoglycerate, the second of the two high-energy intermediates that generate ATP in glycolysis (12). Three isoforms of enolase have been identified and named as enolase-α, -β, and -γ. Enolase-α expression has been detected in almost all of adult tissues, whereas enolase-β is expressed predominantly in muscle and enolase-γ is detected only in nerve tissues (13, 14). These three isoforms may exist as either homodimers or heterodimers.

Diverse functions of enolase-α have been reported in the ecosystem. It has been identified as a heat shock protein in yeast (15), an immunodominant antigen in *Candida albicans* (16), and toxin B in *Clostridium difficile* (17). It also known as a component of the centrosome in HeLa cells (18) and as a molecule associated with connective tissue disorders (19). Enolase-α is considered to have potential roles in tumorigenesis. Tumor cells possess higher metabolic rate than surrounding normal tissues,
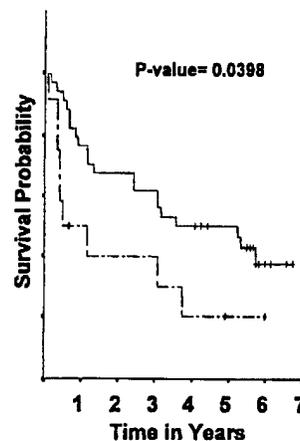
and enolases, the representative glycolytic enzyme, are an important factor in cell metabolism. There is evidence to suggest that enolase-α may involve cancer invasion and metastasis. Enolase-α has a COOH terminus that spans plasma membrane. With this domain, monocytes, neutrophils, and some cancer cell lines, such as U937, are capable of binding with, activating, and stabilizing plasminogen. By doing so, they have the capacity to clear a path for themselves through the macromolecular barriers of basement membrane and other extracellular matrix (20). Additionally the gene encoding enolase-α (*ENO-1*) maps to a region of human chromosome 1(1p35-p36) that is often deleted in several types of human malignancies, including neuroblastoma, melanoma, pheochromocytoma, and carcinoma of the breast and liver (21). Furthermore, as described earlier, the capability of enolase-α to compete with TBP to repress transcription of oncogene *c-myc* suggests a potential mechanism for how enolase-α may be involved in tumorigenesis.

To demonstrate the relevance of this finding in primary

tumors, we used a monoclonal anti-enolase-α antibody to ana-
lyze enolase-α expression status in NSCLC and its potential role
in molecular classification of the tumors. We found that eno-
lase-α is localized in both the cytoplasm and the nucleus in
various cell types of normal lung tissue, including bronchial
epithelium, a finding that is consistent with previous reports (8).
However, 26% of the primary NSCLC exhibits substantial
down-regulation of the molecule, and this down-regulation pro-
portionally reduces staining in both the cytoplasm and the
nucleus, supporting the notion that the proteins in the cytoplasm
and nucleus are both enolase-α. Interestingly, tumors with eno-
lase-α down-regulation tend to be larger than those without
down-regulation, suggesting that the down-regulation is associ-
ated with tumor progression. The biological role of the down-
regulation in NSCLC needs further investigation.

The association of the down-regulation of enolase-α with a
poorer clinical outcome further supports the importance of this
molecule in determining tumor aggressiveness in patients with
NSCLC. It also indicates the importance of proteomic ap-
proaches in identifying potential biomarkers useful in cancer
detection and classification. Our results should be validated in
larger and independent studies to reach a definitive conclusion.
It would also be interesting to determine whether up-regulation
of enolase-α might have a therapeutic role in tumors lacking the
molecule.

ACKNOWLEDGMENTS

REFERENCES

1. Ginsberg R. J., Vokes, E. E., and Rosenzweig, K. Non-small cell
lung cancer. *In:* V. T. DeVita, Jr., S. Hellman, and S. A. Rosenberg
(eds.), Cancer: Principles and Practice of Oncology, Ed. 6, pp. 925–983.
Philadelphia-New York: Lippincott-Raven, 2001.

2. Weinberg, R. A. Oncogenes, anti-oncogenes, and the molecular basis
of multistep carcinogenesis. Cancer Res., *49:* 3713–3721, 1989.

3. Marcu, K. B., Bossone, S. A., and Patel, A. J. *myc* function and
regulation. Annu. Rev. Biochem., *61:* 809–860, 1992.

4. Potter, M., and Marcu, K. B. The *c-myc* story: where we've been,
where we seem to be going. Curr. Topics. Microbiol. Immunol., *224:*
1–17, 1997.

5. Dalla-Favera, R., and Gaidano, G. Molecular pathogenesis of T-cell
non-Hodgkin's lymphomas. *In:* V. T. DeVita, Jr., S. Hellman, and S. A.
Rosenberg (eds.), Cancer, Principles and Practice of Oncology, Ed. 6,
pp. 2228–2230. Philadelphia-New York: Lippincott-Raven, 2001.

6. Ray, R., and Miller, D. M. Cloning and characterization of a human
c-myc promoter-binding protein. Mol. Cell. Biol., *11:* 2154–2161, 1991.

7. Ray, R. B. Induction of cell death in murine fibroblasts by a *c-myc*
promoter binding protein. Cell Growth Differ., *6:* 1089–1096, 1995.

8. Ghosh, A. K., Steele, R., and Ray, R. B. Functional domain of *c-myc*
promoter binding protein-1 involved in transcriptional repression and
cell growth regulation. Mol. Cell. Biol., 2880–2886, 1999.

9. Chaudhary, D., and Miller, D. M. The *c-myc* promoter binding
protein (MBP-1) and TBP bind simultaneously in the minor groove of
the *c-myc* P2 promoter. Biochem., *34:* 3438–3445, 1995.

10. Subramanian, A., and Miller, D. M. Structural analysis of α-
enolase: mapping the functional domains involved in down-regulation
of the *c-myc* proto-oncogene. J. Biol. Chem., *275:* 5958–5965, 2000.

11. Feo, S., Arcuri, D., Piddini, E., Passotino, R., and Giallonogo, C.
ENO-1 gene product binds to the *c-myc* promoter and acts as transcrip-
tional repressor. FEBS Lett., *473:* 47–52, 2000.

12. Harris, R. A. Carbohydrate metabolism 1: major metabolic path-
ways and their control. *In:* T. M. Devlin (ed.), Textbook of Biochem-
istry with Clinical Correlations, Ed. 5, pp. 597–664. New York: Wiley-
Liss, 2002.

13. Deloulme, J. C., Helies, A., Ledig, M., Lucas, M., and Sensenbren-
ner, M. A comparative study of the distribution of α- and γ–enolase
subunit in cultured rat neural cells and fibroblasts. Int. J. Dev. Neurosci.,
15: 183–194, 1997.

14. Sensenbrenner, M., Lucas, M., and Deloume, J. C. Expression of
two neuronal markers, growth-associated protein 43 and neuron-specific
enolase, in rat glial cells. J. Mol. Med., *75:* 653–663, 1997.

15. Ida, H., and Yahara, I. Durable synthesis of high molecular weight
heat shock proteins in G_0 cells of the yeast and other eucaryotes. J. Cell
Biol., *99:* 199–207, 1984.

16. Sundrom, P., and Aliaga, G. R. Molecular cloning of cDNA and
analysis of protein secondary structure of *Candida albicans* enolase, an
abundant, immunodominant glycolytic enzyme. J. Bacteriol., *174:*
6789–6799, 1992.

17. Bisseret, F., Keith, G., Rihn, B., Amiri, I., Werneburg, B., Girardot,
R., Baldacini, O., Green, G., Nguyen, V. K., and Monteil, H. *Clostrid-
ium difficile* toxin B: characterization and sequence of three peptides.
J. Chromatogr., *490:* 91–100, 1989.

18. Johnstone, S. A., Waisman, D. M., and Rattner, J. B. Enolase is
present at the centrosome of HeLa cells. Exp. Cell Res., *202:* 458–463,
1992.

19. Moscato, S., Pratesi, F., Sabbatini, A., Chimenti, D., Scavuzzo, M.,
Passatino, R., Bombardieri, S., Giallongo, A., and Migliorini, P. Surface
expression of a glycolytic enzyme, α-enolase, recognized by autoanti-
bodies in connective tissue disorders. Eur. J. Immunol., *30:* 3575–3584,
2000.

20. Redlitz, A., Fowler, B. J., Plow, E. F., and Miles, L. A. The role of
an enolase-related molecule in plasminogen binding to cells. Eur. J. Bio-
chem., *227:* 407–415, 1995.

21. Weith, A., Brodeur, G. M., Bruns, G. A., Matise, T. C., Mischke,
D., Nizetic, D., Seldin, M. F., van Roy, N., and Vance, J. Report of the
second international workshop on human chromosome 1 mapping 1995.
Cytogenet. Cell Genet., *72:* 114–144, 1996.

Lack of Interleukin-10 Expression Could Predict Poor Outcome in Patients with Stage I Non-Small Cell Lung Cancer[1]

Jean-Charles Soria, Chulso Moon,
Bonnie L. Kemp, Diane D. Liu, Lei Feng,
Ximing Tang, Yoon-Soo Chang, Li Mao, and
Fadlo R. Khuri[2]

Departments of Thoracic/Head and Neck Medical Oncology [J.-C. S.,
C. M., X. T., Y-S. C., L. M.], Pathology [B. L. K.], and Biostatistics
[D. D. L., L. F.], The University of Texas M. D. Anderson Cancer
Center, Houston, Texas 77030, and Winship Cancer Institute, Emory
University, Atlanta, Georgia 30322 [F. R. K.]

ABSTRACT

Purpose: Interleukin-10 (IL-10) may play an important role in controlling tumor growth and metastasis. Some reports have shown that IL-10 can be a potent inhibitor of tumor growth, but others suggest that IL-10 expression by the tumor is an adverse prognostic factor. Because normal bronchial epithelial cells constitutively produce IL-10, we decided to test the prognostic value of IL-10 in a well-defined population of patients with stage I non-small cell lung cancer (NSCLC) treated in a single institution.

Patients and Methods: Using immunohistochemical analysis, we retrospectively analyzed IL-10 expression in specimens from 138 patients with completely resected clinical/radiographic stage I NSCLC for whom clinical follow-up data were available.

Results: IL-10 expression was retained (IL-10 labeling index ≥ 10%) in 94 patients (68.1%) and lost in 44 patients (31.9%). The duration of overall, disease-specific, and disease-free survival in the 44 patients lacking IL-10 expression was worse than in the 94 patients with IL-10 expression ($P = 0.08$, 0.02, and 0.05, respectively; Log-rank test). Interestingly, IL-10 expression was observed more frequently in tumors with squamous cell histology than in tumors of other histological subtypes ($P = 0.04$; χ^2 test). Multivariate analysis confirmed the independent prognostic value of IL-10 expression for disease-specific survival ($P = 0.04$).

Conclusion: Lack of IL-10 expression by the tumor was associated with a significantly worse outcome of early stage NSCLC. The mechanisms underlying this clinically and biologically important finding need to be further explored.

INTRODUCTION

Lung cancer is a major cause of mortality worldwide. Last year, in the United States alone, an estimated 169,400 new cases of lung cancer were diagnosed, and an estimated 154,900 deaths from lung cancer occurred (1). Improving the survival rate of patients with this disease requires a better understanding of tumor biology and the subsequent development of novel therapeutic strategies. One area of intense lung cancer research has been in assessing the prognostic factors of NSCLC,[3] focusing on stage I disease and molecular factors (2–5). This avenue of investigation may lead to the identification of patients with the highest risk stage I NSCLC or of those who are most likely to benefit from adjuvant or chemopreventive approaches.

IL-10 is thought to play a potential pathogenic or therapeutic role in a number of human conditions, such as inflammation, autoimmunity, and cancer (6). The immunomodulatory effects of IL-10 have yielded mixed results in various tumor systems. On one hand, because many tumor types express IL-10, its role in helping tumors evade immunosurveillance has been suggested (7, 8). IL-10 inhibits the tumoricidal capacity of macrophages and the cytotoxicity and cytokine production of tumor-specific T cells and blocks the presentation of tumor antigens by antigen-presenting cells (9, 10). On the other hand, *in vivo* studies in different animal models have demonstrated that IL-10 is a potent inhibitor of tumor growth and metastasis (11–14). Additionally, systemic administration of IL-10 has inhibited tumor metastasis and stimulated antitumor immune responses in murine models (15). Nevertheless, recent data generated by analyzing human lung tissue samples suggest that IL-10 produced by NSCLC is a predictor of poor outcome (16).

Because IL-10 is constitutively expressed in normal bronchial epithelial cells, we hypothesized that loss of IL-10 expression by lung tumors might be a prognostic factor for survival. Therefore, we decided to analyze the prognostic value of IL-10 expression in a homogeneous population of 138 patients with stage I NSCLC.

PATIENTS AND METHODS

Study Population. A total of 595 consecutive patients with stage I NSCLC underwent definitive surgical resection, defined as a lobectomy or a pneumonectomy, from 1975 to 1990

[3] The abbreviations used are: NSCLC, non-small cell lung cancer; SCC, squamous cell carcinoma; TNM, Tumor-Node-Metastasis; CI, confidence interval; IL, interleukin; TIMP, tissue inhibitor of metalloprotease; NK, natural killer; MMP, matrix metalloprotease.

Table 1 IL-10 status in stage I NSCLC tumors according to clinicopathological features of patients

| | No. of patients (n = 138) | IL-10 expression | | P |
		Positive (n = 94)	Negative (n = 44)	
Age: median (range)	64 (37–82)	64 (37–82)	65 (45–76)	0.28
Sex				
Male	106	68	38	0.07
Female	32	26	6	
Race				
Caucasian	120	84	36	0.22
Other	18	10	8	
Smoker				
Yes	119	79	40	0.27[a]
No	9	8	1	
Unknown	10	7	3	
Histology of tumors				
SCC	58	45	13	0.04
Adenocarcinoma and others	80	49	31	
TNM stage				
$T_1N_0M_0$	65	44	21	0.92
$T_2N_0M_0$	73	50	23	
5-year overall survival rate	51.5%	56.6%	40.9%	
(95% CI)	(43.8%, 60.6%)	(47.3%, 67.7%)	(28.7%, 58.4%)	

[a] P calculated comparing smoking vs. nonsmoking patients.

at The University of Texas M. D. Anderson Cancer Center. We retrospectively examined 138 cases for which both tissue samples and a median follow-up period of >5 years were available at the time of this study. The patient population was identified through a search of the Tumor Registry database maintained by the Department of Medical Informatics at The University of Texas M. D. Anderson Cancer Center. Survival status was verified and updated from Tumor Registry records as of December 1, 2000.

The study population consisted of 106 men and 32 women; 120 patients were Caucasian, and 18 patients were of other ethnicities (Table 1). The mean age of patients at surgery was 63 years. Histological subtypes included 58 cases of SCC, 60 cases of adenocarcinoma, 10 cases of bronchioalveolar carcinoma, 5 cases of large cell carcinoma, 3 cases of adenosquamous carcinoma, and 2 cases unclassified.

Immunohistochemical Staining for IL-10 Protein. All available tissue blocks from each patient were reviewed for the presence of tumor by a thoracic pathologist (B. L. K.). Paraffin-embedded, 4-μm-thick tissue sections from all 154 primary tumors were stained for IL-10 protein using a primary goat polyclonal antihuman IL-10 antibody (AF-217-NA; R&D Systems, Minneapolis, MN). Slides were deparaffinized through a series of xylene baths. Rehydration was performed using graded alcohol. The sections were then immersed in methanol containing 0.3% hydrogen peroxidase for 20 min to block the endogenous peroxidase activity and incubated in 2.5% blocking serum to reduce nonspecific binding. Sections were incubated overnight at 4°C with primary anti-IL-10 antibody at a dilution of 1:75 (1.33 μg/ml). The sections were then processed using a standard avidin-biotin immunohistochemical assay according to the manufacturer's recommendations (Vector Laboratories, Bur-

lingame, CA). Diaminobenzidine was used as a chromogen, and commercial hematoxylin was used for counterstaining. Routinely processed tissue sections of normal lymph nodes and tonsils were used as positive staining controls and also stained with the primary antibody omitted to confirm staining specificity. Normal bronchial epithelial cells that constitutively produce IL-10 were also used as internal positive controls (17).

The IL-10 labeling index was defined as the percentage of tumor cells displaying cytoplasmic immunoreactivity and calculated by counting IL-10-stained tumor cells among ≥1000 tumor cells for each section. Representative areas of each tissue section were selected, and cells were counted in at least four fields (magnified 400 times) in these areas. On the basis of previous reports, if ≥10% of the tumor cells were positive for IL-10, the case was considered to be IL-10 positive (18, 19). Tumors with <10% of the cells stained were counted as negative. All slides were scored concomitantly by a pathologist (X. T.) and another investigator (J-C. S.). Immunohistochemical analysis was performed in a blinded manner with respect to clinical information about the subjects.

Statistical Analysis. Overall, disease-specific, and disease-free survival were analyzed in this study. Survival curves were estimated by the Kaplan-Meier method. The Log-rank test was used to compare patient's survival time between groups. The Fisher exact and χ^2 tests were used to analyze the association between two categorical variables. The Wilcoxon rank-sum test was used for differences in median of age. The Cox proportional hazards model was used for univariate analysis to evaluate the association between survival time and risk factors and for multivariate analysis to model the risks of IL-10 expression on survival time, with adjustment for clinical and histopathological parameters (age, sex, race, tumor histology,
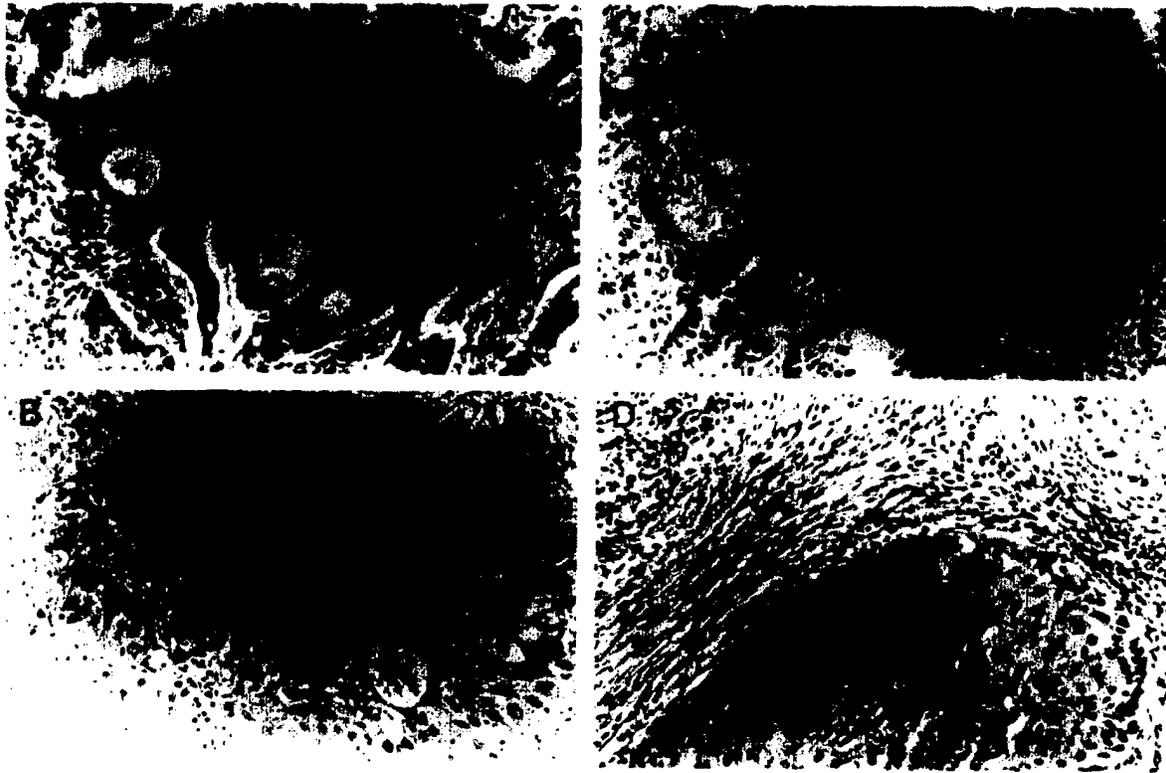
Fig. 1 Immunohistochemical staining patterns of IL-10 in stage I NSCLC. *A,* a well-differentiated adenocarcinoma with most cancer cells expressing IL-10 in the cytoplasm. *B,* a SCC with most carcinoma cells positive for IL-10. *C,* a bronchioalveolar carcinoma tumor with IL-10 expression. *D,* a SCC tumor negative for IL-10 expression (original magnification, ×400).

and tumor size). All statistical tests are two sided, and a $P < 0.05$ was considered to be statistically significant.

All survival curves were calculated from the date of surgery. Overall survival took all deaths (cancer related or not) into account. Disease-specific survival time was calculated from the date of surgery to death from cancer-related causes. Disease-free survival time was calculated from the date of surgery to relapse or death from cancer-related causes.

RESULTS

A total of 138 formalin-fixed, paraffin-embedded NSCLC tumor specimens was stained using a standard immunohisto-chemical technique reported previously for the identification of IL-10 expression (18, 19). The usual pattern of positive staining for IL-10 in NSCLC was cytoplasmic and not nuclear (Fig. 1, *A–C*). Even if tumors cells were negative for IL-10 staining, normal bronchial epithelial cells in the section were positive and used as an internal positive control of the staining for IL-10. In peribronchial gland cells or alveolar pneumocytes, IL-10 expression was not detectable. Lymphoid cells of tumor areas were occasionally immunostained. Only 20 of 138 samples displayed tumor-infiltrating lymphocytes, therefore hindering any relevant analysis of IL-10 production by infiltrating immune cells. In the positive control tissues (tonsil), the normal stratified squamous

epithelium displayed IL-10-positive cells. In the adjacent lymph nodes, IL-10-positive cells were localized predominantly in the germinal centers (data not shown). IL-10 immunohistochemical staining showed a wide heterogeneity from rare scattered cells to a homogeneous pattern for the vast majority of cells examined, suggesting that phenotypic heterogeneity is a major feature in NSCLC (Fig. 1).

IL-10 expression was observed in 94 (68.1%) of the 138 stage I NSCLC specimens. Lack of staining was observed in 44 tumors (31.9%). Table 1 shows the relationships between the expression of IL-10 and clinicopathological factors. There were no statistically significant differences in TNM stage, sex, smoking status, age, and race between the groups with IL-10-positive and -negative staining. Interestingly, IL-10 expression was more prevalent in the SCC subtype than it was in other histological subtypes. Forty-five (77.6%) of the 58 cases of SCC exhibited IL-10 expression, whereas 49 (61.3%) of 80 patients with non-SCC tumors (mainly adenocarcinoma) showed IL-10 expression ($P = 0.04$; χ^2 test).

We subsequently analyzed the relationship between IL-10 expression and length of survival. The median follow-up time for the patient population was 10.6 years. Fig. 2*A* shows the Kaplan-Meier overall survival curves for patients whose tumors were IL-10 positive and negative. Patients with tumors that were
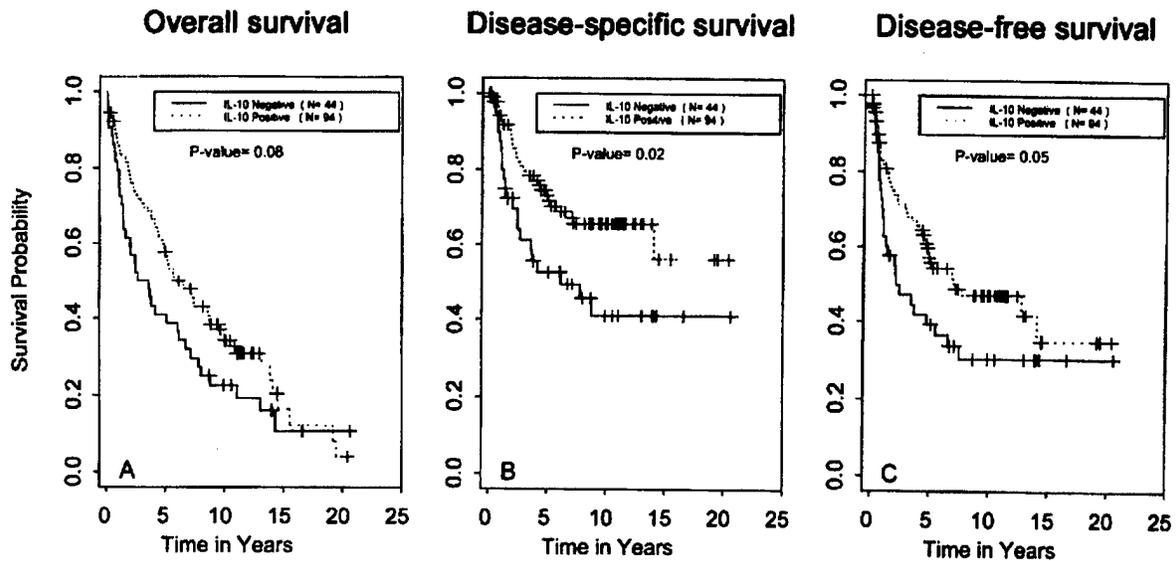
Overall survival   Disease-specific survival   Disease-free survival

Fig. 2 Survival curves of patients with IL-10-positive and -negative NSCLC. The patients lacking IL-10 expression (*solid line, n* = 44) had worst outcomes than the patients with IL-10 expression (*broken line, n* = 94) for overall (*A*), disease-specific (*B*), and disease-free survival (*C*).

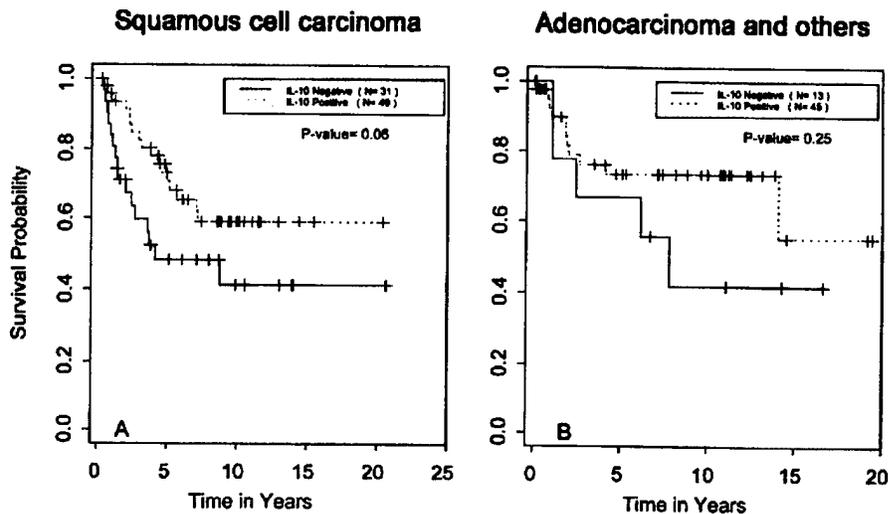## Squamous cell carcinoma   Adenocarcinoma and others

Fig. 3 *A*, disease-specific survival curve of patients with stage I SCC according to IL-10 expression; *B*, disease-specific survival curve of patients with adenocarcinoma or other histological subtypes according to IL-10 expression.

IL-10 negative had a shorter survival time than did patients with tumors that were IL-10 positive (P = 0.08; Log-rank test). Five-year overall survival rate for patients whose tumors were IL-10 positive was 56.6% (95% CI = 47.3–67.7%) and 40.9% (95% CI = 28.7–58.4%) for patients whose tumors were IL-10 negative (Table 1). Fig. 2*B* shows that patients with negative IL-10 expression had significantly shorter disease-specific survival times than did patients with positive IL-10 expression (P = 0.02; Log-rank test). A comparison of disease-free survival curves in IL-10-negative and -positive patients yielded similar results (P = 0.05; Log-rank test; Fig. 2*C*). The prognostic significance of IL-10 expression on disease-specific survival

was further explored in each major histological subtype. IL-10 negativity was a borderline significant adverse prognostic factor among patients with non-SCC tumors (P = 0.06; Log-rank test; Fig. 3*A*). A similar trend was observed for patients with SCC of the lung, but this trend was not significant (P = 0.25; Log-rank test; Fig. 3*B*). Univariate Cox proportional hazards model was used to evaluate the association between IL-10, clinicopathological variables (age, sex, race, histological subtype, and TNM), and survival time. Table 2 shows the results on disease-specific survival. In multivariate Cox proportional hazards model, among all clinicopathological variables, IL-10 expression was the only significant independent prognostic indicator

Table 2 Univariate and multivariate Cox proportional hazards model on disease-specific survival

	Univariate			Multivariate		
	Hazard ratio	95% CI	*P*	Hazard ratio	95% CI	*P*
Age	1.0	0.97–1.03	0.92			
Sex (Male or female)	0.88	0.48–1.64	0.69			
Race (Caucasian or other)	0.49	0.25–0.99	0.047	0.58	0.28–1.2	0.13
Histological subtype (SCC or other)	0.72	0.39–1.30	0.27			
Tumor size (T1 or T2)	0.73	0.42–1.28	0.28			
IL-10 (+ or −)[a]	0.51	0.29–0.89	0.02	0.55	0.31–0.98	0.04

[a] +, IL-10 labeling index $\geq$ 10%; −, IL-10 labeling index < 10%.

for disease-specific survival. The hazard of cancer death for patients whose tumor was IL-10 positive was only 55% of the hazard for patients whose tumor was IL-10 negative ($P = 0.04$, Cox model).

DISCUSSION

Human lung cancer displays an extremely aggressive clinical course and represents the leading cause of malignancy-related mortality in the United States (1). This behavior may reflect an increased capacity to evade detection and containment by host immune response. Because IL-10 demonstrates *in vitro* immunosuppressive activities (9, 10), some groups have hypothesized that IL-10 production by cancer cells may help the tumor evade immunosurveillance (7, 8). Nevertheless, IL-10 is also able to inhibit tumor growth and metastasis in various tumor models (11–14). These conflicting results imply that it is all about "fine tuning" in case of IL-10-mediated immunosuppression or immunostimulation. Because normal bronchial epithelial cells constitutively express IL-10 (17), loss of IL-10 expression by lung cancer cells would represent a specific change in the tumor as compared with its normal epithelial counterpart. In the present study, we explored the prognostic value of IL-10 expression by lung cancer cells in a large and homogeneous population of 138 completely resected clinical/radiographic stage I NSCLC for whom a median follow-up of 10.6 years was available. We have demonstrated that IL-10 is retained in a significant percentage of stage I NSCLCs. Overall, 94 (68.1%) of 138 tumors expressed IL-10 in $\geq$10% tumor cells, whereas loss of IL-10 expression was observed in 44 patients (31.9%). Our data show that lack of IL-10 expression is a poor prognostic factor in patients with stage I NSCLC. The poor prognostic value of lack of IL-10 expression was observed for disease-specific and -free survival, with a trend for overall survival. Furthermore, multivariate analysis confirmed the independent prognostic value of lack of IL-10 expression. The prognostic value of IL-10 was retained even when we changed the cutoff level of positivity from 10% (18) to 5 or 15%. Our results are in contrast to a previous report by Hatanaka *et al.* (16), who suggested that IL-10 expression by the tumor was an indicator of poor prognosis. We have analyzed IL-10's prognostic value in a large and homogeneous population of patients with early stage lung cancer ($n = 138$), whereas Hatanaka *et al.* performed their analysis using a smaller and more heterogeneous population that included 82 patients with stage I–IIIb disease. Furthermore, the fact that all of the patients in our study were treated at a single institution and received lengthy follow-up care after

surgery helps to increase the credibility of our survival analysis. Finally, Hatanake *et al.* (16) evaluated IL-10 expression by RT-PCR as opposed to immunohistochemistry in this study. Thus, our different results may be related in part to differences in patient population and the technique used to evaluate IL-10 expression. Indeed, we evaluated IL-10 expression at the protein level as compared with the mRNA level for Hatanake *et al.* Furthermore, both studies were retrospectively conducted and therefore potentially subject to some degree of selection bias.

We have analyzed IL-10 expression by performing immunohistochemical analysis with a polyclonal antihuman IL-10 antibody reported previously (18, 19). Other anti-IL-10 antibodies have also been used to evaluate IL-10 expression in paraffin-embedded tissue sections (17, 20). A good concordance between reverse transcription-PCR analysis and immunohistochemical analysis for IL-10 has been suggested in different reports (7, 17). We have used internal and external positive controls to assess the specificity of the staining. We found that even if tumor cells were negative for IL-10 staining, normal bronchial epithelial cells in the section (when present) were positive (17), thus ruling out a false negative result.

Although the mechanisms underlying the current data are not clear, there are several potential explanations for the poor outcome of patients with IL-10-negative tumors. Several laboratories have demonstrated that IL-10 is a potent inhibitor of tumor growth and metastasis in multiple animal models and tumor types, including melanoma, breast and prostate cancers, and Burkitt's lymphoma (11, 13, 20, 21). *In vivo*, the effects of IL-10 may be multifold. They can be related to direct inhibition of IL-10 on the angiogenic process *per se* or indirectly by affecting the angiogenic capacity or signals from tumor and/or tumor-infiltrating cells. Compelling evidence indicates that the antiangiogenic effect of IL-10 results from the inhibition of angiogenic factor release and production by the tumor and/or stromal cells. IL-10 induces production of TIMP-1, an inhibitor of angiogenesis, and inhibits MMP-2 and MMP-9 secretion by cancer cell lines, blocking the induction of microvessel formation *in vitro* (20, 22). It has also been suggested that IL-10 can directly inhibit endothelial cell response to angiogenic factors (21). Moreover, in murine mammary tumors, the antimetastatic and antitumor activity resulting from IL-10 gene transfer is related to enhanced production of nitric oxide (23).

One of the major roles of IL-10 in the regulation of immune responses involves its deactivating effect on macrophages (6). From the many cells and cell products within a tumor that serve as inducers or modulators of angiogenesis, macrophages

have emerged as a major component. IL-10 secreted by the tumor cells may prevent the migration of macrophages from the periphery into the tumor tissue, thus preventing macrophage infiltration (24). IL-10 also inhibits the expression of angiogenic factors (vascular endothelial growth factor, IL-1β, tumor necrosis factor-α, IL-6, and MMP-9) in tumor-associated macrophages (25). These changes correlate with decreased neovascularization of the tumors. Alternatively, the inhibitory effect of IL-10 on tumor metastasis has been suggested to be mediated through a NK cell-dependent mechanism (6, 12). IL-10 is able to affect the activities of NK cells, and NK cells were recently shown to contribute to the antiangiogenic effects of IL-12 through the killing of endothelial cells (26).

The observation that IL-10 expression differs among histological subtypes highlights the biological differences among different subtypes of NSCLC. Different abnormalities in oncogenes and tumor suppressor genes among histological subtypes of NSCLC are well known. Indeed, K-*ras* mutations are much more common in adenocarcinomas than in SCCs, whereas cyclin B1 overexpression or the *p53* mutant immunophenotype is more frequent in SCCs than in adenocarcinoma (2, 27, 28).

In conclusion, we found that a lack of IL-10 expression is a prognostic factor of poor outcome in stage I NSCLC. This result may be explained by the antitumor effects of IL-10, which contrast with the immunomodulatory effects that this cytokine displays *in vitro*. The mechanisms behind IL-10 antitumor effects might include inhibition of angiogenesis, stimulation of TIMPs, inhibition of MMP secretion, and inhibition of macrophage activity (20–25). Nevertheless, this result needs to be interpreted with caution because of potential limitations in the present study: (*a*) IL-10 production by tumor-infiltrating lymphocytes was not addressed because only a small fraction of our tissue samples displayed immune infiltrating cells; and (*b*) the role of IL-10 in cancer progression or regression might be very different according to the level of cytokine produced by the tumor and infiltrating immune cells. Additional studies are clearly required to confirm the present data and resolve the role of IL-10 in tumor growth and metastasis. We plan to conduct additional studies that will help in assessing the clinical importance of the present IL-10 findings and in understanding their possible mechanisms. These studies will be conducted using resected tissue from patients with stage I NSCLC, analyze the expression of MMPs and TIMPs, microvessel density, and the presence of tumor-infiltrating lymphocytes and their phenotype, and relate these factors to IL-10 expression by the tumor and to overall prognosis.

ACKNOWLEDGMENTS

REFERENCES

1. Jemal, A., Thomas, A., Murray, T., and Thun, M. Cancer statistics, 2002. CA Cancer J. Clin., *52:* 23–47, 2002.

2. Soria, J. C., Jang, S. J., Khuri, F. R., Hassan, K., Liu, D., Hong, W. K., and Mao, L. Overexpression of cyclin B1 in early-stage non-small cell lung cancer and its clinical implication. Cancer Res., *60:* 4000–4004, 2000.

3. Zhou, X., Kemp, B. L., Khuri, F. R., Liu, D., Lee, J. J., Wu, W., Hong, W. K., and Mao, L. Prognostic implication of microsatellite alteration profiles in early-stage non-small cell lung cancer. Clin. Cancer Res., *6:* 559–565, 2000.

4. Khuri, F. R., Lotan, R., Kemp, B. L., Lippman, S. M., Wu, H., Feng, L., Lee, J. J., Cooksley, C. S., Parr, B., Chang, E., Walsh, G. L., Lee, J. S., Hong, W. K., and Xu, X. C. Retinoic acid receptor-beta as a prognostic indicator in stage I non-small cell lung cancer. J. Clin. Oncol., *18:* 2798–2804, 2000.

5. Khuri, F. R., Wu, H., Lee, J. J., Kemp, B. L., Lotan, R., Lippman, S. M., Feng, L., Hong, W. K., and Xu, X. C. Cyclooxygenase-2 overexpression is a marker of poor prognosis in stage I non-small cell lung cancer. Clin. Cancer Res., *7:* 861–867, 2001.

6. Howard, M., and O'Garra, A. Biological properties of interleukin 10. Immunol. Today, *13:* 198–200, 1992.

7. Smith, D. R., Kunkel, S. L., Burdick, M. D., Wilke, C. A., Orringer, M. B., Whyte, R. I., and Strieter, R. M. Production of interleukin-10 by human bronchogenic carcinoma. Am. J. Pathol., *145:* 18–25, 1994.

8. Young, M. R., Wright, M. A., Lozano, Y., Matthews, J. P., Benefield, J., and Prechel, M. M. Mechanisms of immune suppression in patients with head and neck cancer: influence on the immune infiltrate of the cancer. Int. J. Cancer, *67:* 333–338, 1996.

9. Rohrer, J. W., and Coggin, J. H. CD81 T cell clones inhibit antitumor T cell function by secreting IL-10. J. Immunol., *155:* 5719–5727, 1995.

10. Beissert, S., Hosoi, J., Grabbe, S., Asahina, A., and Granstein, R. D. IL-10 inhibits tumor antigen presentation by epidermal antigen presenting cells. J. Immunol., *154:* 1280–1286, 1995.

11. Kundu, N., Beaty, T. L., Jackson, M. J., and Fulton, A. M. Antimetastasic and antitumor activities of interleukin 10 in a murine model of breast cancer. J. Natl. Cancer Inst. (Bethesda), *88:* 536–541, 1996.

12. Zheng, L. M., Ojcius, D. M., Garaud, F., Roth, C., Maxwell, E., Li, Z., Rong, H., Chen, J., Wang, X. Y., Catino, J. J., and King I. Interleukin-10 inhibits tumor metastasis through an NK cell-dependent mechanism. J. Exp. Med., *184:* 579–584, 1996.

13. Huang, S., Xie, K., Bucana, C. D., Ullrich, S. E., and Bar-Eli, M. Interleukin 10 suppresses tumor growth and metastasis of human melanoma cells: potential inhibition of angiogenesis. Clin. Cancer Res., *2:* 1969–1979, 1996.

14. Giovarelli, M., Musiani, P., Modesti, A., Dellabona, P., Casorati, G., Allione, A., Consalvo, M., Cavallo, F., di Pierro, F., De Giovanni, C., Musso, T., and Forni, G. Local release of IL-10 by transfected mouse mammary adenocarcinoma cells does not suppress but enhances antitumor reaction and elicits a strong cytotoxic lymphocyte and antibody-dependent immune memory. J. Immunol., *155:* 3112–3123, 1995.

15. Berman, R. M., Susuki, T., Tahara, H., Robbins, P. D., Narula, S. K., and Lotze, M. T. Systemic administration of cellular IL-10 induces an effective, specific, and long-lived immune response against established tumors in mice. J. Immunol., *157:* 231–238, 1996.

16. Hatanaka, H., Abe, Y., Kamiya, T., Morino, F., Nagata, J., Tokunaga, T., Oshika, Y., Suemizu, H., Kijima, H., Tsuchida, T., Yamazaki, H., Inoue, H., Nakamura, M., and Ueyama, Y. Clinical implications of interleukin (IL)-10 induced by non-small cell lung cancer. Ann. Oncol., *11:* 815–819, 2000.

17. Bonfield, T. L., Konstan, M. W., Burfeind, P., Panuska, J. R., Hilliard, J. B., and Berger, M. Normal bronchial epithelial cells constitutively produce the anti-inflammatory cytokine interleukin-10, which is downregulated in cystic fibrosis. Am. J. Respir. Cell Mol. Biol., *13:* 257–261, 1995.

18. Huang, M., Wang, J., Lee, P., Sharma, S., Mao, J. T., Meissner, H., Uyemura, K., Modlin, R., Wollman, J., and Dubinett, S. M. Human non-small cell lung cancer cells express a type 2 cytokine pattern. Cancer Res., *55:* 3847–3853, 1995.

19. Fujieda, S., Lee, K., Sunaga, H., Tsuzuki, H., Ikawa, H., Fan, G. K., Imanaka, M., Takenaka, H., and Saito, H. Staining of interleukin-10 predicts clinical outcome in patients with nasopharyngeal carcinoma. Cancer, *85:* 1439–1445, 1999.

20. Stearns, M. E., Garcia, F. U., Fudge, K., Rhim, J., and Wang, M. Role of interleukin 10 and transforming growth factor β 1 in the angiogenesis and metastasis of prostate primary tumor lines from orthotopic implants in severe combined immunodeficiency mice. Clin. Cancer Res., 5: 711–720, 1999.

21. Cervenak, L., Morbidelli, L., Donati, D., Donnini, S., Kambayashi, T., Wilson, J. L., Axelson, H., Castanos-Velez, E., Ljunggren, H. G., Malefyt, R. D., Granger, H. J., Ziche, M., and Bejarano, M. T. Abolished angiogenicity and tumorigenicity of Burkitt lymphoma by interleukin-10. Blood, 96: 2568–2573, 2000.

22. Stearns, M. E., Fudge, K., Garcia, F., and Wang, M. IL-10 inhibition of human prostate PC-3 ML cell metastases in SCID mice: IL-10 stimulation of TIMP-1 and inhibition of MMP-2/MMP-9 expression. Invasion Metastasis, 17: 62–74, 1997.

23. Kundu, N., Dorsey, R., Jackson, M. J., Guiterrez, P., Wilson, K., Fu, S., Ramanujam, K., Thomas, E., and Fulton, A. M. Interleukin-10 gene transfer inhibits murine mammary tumors and elevates nitric oxide. Int. J. Cancer, 76: 713–719, 1998.

24. Richter, G., Kruger-Kasagakes, S., Hein, G., Huls, C., Schmitt, E., Diamantstein, T., and Blankenstein, T. Interleukin-10 transfected into Chinese hamster ovary cells prevents tumor growth and macrophage infiltration. Cancer Res., 53: 4134–4137, 1993.

25. Di Carlo, E., Coletti, A., Modesti, A., Giovarelli, M., Forni, G., and Musiani, P. Local release of interleukin-10 by transfected mouse adenocarcinoma cells exhibit pro- and anti-inflammatory activity and results in a delayed tumor rejection. Eur. Cytokine Netw., 9: 61–68, 1998.

26. Yao, L., Sagadari, C., Furuke, K., Bloom, E. T., Teruya-Feldstein, J., and Tosato, G. Contribution of natural killer cells to inhibition of angiogenesis by IL-12. Blood, 93: 1612–1621, 1999.

27. Rossell, R., Li, S., Skacel, Z., Mate, J. L., Maestre, J., Canela, M., Tolosa, M., Tolosa, E., Armengol, P., Barnadas, A., and Ariza, A. Prognostic impact of mutated K-ras gene in surgically resected non-small cell lung cancer patients. Oncogene, 8: 2407–2412, 1993

28. Kishimoto, Y., Murakami, Y., Shiraishi, M., Hayashi, K., and Sekiya, T. Aberrations of the p53 tumor suppressor gene in human non-small cell carcinomas of the lung. Cancer Res., 52: 4799–4804, 1992.

Association of a functional tandem repeats in the downstream of human telomerase gene and lung cancer

Luo Wang[1], Jean-Charles Soria[1], Yoon-Soo Chang[1], Ho-Young Lee[1], Qingyi Wei[2] and Li Mao*[1]

[1]Department of Thoracic/Head and Neck Medical Oncology, The University of Texas MD Anderson Cancer Center, Houston, TX 77030, USA; [2]Department of Epidemiology, The University of Texas MD Anderson Cancer Center, Houston, TX 77030, USA

Chemoprevention has been widely explored as a promising strategy for controlling the incidence of lung cancer, the leading cause of cancer-related death. To maximize the benefit of lung cancer chemoprevention, it is important to identify individuals at high risk for the disease. The genetic background has been shown to play an important role in one's risk of developing lung cancer. We report here the identification of a polymorphic tandem repeats minisatellite (termed MNS16A) in the downstream region of the human telomerase gene. This minisatellite is located upstream of an antisense transcript from the human telomerase gene locus and was demonstrated to have promoter activity. The promoter activity was significantly lower in the construct containing the shorter repeats, suggesting that the MNS16A variant may have a relevance of functionality. To explore the role of this novel polymorphism in lung cancer, we conducted a pilot hospital-based case–control study by identifying the MNS16A genotype with genomic DNA from 53 lung cancer patients and 72 cancer-free controls. We found four different alleles and classified them as shorter (S) or longer (L) on the functional basis of the length of the repeats in the controls. The MNS16A genotype distributions of the SS, SL, and LL genotypes were 11, 32, and 57%, respectively, in the cases, and 14, 40, and 46%, respectively, in the controls. Compared with the SS + SL genotype, the LL genotype was associated with greater than twofold increased risk of lung cancer (odds ratio = 2.18; 95% confidence interval = 0.92, 5.20) after adjustment for age, sex, ethnicity, and smoking status, suggesting a potential role of MNS16A in lung cancer susceptibility. Larger studies are needed to verify our findings.
Oncogene (2003) 22, 7123–7129. doi:10.1038/sj.onc.1206852

Keywords: minisatellite; tandem repeats; VNTR; hTERT; lung cancer

Introduction

Lung cancer is the leading cause of cancer-related death for both men and women in the United States (ACS, 2003). Despite improvements in diagnosis and therapy, the overall survival of patients with lung cancer remains dismal (Parkin et al., 1999). One of the promising approaches to the prevention of lung cancer is the use of chemopreventive agents. Since preventive treatment may be long term and because the agents used may have certain side effects, it is important to limit chemopreventive treatment to those individuals at high risk of developing lung cancer.

Tobacco smoking is the most important etiologic factor in lung cancer development. However, less than 15% of heavy smokers are expected to develop lung cancer in their lifetime, suggesting the presence of other factors important for the development of the disease. An individual's genetic variation has been shown to play an important role in one's susceptibility to lung cancer. For instance, polymorphism in genes involving detoxification enzymes (Bouchardy et al., 2001) and DNA repairs (Goode et al., 2002) has been shown to play a role in susceptibility to lung cancer. In a recent study, we found that a C/T polymorphism in the promoter region of a novel cytosine DNA-methyltransferase 3B6 is associated with the risk of lung cancer development (Shen et al., 2002), suggesting that the role of polymorphisms in many other genes involved in carcinogenesis of lung cancer needs to be explored.

Human telomerase (hTERT) gene is located to chromosome 5p15.33 and encodes a ribonucleoprotein enzyme that extends chromosome ends that have been shortened during successive cycles of cell division (Greider and Blackburn, 1985). Telomerase is composed of an RNA component, a catalytic protein subunit, and other telomerase-associated proteins whose functions remain to be established (Feng et al., 1995). Telomerase is expressed in the vast majority of human malignant cell lines and tumors, but not in the corresponding benign tissues (Dhaene et al., 2000). Studies of human tumors and human tumor cell lines have shown that telomerase activation plays a critical role in tumorigenesis, including lung tumorigenesis, by sustaining cellular immortality (Kim et al., 1994; Hiyama et al., 1995; Albanell et al., 1997). Overexpression of the RNA component of human telomerase has been observed at a very early

*Correspondence: L Mao, Department of Thoracic/Head and Neck Medical Oncology, The University of Texas MD Anderson Cancer Center, Box 432, 1515 Holcombe Boulevard, Houston, TX 77030, USA; E-mail: lmao@mdanderson.org

stage in the pathogenesis of nonsmall-cell lung cancer (NSCLC) (Yashima et al., 1997). However, such expression is not limited to the cells that harbor telomerase activity. By contrast, expression of hTERT is more closely associated with telomerase activity (Meyerson et al., 1997; Nakamura et al., 1997). In our previous studies, we demonstrated that hTERT expression occurred early in lung carcinogenesis and was associated with a poorer clinical outcome in patients with early-stage NSCLC (Soria et al., 2001; Wang et al., 2002). Interestingly, during these studies, we noticed the presence of an antisense transcript signal detected by in situ hybridization in cells expressing hTERT, suggesting the existence of an antisense hTERT mRNA, which might play a role in regulation of hTERT expression. To identify genetic variation in hTERT that may participate in the regulation of hTERT expression, we sequenced this locus and found a novel polymorphic tandem repeats minisatellite, termed MNS16A, in the downstream region of the hTERT gene locus. The region containing MNS16A was demonstrated to have a promoter activity that was influenced by the length of the MNS16A tandem repeats, suggesting a potential role of this minisatellite in regulating expression of the antisense hTERT mRNA. In this study, we also provided preliminary evidence of a possible association between MNS16A variable number of tandem repeats (VNTR) and risk of lung cancer.

Results

hTERT clusters with minisatellites and microsatellites, including a unique functional tandem repeats minisatellite in the downstream region of the gene

The hTERT gene is located at chromosome 5p15.33 and has 16 exons (Wick et al., 1999; Bryce et al., 2000). Analysing the genomic sequence published in GenBank (Accession numbers AY007685), we found that the gene contains many minisatellites and microsatellites, which divide the gene into four exon clusters (Figure 1). All the seven reported major conserved motifs of the telomerase subunit (Xiong and Eickbush, 1990) are located in the second and third clusters. The fourth cluster contains exons 13–16; however, it is further divided by minisatellites or microsatellites (Figure 1). Interestingly, during our earlier studies in which we used in situ hybridization to evaluate hTERT mRNA expression as a biomarker in lung tumorigenesis and progression (Soria et al., 2001; Wang et al., 2002), we found that with single-strand sense RNA riboprobes specific to the antisense mRNA sequences of various hTERT exons, a strong positive signal could be detected in cells with active telomerase but not in cells of telomerase-negative alternative-lengthening-of-telomeres cell line KB319 (Figure 2). This finding suggested the presence of hTERT antisense sequences. Further study showed that the antisense RNA transcript was initiated at the downstream of hTERT gene and had two major starting points at nt
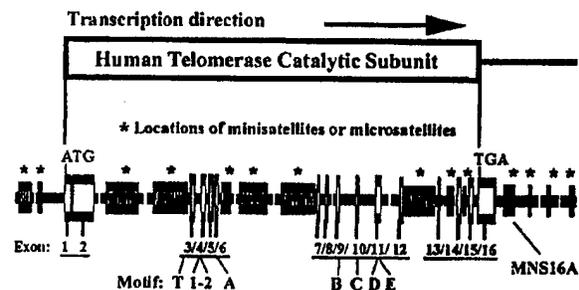
Chromosome location: 5p15.33

Figure 1 Genomic structure of the human telomerase gene (hTERT)

22156 and nt 22163 (GenBank AF128894), respectively (unpublished data).

In the study reported here, we found a unique tandem repeats sequence, which we termed MNS16A, in the putative promoter region of this antisense RNA transcript. This repeats sequence was a typical minisatellite with two different VNTR alleles in the cancer cell lines tested (Figure 3a). These two VNTR alleles were named as VNTR-302 and VNTR-243 on the basis of the PCR fragment size. The core sequence of MNS16A is a 23 bp tandem repeat of TCC TCT TAT CTC CCA GTC TCA TC or a 26 bp sequence with a CAT insertion. The VNTR-302 contains two 23 bp repeats and three 26 bp repeats, while the VNTR-243 contains one 23 bp repeat and two 26 bp repeats (Figure 3b). Interestingly, analysis with Transcription Element Search Software (TESS; URL: http://www.cbil.upenn.edu/tess) showed that the 26 bp tandem repeat with a CAT trinucleotide is a binding site for the transcription factor GATA-1, prompting us to investigate whether this tandem repeat plays a role in promoter activity.

The promoter activity of MNS16A depends on the length of the VNTR sequence size. Luciferase assay was performed to characterize the potential promoter activity of MNS16A (Figure 3c). We found that promoter activity was twice as strong with the pGL3-570(S) forward construct as it was with the pGL3-570(R) reverse construct, indicating the presence of a promoter in this region containing the MNS16A sequence. Promoter activity was much weaker with the pGL3-660(S) construct, which contains the VNTR-302, than with the pGL3-570(S) construct, which contains the VNTR-243. This suggested that promoter activity depended on the length of MNS16A VNTR and MNS16A functioned as a repressor for this promoter. This observation was further confirmed by using two additional constructs, pGL3-243 and pGL3-302, that contained only the tandem repeats VNTR-243 or VNTR-302 (data not shown). The structure of the core promoter that initiated the antisense transcript is illustrated in Figure 3d. It was interesting that the NSCLC cell line H460, which has a VNTR-302/243 genotype, showed a stronger antisense hTERT RNA

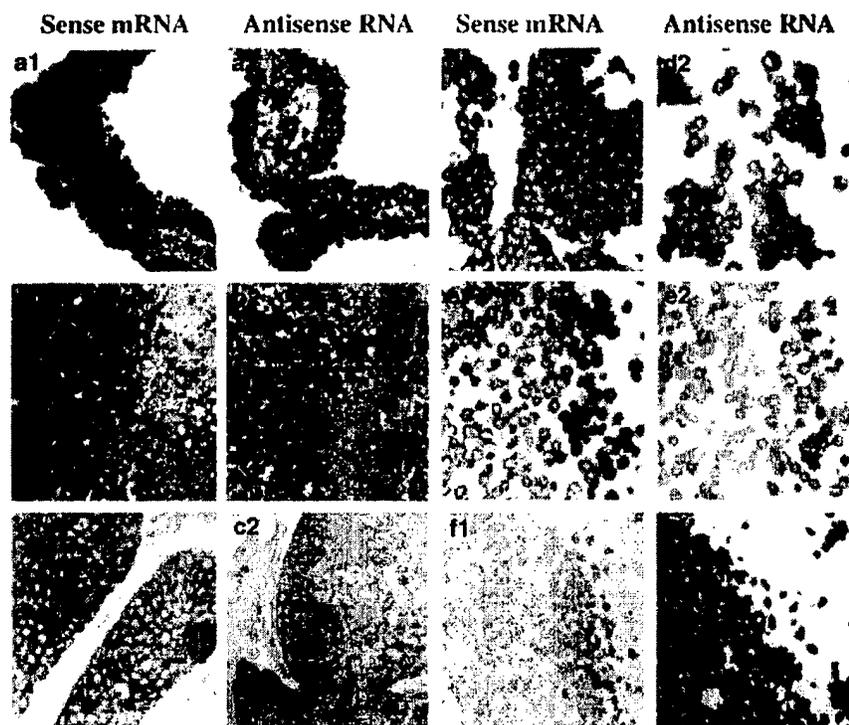Sense mRNA   Antisense RNA   Sense mRNA   Antisense RNA

Figure 2 Antisense *hTERT* RNA expression detected by *in situ* hybridization in primary lung cancers and lung cancer cell lines. The sense mRNAs were detected using the single-strand antisense riboprobe and the antisense RNAs were detected with the the sense riboprobe. (a) Bronchioalveolar carcinoma; (b) large-cell carcinoma; (c) squamous cell carcinoma; (d) lung cancer cell line A549; (e) lung cancer cell line H157; (f) telomerase-negative alternative-lengthening-of-telomeres cell line KB319

expression level and telomerase activity (Soria *et al.*, 2001) than cell lines H157 and SK-MES, which have a VNTR-302/302 genotype.

MNS16A polymorphic allele associated with lung cancer susceptibility. In addition to MNS16A VNTR-243 and VNTR-302 observed in the cancer cell lines (Figure 3a), two other rare alleles, VNTR-272 and VNTR-333, were also identified (data not shown). We classified the alleles VNTR-243 and VNTR-272 as short repeats (S allele), while VNTR-302 and VNTR-333 as long repeats (L allele). To explore the role of this novel polymorphism in lung cancer, we conducted a pilot hospital-based case–control study. The MNS16A genotype was determined with the genomic DNA from the tumor and blood samples of 53 lung cancer patients who were diagnosed with NSCLC and underwent surgery, and blood samples of 72 cancer-free controls who enrolled into our various clinical chemoprevention trials ($n = 57$) and who were seen at MD Anderson without clinical evidence of lung cancer ($N = 15$). For smoking status, 'ever smokers' were defined as those who smoked more than 100 cigarettes in their lifetime, of which they were 'former smokers' if they quit more than a year or 'current smokers' otherwise. Although there was no gender difference between the cases and controls, the cases (mean±s.d., 65.5±9.6 years) were younger than the controls (54.9±10.3 years), and there were more Caucasians and current smokers in the cases (41.5 and

96.2%, respectively) than in the controls (90.3 and 15.3%, respectively) (Table 1). These differences were adjusted for in the multivariate logistic regression analysis. We found four different alleles and classified them as shorter (S) or longer (L) on the functional basis of the length of the repeats in the controls. The MNS16A genotype distributions of the SS, SL, and LL genotypes were 11, 32, and 57%, respectively, in the cases, and 14, 40, and 46%, respectively, in the controls, which was not statistically different (Table 2). Compared with the SS + SL genotype, the LL genotype was associated with greater than twofold increased risk of lung cancer (odds ratio = 2.18; 95% confidence interval = 0.92, 5.20), after adjustment for age, sex, ethnicity, and smoking status (Table 2). These data suggest a potential role of MNS16A in lung cancer susceptibility. However, this pilot study was small and less than optimal; larger studies with a more rigorous study design and sufficient power are warranted to substantiate these findings.

Discussion

Minisatellite sequences are mutated at a high rate in germ cells (Jeffreys *et al.*, 1987) but are relatively stable in somatic cells (Jeffreys *et al.*, 1994), creating non-
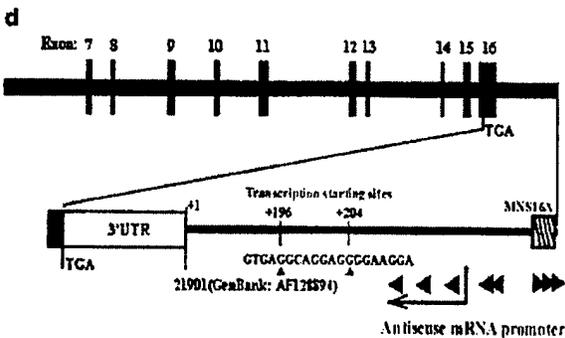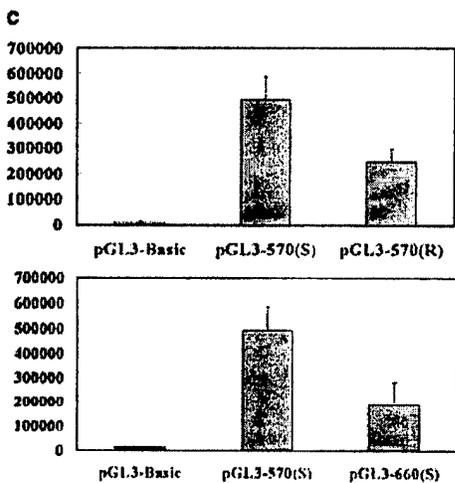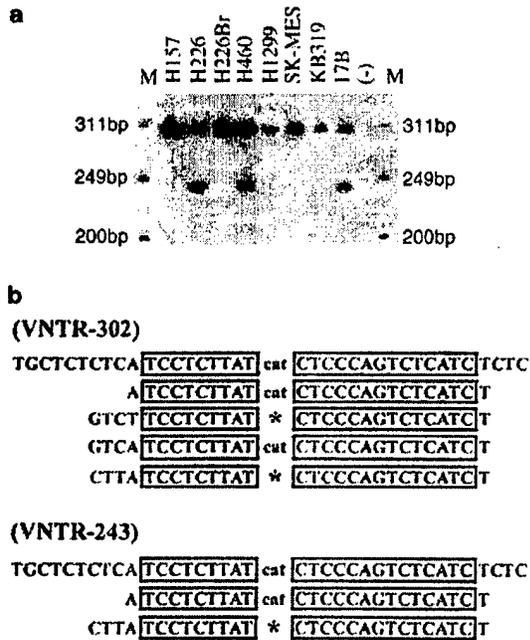
a

311bp — 311bp
249bp — 249bp
200bp — 200bp

M H157 H226 H226Br H460 H1299 SK-MES KB319 17B (-) M

b

(VNTR-302)

TGCTCTCTCA|TCCTCTTAT| cat |CTCCCAGTCTCATC|TCTC
A|TCCTCTTAT| cat |CTCCCAGTCTCATC|T
GTCT|TCCTCTTAT| * |CTCCCAGTCTCATC|T
GTCA|TCCTCTTAT| cat |CTCCCAGTCTCATC|T
CTTA|TCCTCTTAT| * |CTCCCAGTCTCATC|T

(VNTR-243)

TGCTCTCTCA|TCCTCTTAT| cat |CTCCCAGTCTCATC|TCTC
A|TCCTCTTAT| cat |CTCCCAGTCTCATC|T
CTTA|TCCTCTTAT| * |CTCCCAGTCTCATC|T

c

pGL3-Basic   pGL3-570(S)   pGL3-570(R)

pGL3-Basic   pGL3-570(S)   pGL3-660(S)

d

Exon: 7 8   9   10   11   12 13   14 15 16

TGA

Transcription starting sites
+1 +196 +204

3'UTR   MNS16A

TGA

GTGACGCACGAGGCGAAGGA
21901(GenBank: AF128391)

Antisense mRNA promoter

Figure 3 Genotypes of MNS16A, sequence, and function of MNS16A VNTR. M means DNA marker. (a) Genotype pattern of cancer cell lines; (b) sequences of 302 bp (L) allele and 243 bp (S) allele; (c) promoter activity of MNS16A VNTR measured by luciferase assay; (d) structure of the core promoter that initiated the antisense transcript

Table 1 Distribution of selected variables in lung cancer patients and cancer-free controls

Variable	Cases (n = 53)		Controls (n = 72)		P[a]
	No.	%	No.	%	
Age (years)					<0.001
<60	11	20.8	47	65.3	
≥60	42	79.2	25	34.7	
Sex					0.347
Male	31	58.5	36	50.0	
Female	22	41.5	36	50.0	
Ethnicity					0.204
Caucasians	51	96.2	65	90.3	
African-American	2	3.8	7	9.7	
Smoking status[b]					0.004
Never	7	13.2	12	16.7	
Former	24	45.3	49	68.0	
Current	22	41.5	11	15.3	

[a]Two-sided χ^2-test. [b]In all, 12 patients and three controls did not provide information on smoking

inherited individual variations. However, in cells transformed by γ-irradiation or genotoxic carcinogens, the frequencies of minisatellite mutations are increased compared to that in the corresponding nonmalignant immortalized cells (Paquette and Little, 1992; Honma *et al.*, 1994). Minisatellite mutations have also been found in various human tumors (Thein *et al.*, 1987; Matsumura and Tarin, 1992) and experimental animal tumors induced by chemical carcinogens (Ledwith *et al.*, 1990, 1995). Studies have shown high rearrangement frequencies in different types of cancers for two atypical minisatellites, the AT-rich ApoB locus and the VNTR locus D1S7, which have an atypically short repeat unit and may be susceptible to polymerase slippage (Hoff-Olsen *et al.*, 1995; Kaplanski *et al.*, 1997). Somatic mutations in the D1S7 locus have been found to be associated with microsatellite instability in human colorectal carcinomas (Kaplanski *et al.*, 1997). Minisatellite instability has also been demonstrated to exist in severe-combined-immunodeficiency fibroblasts, which have a mutation in the catalytic subunit of DNA-dependent protein kinase, suggesting that this subunit may be involved in the stable maintenance of minisatellite sequences in the genome (Imai *et al.*, 1997).

Single nucleotide polymorphism within genes or potential functional components of genes has been shown to be associated with susceptibility to various diseases, including lung cancer (Wei *et al.*, 2000; Spitz *et al.*, 2001). For instance, in our recent study on different genetic variants of DNA methyltransferase 3B,

Table 2 Logistic regression analysis of hTERT genotype in lung cancer patients and cancer-free controls

	Cases (n = 53)		Controls (n = 72)		P-value[a]	OR	(95% CI)[b]
	No.	%	No.	%			
hTERT genotype					0.492[c]		
SS	6	11.3	10	13.9		Ref.	
SL	17	32.1	29	40.3		1.82	(0.42–7.84)
LL	30	56.6	33	45.8		3.49	(0.82–14.8)
SS + SL	23	43.4	39	54.2		Ref.	(0.79–1.50)
LL	30	56.6	33	45.8	0.243[d]	2.18	(0.92–5.20)
L allele frequency	0.726		0.660		0.330[e]		

[a]Two-sided χ^2-test. [b]Adjusted for age, sex, ethnicity, and smoking status. [c]χ^2-test for genotype distribution between cases and controls. The P-value for the test for Hardy–Weinberg equilibrium ($q^2 + 2qp + p^2$, where $q =$ the L allele frequency) of the genotype in the controls was 0.825. [d]χ^2-test using the SS + SL as the reference. The power of this study to detect an OR greater than 2.18 is 0.566. [e]χ^2-test for the L allele frequency between cases and controls

we found that a functional C/T polymorphism in the promoter region could contribute to the risk of lung cancer development (Shen et al., 2002). However, the potential biological consequences of minisatellite polymorphism have not been well recognized. In the study reported here, we identified an antisense hTERT mRNA transcript and its promoter whose activity depended on the length of tandem repeats. To our knowledge, this is the first report of a novel controlling mechanism of gene regulation, which showed that a tandem repeat minisatellite functioned as a part of promoter. The strong presence of the antisense molecule in cancer cell KB319 lacking hTERT expression suggests that expression of the antisense molecule is independent of hTERT. Even if it was possible that the antisense hTERT RNA could act as an inhibitor of hTERT by reducing its transcription or blocking its translation (unpublished data), however, the natural biological function of this antisense mRNA remains unknown and needs further studies. Nevertheless, because activation of telomerase plays an important role in early lung carcinogenesis (Yashima et al., 1997) and is also associated with lung cancer progression (Wang et al., 2002), it is likely that the level of antisense mRNA may contribute to the development of lung cancer.

Szutorisz et al. (2001) identified two polymorphic minisatellites located in intron 2 and intron 6 of human telomerase gene. The polymorphic minisatellite in intron 2 was found to contain binding sites for c-Myc that has been shown to upregulate hTERT transcription. However, there were only minor variations and one deletion seen in the 38 colon carcinomas analysed, which led the authors to conclude that the size rearrangements of the hTERT minisatellites are not required for telomerase expression in colon carcinomas (Szutorisz et al., 2001). However, in a recent work, eight alleles of intron 6 VNTR and four alleles of intron 2 VNTR in hTERT gene locus were identified among 103 unrelated individuals, and in one patient with a kidney tumor, the VNTR in intron 6 was found to have undergone concomitant rearrangements, suggesting that chromosomal rearrangements of these VNTR may be associated with the activation of hTERT in cancer cells (Leem et al.,

2002). Consistent with the above reports, we also found rearrangement of the MNS16A VNTR in 11 primary lung tumors examined in our another study (data not shown). However, the association of the rearrangement with hTERT expression levels has not yet been determined because of the lack of reliable quantitative methods.

Our finding that patients with NSCLC have a higher frequency of the MNS16A LL genotype is important, because it supports the notion that the antisense hTERT mRNA has a biological function, which may be exerted through interference with hTERT levels. Our finding that minisatellite length influences promoter activity, together with the finding that minisatellite length was possibly related to lung cancer susceptibility, suggests a role of minisatellites in regulation of gene expression and contributes to diversity of human cell biology. Further studies with larger cohorts are necessary to validate our findings.

Materials and methods

Tissue, cell specimens, and study population

H157, H226, H226Br, H460, H1299, and H1944 human NSCLC cells were purchased from American Type Culture Collection (Rockville, MD, USA). SK-MES and 17B squamous carcinoma of the head and neck were obtained from Dr Adi Gazdar (University of Texas Southwestern Medical Center, Dallas, TX, USA). The telomerase-negative alternative-lengthening-of-telomeres cell line KB319 was a gift from Drs John Murnane and Laure Sabatier, Radiation Oncology Research Laboratory, University of California, San Francisco, USA (Murnane et al., 1994). Cells were cultured in Dulbecco's modified Eagle's medium supplemented with 10% heat-inactivated fetal calf serum, 2 mM L-glutamine, 100 IU/ml penicillin, and 100 mg/ml streptomycin at 37°C in the presence of 5% CO_2.

Lung cancer tissues were obtained from 53 consecutive patients with NSCLC, who had undergone surgical resection with curative intent at MD Anderson Cancer Center between 1996 and 1998, and for whom archived tissues were available. These specimens were collected from the Department of Pathology and stored at −80°C until use. All patients had consented to the use of their tissue specimens, and the

institutional review board approved the research protocol. The leukocytes (control samples) were obtained from 57 noncancer volunteers (former smokers) recruited for several randomized chemoprevention trials in the Houston metropolitan area and 15 hospital patients without evidence of lung cancer.

RNA in situ hybridization and Telomeric Repeat Amplification Protocol Assay

The riboprobe used in this study was a 620 bp cDNA fragment RT–PCR-amplified from exons 10 to 15 by using the forward primer 5'-TCT TGT TGG TGA CAC CTC ACC-3' and the reverse primer 5'-TAG GTG ACA CGG TGT CGA GT-3'. The PCR fragment was then cloned into the pCR*II-TOPO vector (Invitrogen, Carlsbad, CA, USA). The plasmid was linearized with EcoRV, and the single-strand-specific riboprobe was transcribed *in vitro* with SP6 RNA polymerase (Promega, Madison, WI, USA) by using a DIG RNA Labeling Kit (Roche Diagnostics, Inc., Indianapolis, IN, USA). *In situ* hybridization was performed as previously described (Wang et al., 2002). Detection was performed using a DIG Nucleic Acid Detection Kit (Roche Diagnostics, Inc., Indianapolis, IN, USA) according to the manufacturer's directions. Anti-DIG alkaline phosphatase conjugated antibody was diluted 1 : 500. Nitro-blue tetrazolium and 5-bromo-4-chloro-3-indolyl phosphate were used as chromogens. Slides were then rinsed in TE buffer (10 mM Tris-HCl and 1 mM EDTA, pH 8) and mounted with Aqua-Mount medium (Fisher, Houston, TX, USA). Telomerase activity was measured by using the TRAP-cze Telomerase Detection Kit (Intergen, Purchase, NY, USA) according to the manufacturer's protocol.

Construction of the pGL3-570(S), pGL3-570(R), and pGL3-660(S) plasmids

A 570 bp DNA fragment from the downstream region of hTERT gene (from base 22 141 to base 22 710, Accession number AF128894) was amplified from the cell line H460 by using the forward primer 5'-TTC TGA TGC TGT GAG GCA GG-3' and the reverse primer 5'-GAG AGA TGA GAC TGG GAG ATG-3', and inserted into pGL3-basic vector (Promega). The plasmids with forward and reverse directions identical with the direction of hTERT genomic sequence in GenBank, were constructed and named as pGL3-570(S) and pGL3-570(R), respectively. The PCR reaction was performed in a 12.5-μl volume containing about 50 ng of genomic DNA, 7% dimethyl sulfoxide, 1.5 mM dNTPs, 6.7 mM MgCl₂, 16.6 mM (NH₄)₂SO₄, 67 mM Tris, 10 mM β-mercaptoethanol, 6.7 μM EDTA, 0.5 μM forward, 0.5 μM reverse primer, and 0.625 U of HotStar Taq DNA Polymerase (Qiagen, Inc., Chatsworth, CA, USA). Amplification was carried out with an initial denaturing step at 95°C for 15 min, followed by 40 cycles of 95°C for 30 s, 60°C for 1 min, and 72°C for 1 min in a thermal cycler (Hybaid; PCR Express, Middlesex, UK) with a last extension step of 72°C for 10 min. The sequences of plasmids were confirmed by using an AmpliCycle sequencing kit according to the manufacturer's instructions (Applied Biosystems, Foster City, CA, USA). A 660 bp DNA fragment was also amplified using the same set of primers (containing additional repeats sequence) to construct the plasmid pGL3-660(S).

Construction of pGL3-302(S), pGL3-302(R) and pGL3-243(S), pGL3-243(R) plasmids

Two smaller DNA fragments containing a 243 or 302 bp tandem repeat sequence (MNS16A) within the 570 or 660 bp fragment described above were amplified by using the forward primer S3-H 5'-AAA GCT TCT TCT GAT CTC TGA AGG G-3' and the reverse primer E17AS4-H 5'-AAA GCT TGC CTG AGG AAG GAC GTA-3'. These two fragments were also inserted into pGL3-basic vector. The plasmids with forward and reverse directions identical with the direction of hTERT genomic sequence in GenBank were constructed and named pGL3-302(S) and pGL3-302(R), respectively, and pGL3-243(S) and pGL3-243(R), respectively.

Transient transfection and luciferase assay

The plasmids were transfected into lung cancer cell line H1299 using Lipofect.AMINE reagent (GIBCO BRL, Grand Island, NY, USA) according to the manufacturer's protocol. Briefly, 5 × 10⁴ cells were spread into 24-well plates and incubated overnight. Then, 250 ng of plasmids and 50 ng of pCMVsport-beta gal (GIBCO BRL, Grand Island, NY, USA), which was used as the internal control to monitor the transfection efficiency, were added. After 6 h, the medium was replaced with a medium containing 10% fetal calf serum and 36 h later, the cells were harvested with cell lysis buffer. In each experiment, transfection was performed in triplicate and luciferase activity was measured by using a Luciferase Assay System (Promega Co., Madison, WI, USA) with a luminometer. β-galactosidase activity was measured with Beta-galactosidases Enzyme Assay System with a report lysis buffer (Promega) following the manufacturer's instructions. The values of luciferase activities were normalized against those of β-galactosidase expressed by plasmid pCMVsport-β gal.

Genotyping of MNS16A

For genotyping of MNS16A, genomic DNA was extracted from leukocytes of surgically resected lung tissues. Briefly, the tissue was digested in 200 μl of 50 mM Tris-HCl (pH 8.0) containing 1% sodium dodecyl sulfate and proteinase K, and incubated at 42°C for 24 h. DNA was purified using phenol–chloroform extraction followed by ethanol precipitation. 'Hot-PCR' was used to determine the MNS16A genotype by using the forward primer 5'-AGG ATT CTG ATC TCT GAA GGG TG-3', located at nt 22591, and the reverse primer 5'-TCT GCC TGA GGA AGG ACG TAT G-3', located at nt 22871. Briefly, the reverse primer was endlabeled with γ-³²P-ATP by using T4 polynucleotide kinase. The PCR reaction was performed in a 12.5-μl volume with an additional 0.02 μM of hot primer under the condition same as that mentioned above. Omission of DNA was used as a negative control. The PCR products were mixed with loading buffer, separated by electrophoresis on a 6% urea/formamide-denaturing polyacrylamide gel, and exposed to X-ray film.

Three different MNS16A genotypes, that is, LL-genotype (homozygotes), SS-genotype (homozygotes), and SL-genotype (heterozygotes), were defined on the basis of the functional structure of this tandem repeat minisatellite. (There are three GATA-1 binding sites in LL-genotype, while only two such sites in SS-genotype.)

References

Albanell J, Lonardo F, Rusch V, Engelhardt M, Langenfeld J, Han W, Klimstra D, Venkatraman E, Moore MA and Dmitrovsky E. (1997). *J. Natl. Cancer Inst.*, **89**, 1609–1615.

Bouchardy C, Benhamou S, Jourenkova N, Dayer P and Hirvonen A. (2001). *Lung Cancer*, **32**, 109–112.

Bryce LA, Morrison N, Hoare SF, Muir S and Keith WN. (2000). *Neoplasia*, **2**, 197–201.

Dhaene K, Van Marck E and Parwaresch R. (2000). *Virchows Arch.*, **437**, 1–16.

Feng J, Funk WD, Wang SS, Weinrich SL, Avilion AA, Chiu CP, Adams RR, Chang E, Allsopp RC, Yu J, Le S, West MD, Harley CB, Andrews WH, Greider CW and Villeponteau B. (1995). *Science*, **269**, 1236–1241.

Greider CW and Blackburn EH. (1985). *Cell*, **43**, 405–413.

Goode EL, Ulrich CM and Potter JD. (2002). *Cancer Epidemiol. Biomarkers Prev.*, **11**, 1513–1530.

Hiyama K, Hiyama E, Ishioka S, Yamakido M, Inai K, Gazdar AF, Piatyszek MA and Shay JW. (1995). *J. Natl. Cancer Inst.*, **87**, 895–902.

Hoff-Olsen P, Meling GI and Olaisen B. (1995). *Hum. Mutat.*, **5**, 329–332.

Honma M, Mizusawa H, Sasaki K, Hayashi M, Ohno T, Tanaka N and Sofuni T. (1994). *Mutat. Res.*, **304**, 167–179.

Imai H, Nakagama H, Komatsu K, Shiraishi T, Fukuda H, Sugimura T and Nagao M. (1997). *Proc. Natl. Acad. Sci. USA*, **94**, 10817–10820.

Jeffreys AJ, Tamaki K, MacLeod A, Monckton DG, Neil DL and Armour JA. (1994). *Nat. Genet.*, **6**, 136–145.

Jeffreys AJ, Wilson V, Kelly R, Taylor BA and Bulfield G. (1987). *Nucleic Acids Res.*, **15**, 2823–2836.

American Cancer Society Inc. (2003). *Cancer facts & figures*, American Cancer Society: Atlanta, GA. pp. 2–5.

Kaplanski C, Srivatanakul P and Wild CP. (1997). *Int. J. Cancer*, **72**, 248–254.

Kim NW, Piatyszek MA, Prowse KR, Harley CB, West MD, Ho PL, Coviello GM, Wright WE, Weinrich SL and Shay JW. (1994). *Science*, **266**, 2011–2015.

Ledwith BJ, Storer RD, Prahalada S, Manam S, Leander KR, van Zwieten MJ, Nichols WW and Bradley MO. (1990). *Cancer Res.*, **50**, 5245–5249.

Ledwith BJ, Joslyn DJ, Troilo P, Leander KR, Clair JH, Soper KA, Manam S, Prahalada S, van Zwieten MJ and Nichols WW. (1995). *Carcinogenesis*, **16**, 1167–1172.

Leem S-H, Londoño-Vallejo JA, Kim J-H, Bui H, Tubacher E, Solomon G, Park J-E, Horikawa I, Kouprina N, Barrett JC and Larionov V. (2002). *Oncogene*, **21**, 769–777.

Matsumura Y and Tarin D. (1992). *Cancer Res.*, **52**, 2174–2179.

Meyerson M, Counter CM, Eaton EN, Ellisen LW, Steiner P, Caddle SD, Ziaugra L, Beijersbergen RL, Davidoff MJ, Liu Q, Bacchetti S, Haber DA and Weinberg RA. (1997). *Cell*, **90**, 785–795.

Murnane JP, Sabatier L, Marder BA and Morgan WF. (1994). *EMBO J.*, **13**, 4953–4962.

Nakamura TM, Morin GB, Chapman KB, Weinrich SL, Andrews WH, Lingner J, Harley CB and Cech TR. (1997). *Science*, **277**, 955–959.

Paquette B and Little JB. (1992). *Cancer Res.*, **52**, 5788–5793.

Parkin DM, Pisani P and Ferlay J. (1999). *CA Cancer J. Clin.*, **49**, 33–64.

Shen H, Wang L, Spitz MR, Hong WK, Mao L and Wei QY. (2002). *Cancer Res.*, **62**, 4992–4995.

Soria JC, Moon C, Wang L, Hittelman WN, Jang SJ, Sun S-Y, Lee JJ, Liu D, Kurie JM, Morice RC, Lee JS, Hong WK and Mao L. (2001). *J. Natl. Cancer Inst.*, **93**, 1257–1263.

Spitz MR, Wu X, Wang Y, Wang LE, Shete S, Amos CI, Quo Z, Lei L, Mohrenweiser H and Wei Q. (2001). *Cancer Res.*, **61**, 1354–1357.

Szutorisz H, Palmqvist R, Roos G, Stenling R, Schorderet DF, Reddel R, Lingner J and Nabholz M. (2001). *Oncogene*, **20**, 2600–2605.

Thein SL, Jeffreys AJ, Gooi HC, Cotter F, Flint J, O'Connor NT, Weatherall DJ and Wainscoat JS. (1987). *Br. J. Cancer*, **55**, 353–356.

Wang L, Soria JC, Kemp BL, Liu DD, Mao L and Khuri FR. (2002). *Clin. Cancer Res.*, **8**, 2883–2889.

Wei Q, Cheng L, Amos CI, Wang LE, Guo Z, Hong WK and Spitz MR. (2000). *J. Natl. Cancer Inst.*, **92**, 1764–1772.

Wick M, Zubov D and Hagen G. (1999). *Gene*, **232**, 97–106.

Xiong Y and Eickbush TH. (1990). *EMBO J.*, **9**, 3353–3362.

Yashima K, Litzky LA, Kaiser L, Rogers T, Lam S, Wistuba II, Milchgrub S, Srivastava S, Piatyszek MA, Shay JW and Gazdar AF. (1997). *Cancer Res.*, **57**, 2373–2377.

#370 Altered and focused expression of CD9 in invasive cervical cancer: Correlation with lymphatic vessel invasion and tumor progression. Georg Walter Sauer, Jasmin Windisch, Christian Kurzeder, Volker Heilmann, Rolf Kreienberg, and Helmut Deissler. *University of Ulm Medical School, Ulm, Germany.*

Lymphovascular space invasion plays a critical role in the progression of cervical cancer. It is associated with an unfavourable prognosis even in patients with early stage disease. Therefore, identification and functional characterization of molecules that are predominantly expressed in tumors with lymphatic vessel involvement may help to improve the clinical assessment of cervical neoplasias with unclear prognosis. For a number of malignant diseases, the level of expression of CD9, a tetraspanin adaptor protein involved in various fundamental cellular processes, was found to be inversely correlated with tumor invasiveness, ability to form metastases, and poor clinical outcome. We demonstrate that cervical carcinoma locally re-expresses CD9 at sites of lymphovascular space and blood vessel invasion. This suggests a functional role of CD9 in transendothelial migration as a crucial step in the formation of metastases. In addition, local re-expression of CD9 defines a subgroup of patients with low-grade tumors according to conventional histopathological classification and poor prognosis. We postulate therefore that occurrence of clusters of cells with strong CD9 expression is a marker for high risk recurrence in early-stage cervical cancer that may provide a basis for a decision in favour of additional treatment of these patients.

#371 Frequent overexpression of hepatoma-derived growth factor in early stage non-small cell lung cancer (NSCLC) development. Hening Ren, Xi Ming Tang, Lei Feng, J. Jack Lee, Allen D. Everett, and Li Mao. *The Univ of Texas MD Anderson Cancer Center, Houston, TX and University of Virginia Health Sciences Center, Charlottesville, VA.*

Hepatoma-derived growth factor (HDGF) is a heat-liable protein identified in the conditioned medium of the human hepatoma-derived HuH-7 cell line by proliferation assay of Swiss 3T3 cells. The 27 kDa protein contains a motif homologous to the consensus sequences of bipartite nuclear localization signal, a DNA-binding PWWP motif, suggesting HDGF's potential role as a nuclear transcriptional factor. Exogenous HDGF is mitogenic for HuH-7 cells, fibroblast and aortic endothelial cells. In esophageal cancer, HDGF level was found to be associated with radiation sensitivity. By means of immunoproteomic approach, we have found that HDGF expression is elevated in lung cancer cells compared to normal lung tissues. We confirmed this finding by comparing mRNA expression of HDGF in 12 lung cancer cell lines to its expression in a normal lung tissue cDNA library by RT-PCR. To determine the role of HDGF in early lung tumorigenesis, HDGF expression in paraffin-embedded tissue sections from 46 patients with stage I NSCLC and normal lung tissue from a non-smoking patient with sarcoma metastases was analyzed by immunohistochemical staining using a rabbit polyclonal anti-HDGF antibody. All 46 patients with NSCLC were treated with curative surgery and followed for an average of more than 6 years. In the normal bronchial epithelium of the non-smoking sarcoma patient, HDGF expression was absent or weakly stained, whereas a strong nuclear staining was observed in most of the adenocarcinoma cells. A mixed cytosolic/nuclei staining was observed in a substential number of squamous carcinoma cells, although the staining was generally weaker than was that seen in adenocarcinoma cells. Interestingly, HDGF staining appeared stronger in poorly differentiated cells with visible cellular atypia and pleomorphism. We used both staining intensity and the percentage of positive cells as indices of HDGF expression in the tumors. We found that HDGF expression was significantly higher in adeno/bronchioaveolar carcinoma histology compared with other histology types (P = 0.0012 by Wilcoxon rank sum test). We further analyzed HDGF expression in the same specimens with other clinical and pathological parameters and biomarkers. Besides a weak association with loss of heterozygosity at several tumor suppressor loci (P = 0.07), no association was observed with the proliferation marker Ki67 or with G2-S regulator cyclin B1. Importantly, we observed an adverse trend in the duration of survival when tumors exhibited a higher level of HDGF (P = 0.095 by log-rank test for disease-specific survival). A larger sample size is needed before reaching a meaningful conclusion. (Supported in part by NCI PO1 CA91844 and DOD DAMD17-01-1-0689).

#372 Distribution and expression of hepatoma-derived growth factor (HDGF) in normal, proliferative and neoplastic human lung tissue and its significance in carcinogenesis of non-small cell lung cancer. Ximing Tang, Hening Ren, Reuben Lotan, Waun Ki Hong, and Li Mao. *University of Texas MD Anderson Cancer Center, Thoracic/Head & Neck Medical Oncology, Houston, TX.*

Hepatoma-derived growth factor (HDGF) is a heat-liable protein that can stimulate the growth of fibroblasts, vascular smooth muscle cells, endothelial cells, and hepatoma cells. However, the function of this mitogen in tumorigenesis remains unknown. Recently, we found that HDGF is highly expressed in lung cancer cell lines by means of immunoproteomic method. Its expression level in tumor tissue

from patients with non-small cell lung cancer (NSCLC) tends to be correlated with negative outcome. In this study, we determined the distribution of HDGF in normal and malignant lung tissues by immunohistochemistry staining of sections of formalin-fixed paraffin-embedded tissue sample from human NSCLC stage I and adjacent lung, and lung tissue. Semi-quantitative assessment of HDGF expression was based on the staining of a reference smooth muscle cells (SMCs) of small vessels as follows: a) negative; b) +1 if ≤2 amount in SMCs; c) +2 if 2-4 x amount in SMCs; d) +3 if >4 x amount in SMCs. HDGF was found in the majority of nuclei of lung adenocarcinoma cells at levels of +2 or +3, but rarely in the cytoplasm. In contrast, HDGF was found in both cytoplasm (+1 or +2) and nuclei (+1 or +2) in most of the squamous carcinoma cells. The degree of staining with was correlated to the grade of cell atypia of tumor cells. Most tumor giant cells possessed much more HDGF (+3) in their nuclei than well-differentiated tumor cells. Many "normal appearing" tumor cells were negative in either adenocarcinoma or squamous carcinoma. HDGF staining was gradually reduced as cells entered mitosis and completely disappeared at metaphase. In areas of hyperplasia and dysplasia adjacent to tumor in alveoli and bronchi almost all of epithelial cells stained strongly positive (+2 or +3). Some new growth SMCs, endothelia, fibroblast cells, macrophages, and lymphoblasts of germinal centers in lymph nodules were stained positively (+1 or +2). In "normal lung" from non-smoker patient with metastatic sarcoma, only 1/3 of bronchial epithelial cells showed positive nuclear stain (+1 or +2). We concluded that HDGF expression pattern suggests that it may play a role in maintaining cell proliferation during DNA synthesis, transcription and early mitosis. The different distribution in cytoplasm and nucleus may be used as marker for distinguishing poorly differentiated adenocarcinoma and squamous carcinoma. Furthermore, its increased expression may be a very early marker of lung tumorigenesis.

#373 Prognostic significance of laminin-5 gamma 2 chain expression in advanced colorectal carcinoma. Seishi Aoki, Yukihiro Nakanishi, Shingo Akimoto, Yoshihiro Moriya, Kimio Yoshimura, Masaki Kitajima, Michiie Sakamoto, and Setsuo Hirohashi. *Keio University School of Medicine, Shinjuku-ku, Tokyo, Japan and National Cancer Center Research Institute and Hospital, Tokyo, Japan.*

(Purpose) The laminin-5 gamma 2 chain (LN5) plays an important role in cell migration during tumor invasion and tissue remodeling. Although this chain has been reported to be expressed in tumor-stroma interface of colorectal carcinoma, prognostic significance of its expression has not been elucidated in these tumors. So we investigated the clinicopathologic significance of LN5 expression in colorectal carcinoma. (Methods) LN5 expression was investigated immunohistochemically in 103 colorectal carcinoma patients with stage II, III and IV. The patients were categorized into 3 groups as follows according to the number of immunopositive tumor cells in the sections containing the maximum diameter of the tumor: +, less than 20 tumor cells were positive; ++, 20- 500 tumor cells were positive; +++, more than 500 tumor cells were positive. (Results) LN5 expression was observed in the cytoplasm of tumor cells, especially those budding from the tumor nests at the invasive front. Few immunopositive tumor cells were observed in large tumor nests showing non-infiltrative growth pattern. No expression was observed in normal colon mucosa. Eighteen (17%) tumors showed +, 60 (58%) showed ++, 25 (24%) showed +++. The increased number of immunopositive tumor cells was significantly associated with synchronous liver metastasis (P=0.048). The univariate (P=0.036) and multivariate (P=0.001) analysis of the patients' survival revealed that the prognosis became significantly poorer in patients with the increased number of immunopositive tumor cells. (Conclusions) Increased LN5 immunoreactivity, suggesting a high invasive potential of tumor cells, was a significant poor prognostic indicator for the patients with colorectal carcinoma.

#374 Malignancy-associated changes (MACs) measured using nuclear structure of morphologically benign cells predict prostate cancer distant metastasis and death in men with biochemical recurrence. Robert W. Veltri, Masood A. Khan, Michael C. Miller, Wesley Bales, Jonathan I. Epstein, Leslie Mangold, and Alan W. Partin. *Johns Hopkins University School of Medicine, Baltimore, MD, Immunicon Corporation, Huntington Valley, PA, and UroCor Inc., Oklahoma City, OK.*

A retrospective clinical study assessed the ability of alterations in nuclear measurements of benign epithelial nuclei juxtaposed to cancer areas to predict metastasis and/or prostate cancer-specific death following biochemical recurrence. We utilized a group 104 radical prostatectomy (RP) biochemical recurrence cases (n=59, non-distant and n=45, distant metastases) with long term follow-up(mean 11.71 +/- 4.18 years). All data were collected under an IRB approved protocol. A single radical prostatectomy (RP) block was selected by the pathologist, and five micron sections were stained with H&E and Feulgen stains. The pathologist marked the H&E master slide for morphologically benign and cancer areas and 125-150 nuclear images were captured from both areas of the Feulgen stained slide

ONCOGENE

nature publishing group

SEARCH | | | my account | e-alerts | subscribe | register

Journal home

Table of contents   Previous Article Next PDF

Original Paper

CACNA2D2-mediated apoptosis in NSCLC cells is associated with alterations of the intracellular calcium signaling and disruption of mitochondria membrane integrity

Giovanni L Carboni[1,3], Boning Gao[2], Masahiko Nishizaki[1], Kai Xu[1], John D Minna[2], Jack A Roth[1] and Lin Ji[1]

[1]Section of Thoracic Molecular Oncology, Department of Thoracic and Cardiovascular Surgery, The University of Texas MD Anderson Cancer Center, Houston, TX 77030, USA

[2]Department of Internal Medicine and Pharmacology, Hamon Center for Therapeutic Oncology Research, University of Texas Southwestern Medical Center, Dallas, TX 75390, USA

[3]Division of General Thoracic Surgery, University Hospital Bern, Switzerland

Correspondence to: L Ji, Department of Thoracic and Cardiovascular Surgery, Box 445, The University of Texas MD Anderson Cancer Center, 1515 Holcombe Blvd, Houston, TX 77030, USA. E-mail: lji@mail.mdanderson.org

Abstract

The CACNA2D2 gene, a new subunit of the Ca^{2+}-channel complex, was identified in the homozygous deletion region of chromosome 3p21.3 in human lung and breast cancers. Expression deficiency of the CACNA2D2 in cancer cells suggests a possible link of it to Ca^{2+} signaling in the pathogenesis of lung cancer and other cancers. We investigated the effects of overexpression of CACNA2D2 on intracellular Ca^{2+} contents, mitochondria homeostasis, cell proliferation, and apoptosis by adenoviral vector-mediated wild-type CACNA2D2 gene transfer in 3p21.3-deficient nonsmall cell lung cancer cell lines. Exogenous expression of CACNA2D2 significantly inhibited tumor cell growth compared with the controls. Overexpression of CACNA2D2 induced apoptosis in H1299 (12.5%), H358 (13.7%), H460 (22.3%), and A549 (50.1%)

Microbiology NEW!
■ Molecular Cell Biology
■ Neuroscience
■ Pharmacology
Physics

browse all publications

cell lines. Levels of intracellular free Ca^{2+} were elevated in AdCACNA2D2-transduced cells compared with the controls. Mitochondria membrane depolarization was observed prior to apoptosis in Ad-CACNA2D2 and Adp53-transduced H460 and A549 cells. Release of cyt c into the cytosol, caspase 3 activation, and PARP cleavage were also detected in these cells. Together, these results suggest that one of the pathways in CACNA2D2-induced apoptosis is mediated through disruption of mitochondria membrane integrity, the release of cyt c, and the activation of caspases, a process that is associated with regulation of cytosolic free Ca^{2+} contents.

Keywords

Abbreviations

ADP, adenosinediphosphate; CACNA2D2, calcium-channel alfa-2-delta-2 subunit; COX IV (I), cytochrome oxidase IV subunit I; cyt C, cytochrome C; DAPK, death-associated protein kinase; DMSO, dimethylsulfoxide; FBS, fetal bovine serum; HBSS, Hanks balanced saline solution; MOI, multiplicity of infection; NSCLC, non-small cell lung cancer; PARP, poly ADP-ribose polymerase; PI, propidiumiodide; TUNEL, terminal deoxynucleotidyl transferase-mediated dUTP nick-end labeling; VACC, voltage-activated calcium channel; XTT, sodium 3,3'-{1-[(phenylamino)carbonyl]-3,4-tetrazolium}-bis(4-methoxy-6-nitro)-benzene sulfonic acid hydrate; wt, wild-type

Introduction

The novel gene CACNA2D2 has recently been identified in the homozygous deletion region of chromosome 3p21.3 in human lung and breast cancers (Gao *et al.*, 2000, Lerman and Minna, 2000). It is characterized structurally as a new α2δ2 auxiliary subunit of the voltage-activated calcium channel (VACC) protein complex. The CACNA2D2 gene spans an ~140 kb genomic locus in the 3p21.3 region, consists of at least 40 exons, and is expressed as a 5.5–5.7 kb mRNA. The CACNA2D2 protein consists of 1146 amino acids with a predicted molecular mass of 130 kDa (Gao *et al.*, 2000). Three splicing variants of CACNA2D2 mRNA have been detected, which result in two protein isoforms with different N-terminals (Angeloni *et al.*, 2000). The CACNA2D2 protein shows a 56% amino-acid sequence homology to that of the α2δ1 subunit of the VACC complexes and shares a similar secondary and tertiary structure with the CACNA2D1, as suggested by

the analysis of hydrophobicity, potential glycosylation sites, and bridge-forming cysteines of the primary sequence (Angeloni et al., 2000). The CACNA2D2 protein is highly expressed in normal lung tissue, but either absent or underexpressed in more than 50% of lung cancers (Gao et al., 2000). Since cancer cells are deficient in CACNA2D2, it has been suggested that CACNA2D2 could be a tumor suppressor gene linking Ca^{2+} signaling with the pathogenesis of lung cancer and other cancers (Gao et al., 2000).

Growing evidence has demonstrated that Ca^{2+} signaling regulates and controls diverse cellular processes such as cell fertilization, development, proliferation, learning and memory, contraction and secretion, and cell death (Berridge et al., 1998,2000). The universality of calcium as an intracellular messenger depends on the enormous range of timing, spatial, and temporal signals it can create in the complicated cellular processes (Berridge et al., 1998,2000). Alteration of the spatial and temporal balances of intracellular calcium by either environmental stimuli or calcium effectors can result in cell death by both necrosis and apoptosis (Lemasters et al., 1998; Berridge et al., 2000; Zhu et al., 2000).

Early loss of CACNA2D2 expression in the pathogenesis of lung cancer (Angeloni et al., 2000), inactivation of expression of other calcium channel-related proteins such as calcium/calmodulin-dependent death-associated protein kinase (DAPK) (Raveh and Kimchi, 2001) and CACNA1G by promoter hypermethylation in various human cancers (Toyota et al., 1999; Ueki et al., 2000; Zochbauer-Muller et al., 2001), and the growing role of Ca^{2+} signaling in cell regulation (Berridge et al., 2000), and especially its involvement in the mitochondria-mediated apoptotic pathway (Rutter and Rizzuto, 2000; Zhu et al., 2000), motivated us to further investigate the function of the calcium channel protein CACNA2D2 in the regulation of cell proliferation and cell death and in the pathogenesis of human cancers. This study encompasses the effect of the ectopic expression of CACNA2D2 on mitochondria homeostasis, cell proliferation, apoptosis, and intracellular Ca^{2+} contents by adenoviral vector-mediated wild-type (wt)-CACNA2D2 gene transfer in various 3p21.3-deficient NSCLC cell lines. We demonstrated that CACNA2D2-induced apoptosis was mediated through a cellular process involved in the regulation of the intracellular Ca^{2+} contents, the disruption of mitochondria membrane integrity, the release of cyt c, and the activation of downstream caspases.

Results

Exogenous expression of CACNA2D2 inhibits tumor cell growth

To evaluate whether the CACNA2D2 could function as a tumor suppressor or a cell death mediator by inhibition of tumor cell growth in lung cancer, we performed a series of experiments to study the effect of ectopic expression of the CACNA2D2 gene on cell proliferation in various Ad-CACNA2D2-transduced human NSCLC cell lines NCI-H1299, NCI-H460, NCI-H358, and A549, with varying status of 3p21.3 markers (Figure 1). Cells from each line were transduced *in vitro* by the Ad-CACNA2D2 vector administered at various MOIs, and cells treated with PBS, the empty vector Ad-EV, Ad-LacZ, or Ad-GFP were used as controls. The transduction efficiency was determined by examining the GFP-expressing cells in the Ad-GFP transduced cell population under a fluorescence microscope. The transduction efficiency of the adenoviral vectors was greater than 80% at the highest MOI applied for each cell line. Expression of CACNA2D2 was verified by RT-PCR analysis (Figure 1a) and Western blot analysis (Figure 1b), respectively, in Ad-CACNA2D2-transduced NSCLC cells. The transfection by plasmid DNA and the transduction by adenoviral vector are less efficient in A549, H460, and H358 cells than those in H1299 cells. Although the transcription of CACNA2D2 could be detected by RT-PCR (Figure 1a), the protein expression could only be detected at a trace amount by Western blot analysis (Figure 1b) in the CACNA2D2-containing plasmid DNA-transfected A459, H460, and H358 cells. A significantly elevated expression of CACNA2D2 proteins could be detected in all cell lines transduced by the Ad-CACN vector (Figure 1b).

We analysed cell proliferation by determining the viability of cells at 2 and 5 days post-transduction, respectively. Tumor cell growth was significantly inhibited in all the cell lines transduced by the Ad-CACNA2D2 vector 5 days after transduction, compared with what we observed with untreated cells (PBS) or those treated with Ad-EV and Ad-LacZ controls (Figure 1c). The A549 cell line appeared to be the most sensitive to the ectopic expression of CACNA2D2 and showed a more than 60% reduction in cell viability at day 5 (Figure 1c, A549), while moderate reduction of cell viability was observed in Ad-CACNA2D2-transduced H358 (44%), H460 (42%), and H1299 (28%) cells (Figure 1c). Adp53 was used as a positive control and was less effective than Ad-CACNA2D2 in A549 and H460, which contain wt-p53. No significant effect on cell viability was observed in controls treated with PBS, AdEV, and Ad-LacZ.

The effect of enforced expression of the wt-CACNA2D2 gene on tumor growth was further evaluated *in vivo* by direct intratumoral injection of Ad-CACNA2D2 vector, along with PBS and Ad-LacZ vector as controls, into human NSCLC H460 tumor xenografts in *nu/nu* mice (Figure 1d). The growth of tumors was recorded from the first injection until about 20 days after the last injection. Tumor volumes were normalized by calculating the percentage increase in tumor volume after treatment relative to volume at the beginning of treatment in each

group. A significant suppression of tumor growth was observed in H460 tumors treated with Ad-CACNA2D2 vector compared with those control groups treated with PBS ($P<0.0001$) and with Ad-LacZ ($P=0.015$) (Figure 1d). These results obtained *in vivo* are consistent with those observed *in vitro* for effects on inhibition of tumor cell growth and induction of apoptosis in the same cell line.

Induction of apoptosis by exogenous expression of CACNA2D2

One of the physiological functions associated with calcium channel proteins is their ability to induce apoptosis by regulating intracellular Ca^{+2} signaling and several downstream pathways (Lam *et al.*, 1994; Walker and De Waard, 1998; Felix, 1999; Wang *et al.*, 1999a; Zhu *et al.*, 1999,2000). To test whether the growth inhibition by the ectopic expression of CACNA2D2 was caused by induction of apoptosis, we performed FACS analysis with TUNEL reaction and PI staining to examine DNA fragmentation and cell cycle kinetics in Ad-CACNA2D2-transduced cells (Figure 2). Significant induction of apoptosis was observed in Ad-CACNA2D2-transduced A549 (50.1%) (Figure 2a), H460 (22.3%) (Figure 2b), and H358 (18.7%) (Figure 2d) cells at 5 days after transduction compared with cells treated with what was seen with the Ad-EV or Ad-LacZ (from 2 to 10%) control vectors at the same time (Figure 2). However, no significant induction of apoptosis was detected in Ad-CACNA2D2-transduced H1299 cells (Figure 2c) at the same MOIs. The magnitude of and trend toward the induction of apoptosis in these Ad-CACNA2D2-treated cells paralleled the degree and trend towards growth inhibition (Figure 1c). The correlation coefficients between the relative cell viability and the relative apoptotic cell populations in Ad-CACNA2D2-treated cells versus PBS-treated controls/PBS are significant ($P<0.05$) in all four NSCLC cell lines A549, H1299, H460, and H358 cells ($r=-0.96198, -0.79416, -0.99436,$ and -0.95744, respectively), but with a less degree of correlation in H1299 cells which are less sensitive to exogenous expression of CACNA2D2, suggesting that the growth inhibition by the ectopic expression of CACNA2D2 might be mediated by the induction of apoptosis. We saw no significant alteration in cell cycle kinetics, such as G1 arrest or G2/M arrest, in these Ad-CACNA2D2-transduced cells (data not shown).

Upregulation of intracellular free cytosolic Ca^{2+}

CACNA2D2 is structurally related to the $\alpha2\delta2$ subunit of the VACC protein complex, which has been suggested to regulate Ca^{+2} trafficking through the channel and the retention of VACC at the plasma membrane without significant change in such properties as channel gating or permeation (Wang *et al.*, 1999b; Marais *et al.*, 2001). To examine whether the ectopic overexpression of this CACNA2D2 subunit would increase free cytosolic Ca^{2+} influx, we measured

changes in the levels of intracellular Ca^{2+} in Ad-CACNA2D2-transduced cells by a sensitive FACS and fluorescence image analysis with fluorescent Fluo3-AM staining (Kao et al., 1989). Fluo3-AM dye binds specifically to free Ca^{2+} and shows an increase of emission fluorescence at 530 nm upon excitation at 488 nm. The fluorescence intensity depends on how much free Ca^{2+} is bound. We detected a significant increase of fluorescence emission in Ad-CACNA2D2-transduced H460 ($P=0.015$ and 0.03) (Figure 3a (panel c) and b) and A549 ($P=0.001$ and 0.002) (Figure 3a (panel g) and b) 48 h after treatment, but this was not seen in the untreated cells and the p53-transduced cells (Figures 2a (panels a and e) and 3b), but not a significant increase in Ad-CACNA2D2-transduced H1299 cells (Figure 3b). An increase in the level of fluorescence emission in Adp53-treated cells (Figure 3a (panels b and f) and b) was also detected, but exhibited a lower magnitude and a slower manifestation (the peak emission was registered 72–96 h post-treatment) than that in Ad-CACNA2D2-transduced cells (the peak emission was registered 48 h post-treatment). The increase of free cytosolic Ca^{2+} occurred shortly prior to apoptosis in these Ad-CACNA2D2-treated cells, suggesting a possible association of the induction of apoptosis by CACNA2D2 activity and the regulation of intracellular Ca^{2+} signaling, homeostasis, or both. However, this experimental setting does not allow to link mechanistically the Ca^{2+} increase to the apoptotic induction. The Fluo3-AM loading and staining conditions were optimized and confirmed by treating cell samples with 2 μg of ionomycin (a ionophore) (Kochegarov et al., 2001) as a positive control, which showed uniform fluorescence emission increase in all treated cells (Figure 3a, panels d and e).

Interruption of mitochondria membrane potential

Depolarization of mitochondria and loss of mitochondria membrane potential can be a rate-limiting step in apoptosis as well as in necrotic cell death (Kroemer and Reed, 2000; Vieira et al., 2000). The emerging evidence suggests that an excessive influx of Ca^{2+} represents a prototypical example of a cell death stimulus where mitochondria membrane depolarization precedes cyt c release (Reed and Kroemer, 2000; Vieira et al., 2000). To investigate further the impact of the observed increase in intracellular free Ca^{2+} influx by ectopic expression of CACNA2D2 on mitochondria membrane integrity, we analysed the changes of mitochondria membrane potential in Ad-CACNA2D2-transduced NSCLC cells by FACS with mitochondria membrane potential-specific fluorescent JC-1 staining (Figure 4). Mitochondria depolarization, as demonstrated by a significant fluorescent shift with an increase in green (540 nm) emission (Figure 4a), was observed in Ad-CACNA2D2-transduced H460 and A549, cells between 24 and 48 h after transduction (Figure 4b), but not in untreated or Ad-LacZ-

transduced cells. After 72 h of transduction by the Ad-CACNA2D2 vector, more than 84% of the A549 cells (Figure 4b, A549) and 80% of H460 (Figure 4b, H460) cells revealed mitochondria membrane depolarization; however, no significant changes were observed in the H1299 cells (Figure 4b, H1299). Adp53 induced similar changes in H460, A549 and H1299 cells (Figure 4). Mitochondria membrane depolarization preceding induction of apoptosis in cells transduced by Ad-CACNA2D2 at the same MOIs (Figure 2) suggests that the mitochondria depolarization mediated by an elevated level of Ca^{2+} influx is an earlier event in CACNA2D2-induced apoptosis.

Cyt c release from mitochondria

Release of cyt c from the mitochondria plays an integral role in apoptosis. To evaluate whether cyt c release might be an integral part of CACNA2D2-mediated apoptosis in a process involving regulation of Ca^{2+} influx and interruption of the mitochondria membrane integrity, we performed Western blot analysis of cyt c in the fractionated mitochondria and cytosolic lysates in Ad-CACNA2D2-treated A549 cells (Figure 5). The release of cyt c from mitochondria to cytosol was detected in both the Ad-CACNA2D2-transduced A549 cells at an MOI of 2500 (viral particles/cell) vp/c (Figure 5a, lanes 3 and 9) and H460 cells at an MOI of 4000 vp/c (Figure 5a, lanes 6 and 12), but no significant changes in cyt c in the cytosol fraction were detected in untreated (PBS) (Figure 5a, lanes 1, 4, 7, and 10) and Ad-LacZ-transduced (Figure 5a, lanes 2, 5, 8, and 11) cells. No significant change in levels of the cyt c in both the mitochondria and cytosol fractions was observed in Ad-CACNA2D2-transduced H1299 cells (data not shown). Cyt c release began at 48 h after transduction and increased over time as demonstrated in Ad-CACNA2D2-transduced A549 cells (Figure 5b). The changes in cell morphology and subcellular localization of cyt c (probed with an anti-human cyt c monoclonal antibody) were demonstrated in fluorescence images of A549 cells transduced with Ad-CACNA2D2 (Figure 5c). The characteristic pattern of the mitochondria distribution of cyt c still remained 24 h after transduction (Figure 5c, panel a) but was lost 48 h after transduction at this MOI (Figure 5c, panel b). The release of cyt c from mitochondria into the cytosol and the typical nuclear changes because of apoptosis were evident 48 h after (Figure 5c, panel b) and 72 h after (Figure 5c, panel c) transduction. The accumulation of apoptotic cell populations was also detected 48 h after transduction and increased in time as shown by FACS with PI staining (Figure 5d). The timing of the CACNA2D2-induced cyt c release was sequential and matched the timing of CACNA2D2-induced changes in intracellular Ca^{2+} influx (Figure 3) and mitochondria membrane potential (Figures 4 and 5d).

Activation of caspase 3 and PARP

Activation of caspases and PARP by translocation of cyt *c* from mitochondria to the cytosol is one of the events that establishes the mitochondrion as an important regulator of cell life and death (von Ahsen *et al.*, 2000; Martinou and Green, 2001). Western blot analysis was performed to evaluate the activation of caspase 3 and PARP downstream of the mitochondria-mediated apoptotic pathway (Figure 6). The activation of both apoptotic executioners, caspase 3 (Figure 6a) and PARP (Figure 6b), was detected in Ad-CACNA2D2-transduced H460 and A549 cells, as demonstrated by the cleaved fragments of the procaspase3 and pro-PARP on the Western blot (Figure 6). These results provide further evidence that CACNA2D2-mediated apoptosis occurs via the mitochondrion.

Discussion

The protein product of the recently cloned CACNA2D2 gene is structurally related to the $\alpha2\delta2$ auxiliary subunit of the voltage-activated calcium channel (VACC) protein complex (Angeloni *et al.*, 2000; Gao *et al.*, 2000). Various VACC protein subunits such as the pore-forming $\alpha1$ unit and the auxiliary β, γ, and $\alpha2\delta$ subunits have been identified and partially characterized (Singer *et al.*, 1991; Castellano *et al.*, 1993; Brown and Gee, 1998; Burgess *et al.*, 1999; Felix, 1999, Hofmann *et al.*, 1999; Varadi *et al.*, 1999; Catterall, 2000; Lacinova *et al.*, 2000). The $\alpha2\delta2$ subunit (CACNA2D2) of VACC is a regulatory subunit (Gao *et al.*, 2000). Mutation of this gene has been found to lead to a phenotype characterized by epilepsy, ataxia, and alterations of calcium currents in cerebellar cells in mice, which is ultimately fatal (Barclay *et al.*, 2001). Although the exact physiological function of CACNA2D2 in nonexcitable cells remains unknown, functional studies of CACNA2D2 have revealed that the activity of CACNA2D2 protein may alter the conductance properties of the pore-forming $\alpha1$ unit as well as their membrane trafficking and, therefore dynamically regulates Ca^{2+} current through the VACC (Gao *et al.*, 2000; Hobom *et al.*, 2000; Hurley *et al.*, 2000; Klugbauer *et al.*, 1999). The very frequent and early loss of expression of CACNA2D2 together with a subset of genes in the 3p21.3 homozygous deletion region of human chromosome 3 in human lung and breast cancers suggest a link between the CACNA2D2 and the regulation of proliferation and cell death in lung cancer pathogenesis, possibly through the regulation of the VACC-mediated Ca^{2+} influx (Angeloni *et al.*, 2000; Gao *et al.*, 2000; Lerman and Minna, 2000). However, no direct evidence has been presented for this link. In this study, we focused on CACNA2D2-mediated apoptosis by adenoviral vector-mediated ectopic expression of the wt-CACNA2D2 gene in the CACNA2D2-deficient NSCLC cells. We presented indirect evidence to link the CACNA2D2-mediated apoptosis with the regulation of the intracellular calcium content, interruption of mitochondria membrane integrity, and activation of downstream

caspases.

Inhibition of tumor cell growth by ectopic expression of CACNA2D2 is concomitant with induction of apoptosis in these Ad-CACNA2D2-transduced NSCLC cells. A significant induction of apoptosis was observed 48 h after transduction. The cell lines most sensitive to CACNA2D2-induced apoptosis were A549 and H460, which contain a wt-p53 gene and are generally resistant to either the transduction of adenoviral vectors or to wt-p53-mediated cell death. Ad-CACNA2D2-transduced H358 cells, which carry a mutated p53 gene, showed remarkable inhibition of cell growth but no significant induction of apoptosis. H1299 cells, which are p53-null, were the most resistant to CACNA2D2-induced growth inhibition and apoptosis *in vitro* and *in vivo*. These results suggest a possible association of the CACNA2D2-mediated apoptosis with the activities of wt-p53, which is very interesting and needs to be explored further.

Based on the evidence that the activity of CACNA2D2 dynamically regulates Ca^{2+} currents in L- and T-type calcium channels (Klugbauer *et al.*, 1999; Gao *et al.*, 2000; Hobom *et al.*, 2000; Hurley *et al.*, 2000), we expected that overexpression of CACNA2D2 might result in an increase in the level of cytosolic Ca^{2+} influx. A significant increase in the basal level of the intracellular free Ca^{2+} was indeed detected in Ad-CACNA2D2-transduced H460 and A549 cells using sensitive free-Ca^{2+}-specific Fluo3-AM staining in a semiquantitative manner. Several factors, however, hinder the accurate determination of the kinetic events of the modulation of Ca^{2+} influx influenced by the adenoviral vector-mediated transient expression of CACNA2D2 protein. Gradual expression of the CACNA2D2 subunit after 24 h of transduction would cause the modulation of intracellular Ca^{2+} influx with time. Since Ca^{2+} is a multivalent messenger, several cytosolic Ca^{2+} binding proteins, such as calmodulin, can bind to the free Ca^{2+} to execute downstream effects on cellular processes, which would significantly reduce the availability of free Ca^{2+}; other Ca^{2+} effectors or mediators, such as calbindin-D, parvalbumin, and calretinin, can buffer the cytosolic increases of Ca^{2+} (Berridge *et al.*, 1998,2000). Furthermore, Ca^{2+} signals have a wide range of spatial and temporal distribution and so are capable of conveying signals in a very complex way (Lemasters *et al.*, 1998; Berridge *et al.*, 2000; Zhu *et al.*, 2000). Together, these factors make it difficult to detect even the global Ca^{2+} oscillations in our experimental setting; therefore, our data may not represent the accurate dynamic changes of intracellular Ca^{2+} contents and influx.

Mitochondria play a major role in apoptosis triggered by many stimuli. Disruption and permeation of the mitochondria membrane are general phenomena associated with the processes of apoptosis and necrotic cell death (Kroemer and Reed, 2000, Vieira *et al.*, 2000). An excessive

mitochondria Ca^{2+} influx has been suggested to be a potent cell death stimulus leading to mitochondria membrane depolarization and cyt c release (Reed and Kroemer, 2000; Vieira et al., 2000). Activation of caspases by translocation of cyt c from mitochondria to the cytosol is a downstream event through which the mitochondrion's role as a regulator of cell life and death has become unquestioned (Chen et al., 2000; von Ahsen et al., 2000; Martinou and Green, 2001). We demonstrated that ectopic expression of CACNA2D2 was associated with the accumulation of intracellular free Ca^{2+} and the collapse of the mitochondria membrane potential prior to cyt c release and nuclear apoptotic changes, suggesting a physiological effect of CACNA2D2 activity in regulating cell survival by indirectly altering the mitochondria membrane integrity in concomitance with cytosolic Ca^{2+} increase. Rupture of the outer membrane results in the release of many proteins such as cyt c and some caspases (Desagher and Martinou, 2000). However, whether this is the result of a direct effect of the CACNA2D2-mediated Ca^{2+} oscillations on mitochondria permeability needs to be further investigated. It would also be interesting to explore the CACNA2D2-mediated Ca^{2+}-signaling pathways involved in activation of the proapoptotic mediators such as Bad and Bax and inactivation of the antiapoptotic factors such as Bcl-2 and Bclx that convey the apoptotic signal to the mitochondrion (Gross et al., 1999; Vieira et al., 2000; von Ahsen et al., 2000).

Together, our results suggest that ectopic expression of CACNA2D2 is capable of inducing apoptosis in several NSCLC cell lines. The induction of apoptosis by CACNA2D2 activity is associated with the regulation of cytosolic Ca^{2+} contents and the activation of the mitochondria pathway. Further identification of the physiological functions of CACNA2D2 in unexcitable cells such as normal bronchial epithelial cells, the evaluation of the cellular modulation of endogenous and exogenous expression of CACNA2D2 in response to environmental stimuli such as DNA-damaging agents and oncogene activities in normal and tumor cells, and the characterization of the effects of CACNA2D2 activity on both L- and T-type calcium channels in the presence and absence of selective inhibitors of the various VACC subtypes will provide us insight into the molecular mechanisms in the CACNA2D2-mediated regulation of cell proliferation and cell death in the pathogenesis of lung cancers and other human cancers.

Materials and methods

Cell lines and cell culture

Four human NSCLC cell lines, A549 (homozygous for multiple 3p21.3 markers and wt-*p53*), NCI-H1299 (homozygous for multiple 3p21.3 markers and homozygous deletion of *p53*), NCI-H358 (retained

heterozygosity of multiple 3p21.3 markers and homozygous deletion of *p53*), and NCI-H460 (homozygous for multiple 3p21.3 markers and wt-*p53*), with varied 3p21.3 and *p53* gene status, and a normal human bronchial epithelial cell line (HBEC) or fibroblast cells were used for *in vitro* experiments. The multiple 3p21.3 markers located in the 630 kb region used for this analysis were described previously (Fondon *et al.*, 1998). The A549 line was maintained in Ham's F12 medium supplemented with 10% fetal calf serum. The H1299, H358, and H460 lines were maintained in RPMI-1640 medium supplemented with 10% fetal calf serum and 5% glutamine.

Recombinant adenoviral vectors

The recombinant Ad-CACNA2D2 was constructed using our recently developed ligation-mediated plasmid adenovirus vector construction system, named herein pAd-RAP and pAd-RAP-Shuttle. The CACNA2D2 was assembled as a mammalian gene expression cassette that is driven by a CMV promoter and tailed with a bovine growth hormone (BGH) poly (A) signal sequence. Sequences of the CACNA2D2 gene in the viral vectors were confirmed by automated DNA sequencing. A vector expressing the GFP (green fluorescence protein) gene (Ad-GFP) and a vector carrying the β-galactosidase gene *LacZ* (Ad-LacZ) were used to monitor the efficiency of transduction by the viral vectors and as nonspecific transgene expression controls. Ad-EV, an empty E1-deleted vector, was used as a negative control; Ad-p53, a vector containing the wt-*p53* gene, was used as a positive control for tumor suppression. Viral titers were determined by both optical density measurement (i.e. vp/ml) and plaque assay (i.e. plaque-forming units (PFU)/ml).

Animal experiments

All animals were maintained and animal experiments were performed under NIH and institutional guidelines established for the Animal Core Facility at the University of Texas MD Anderson Cancer Center. Procedures for H460 subcutaneous tumor inoculations in *nu/nu* mice were described previously (Ji *et al.*, 1999). When the average tumor size reaches about 0.5 cm in diameter, mice were injected intratumorally three times within a week with Ad-CACNA2D2 and control vectors at a dose of 3×10^{10} PFU (3×10^{12} vp)/tumor in a volume of 0.2 ml. Differences in tumor volumes between treatment groups were analysed with a mixed model ANOVA using the Statistica software (StatSoft Inc., Tulsa, OK, USA). A difference was considered to be statistically significant when $P=0.05$.

Analysis of CACNA2D2 gene Expression by RT–PCR

Total RNA samples were isolated from Ad-CACNA2D2-transduced

tumor cells using TRIZOL reagent (Life Technologies, Grand Island, NY, USA) as instructed by the manufacturer. The RT reaction was performed using a reverse transcription kit with the oligo-d(T)$_{16}$ as a primer under the conditions recommended by the manufacturer (Perkin-Elmer Applied Biosystems, Foster City, CA, USA). The RT–PCR products amplified with human total RNA as a template and glyceraldehyde-3-phosphate dehydrogenase (GAPDH) primers were used as an internal control. The primers for CACNA2D2 were 5'GACTGACCAACACCACTCTTCTC (sense, within CACNA2D2 cDNA) and 5'CTCATCGTACCTCAGCTCCTTCC (antisense, within the BGH poly (A) signaling region). The PCR was performed using an AmpliTaq PCR Kit and a 9600 PCR instrument according to the manufacturer's instructions (Perkin-Elmer Applied Biosystems).

Cell viability assay

Inhibition of tumor cell growth by treatment with Ad-CACNA2D2 and control vectors was analysed by quantitatively determining cell viability using an improved XTT assay (Roche Molecular Biochemicals, Indianapolis, IN, USA). Briefly, cells were plated in 96-well microtiter plates at 1×10^3 cells/well in 100 μl of medium. One day after the cells were plated, a 100-μl aliquot of medium containing individual adenoviral vectors at various multiplicities of infection MOI in units of vp/cell (vp/c) was placed into each sample well, and phosphate-buffered saline (PBS), Ad-EV, Ad-LacZ, and Adp53 were added as controls. On designated sampling days after transduction, cell growth and viability were quantified by XTT assay as described previously (Nishizaki *et al.*, 2001). The percentage of cell viability was calculated in terms of the absorbency of treated cells relative to the absorbency of untreated control cells. Experiments were repeated at least three times with quadruplicate samples for each treatment in each individual experiment.

Analysis of apoptosis and cell cycle kinetics

Induction of apoptosis in tumor cells treated with various adenoviral vectors was analysed by flow cytometry (FACS) using terminal deoxynucleotidyl transferase-mediated dUTP nickend labeling (TUNEL) reaction with fluorescein (FITC)-labeled dUTP (Roche Molecular Biochemicals, Mannheim, Germany). Briefly, cells were plated in six-well plates (1×10^6 cells/well) and treated by various Ad-CACNA2D2 vectors; PBS, Ad-EV, Ad-LacZ, and Adp53 were used as controls. At designated times after transduction, cells were harvested and washed in PBS. Cells were processed for FACS analysis to determine apoptosis and cell cycle kinetics as described previously (Ji *et al.*, 1999).

Measurement of cytosolic free calcium

The intracellular free Ca^{2+} was measured by FACS and fluorescence image analysis with free-Ca^{2+}-sensitive Fluo3-AM green fluorescent staining (Molecular Probes, Eugene, OR, USA) in Ad-CACNA2D2-transduced A549 and H460 cells. Cells were cultured in 100 mm dishes at about 5×10^6 cells/dish and transduced with adenoviral vectors at varied MOIs. After 24 and 48 h of transduction, cells were collected and washed once with 1×HBSS supplemented with 1 mM Ca^{2+}, 1 mM Mg^{2+}, and 1% fetal bovine serum (FBS). The Fluo3-AM stock solution was prepared by first dissolving 50 μg of Fluo3-AM dye in 20 μl of DMSO containing 20% of the detergent Fluronic F-127 (Molecular Probes) and then mixing it with 117 μl of FBS. The cells were resuspended in 1 ml of HBSS containing the Fluo3-AM dye in a final concentration of 2.5–5.0 μg/ml, depending on the cell type. The anion carrier inhibitor probenecid was added at a final concentration of 4 mM to minimize the dye leakage. The cells were incubated for 45 min at room temperature on an orbital shaker in the dark. Cells were spun down by centrifugation for 5 min at 1500 r.p.m. and washed once with HBSS. Cells were gently resuspended in HBSS containing 4 mM of probenecid and then incubated for 20 min in the dark to allow cellular esterases to cleave the acetoxymethyl group of Fluo3-AM. Fluorescence intensity in the stained cells was measured by FACS analysis at an excitation wavelength of 488 nm and an emission wavelength of 530 nm. Experiments were performed three times independently. To evaluate the conditions of dye loading, 2 μg of ionomycin, an ionophoric antibiotic synthesized by *Streptomyces conglobatus* sp. (Calbiochem, Fremont, CA, USA), was added to each of the cell samples in a separate tube, and the dynamic fluorescence emission was measured by FACS after baseline fluorescence was assessed. For fluorescence imaging analysis of Fluo3-AM stained cells, the cells were cultured in chamber slides (Falcon), and then treated and stained with Fluo3-AM with the same procedure as was described for FACS analysis. The stained cells were examined under a microscope (Nikon Labophot 2) equipped with a digital camera (Nikon DMX1200, Tokyo, Japan) and the analysis software (Nikon ACT-1 V2.0).

Analysis of mitochondria membrane potential by FACS with JC-1 staining

Changes in mitochondria membrane potential in adenoviral vector-transduced cells were measured by flow cytometry with JC-1 (5,5',6,6'-tetrachloro-1,1'3,3'-tetraethylbenzimidazolyl-carbocyanine iodide) staining (Molecular Probes, Eugene, OR, USA). JC-1 exists as a monomer at low concentrations or at low membrane potential and emits green fluorescence at 527 nm. However, at higher concentrations or higher membrane potentials, JC-1 forms J-aggregates and emits maximum red fluorescence at ~590 nm. The measurement of the ratio of the red to green JC-1 fluorescence in cells by flow cytometry is a

sensitive and specific method for monitoring changes in mitochondria potential in living cells during induction of apoptosis by various agents (Ankarcrona et al., 1995; Cossarizza et al., 1995). Cells were cultured in six-well plates and, after reaching ~70% confluence, transduced with various adenoviral vectors at varied MOIs. Cells were collected by centrifugation for 5 min at 2000 r.p.m. at 4°C and resuspended in complete medium containing 10 mg/ml JC-1 at a density of 5×10^5 cells/ml. The cells were incubated for 10 min at room temperature in the dark, washed twice with cold PBS, resuspended in 400 ml of PBS, and analysed immediately by flow cytometry.

For in situ fluorescent staining with JC-1, cells were cultured in chamber slides. At designated time points, the medium was removed and the cells incubated in reduced serum Opti-MEM-I medium (GIBCO BRL, Grand Island, NY, USA) containing 10 μg/ml of JC-1 for 10 min in the dark. After washing and air-drying, stained cells were immediately examined by fluorescence microscopy.

Western blot analysis

Western blot analysis was performed to evaluate the expression of CACNA2D2 protein, the release of cyt *c*, activation of caspase 3 and PARP, and other protein expression in Ad-CACNA2D2 and control vector-transduced cells. For the preparation of crude cell lysates, cells were suspended in SDS–PAGE running buffer containing a complete set of proteinase inhibitors (Roche Molecular Biochemials, Mannheim, Germany) and lysed for 20 min at 4°C. Cell lysates were passed through a 25-gauge needle and briefly sonicated twice for 30 s. For cyt *c* analysis, cell fractionation was performed to separate mitochondria-enriched fractions from cytosol fractions using an Apo-Alert Cell Fractionation Kit (ClonTech, Palo Alto, CA, USA) according to the manufacturer's instructions. Fractionated cell lysates were kept in equal volume in 2×lysis buffer supplemented with 62.5 mM urea. Protein concentrations were assayed using the Bio-Rad protein assay reagent (Bio-Rad Laboratories, Hercules, CA, USA). The crude cell lysates (about 50 μg) were used in standard SDS–PAGE and Western blot analysis.

Immunofluorescence staining

Immunofluorescence staining was performed in cells cultured in chamber slides. At designated time points, the cells were washed twice with cold PBS fixed in 4% paraformaldehyde for 15 min at 4°C and made permeable by incubation for 5 min in a solution containing 0.1% Triton X-100 and 0.1% sodium citrate. The cells were incubated with the primary monoclonal mouse anti-cyt C antibody for 60 min at 37°C, and after washing were incubated with the FITC-labeled secondary rabbit anti-mouse IgG antibodies for 60 min. After three washing steps

in 0.1% Tween 20–PBS solution and air-drying, the slides were mounted with aqueous mounting medium containing 50 μg/ml of PI for nuclear staining and immediately examined under a fluorescence microscope.

Statistics

All the experiments were repeated at least two times with duplicates or triplicates of samples. The results were expressed as mean±s.d. Student's two-sided *t*-test was used to compare the values of the test and control samples. A value of $P<0.05$ was taken as significant.

References

Angeloni D, Wei MH, Duh FM, Johnson BE and Lerman MI. (2000). *Mol. Cell Probes*, 14, 53–54.

Ankarcrona M, Dypbukt JM, Bonfoco E, Zhivotovsky B, Orrenius S, Lipton SA and Nicotera P. (1995). *Neuron.*, 15, 961–973. PubMed

Barclay J, Balaguero N, Mione M, Ackerman SL, Letts VA, Brodbeck J, Canti C, Meir A, Page KM, Kusumi K, Perez-Reyes E, Lander ES, Frankel WN, Gardiner RM, Dolphin AC and Rees M. (2001). *J. Neurosci.*, 21, 6095–6104. PubMed

Berridge MJ, Bootman MD and Lipp P. (1998). *Nature*, 395, 645–648. Article PubMed

Berridge MJ, Lipp P and Bootman MD. (2000). *Nat. Rev. Mol. Cell. Biol.*, 1, 11–21. Article PubMed

Brown JP and Gee NS. (1998). *J. Biol. Chem.*, 273, 25458–25465.

Burgess DL, Davis CF, Gefrides LA and Noebels JL. (1999). *Genome Res.*, 9, 1204–1213. Article PubMed

Castellano A, Wei X, Birnbaumer L and Perez-Reyes E. (1993). *J. Biol. Chem.*,

268, 3450–3455.

Catterall WA. (2000). *Annu. Rev. Cell Dev. Biol.*, **16**, 521–555. Article PubMed

Chen Q, Gong B and Almasan A. (2000). *Cell Death Differ.*, **7**, 227–233. Article PubMed

Cossarizza A, Cooper EL, Quaglino D, Salvioli S, Kalachnikova G and Franceschi C. (1995). *Biochem. Biophys. Res. Commun.*, **214**, 503–510.

Desagher S and Martinou JC. (2000). *Trends Cell Biol.*, **10**, 369–377. Article PubMed

Felix R. (1999). *Receptors Channels*, **6**, 351–362.

Fondon JW, Mele GM, Brezinschek RI, Cummings D, Pande A, Wren J, O'Brien KM, Kupfer KC, Wei MH, Lerman M, Minna JD and Garner HR. (1998). *Proc. Natl. Acad. Sci. USA*, **95**, 7514–7519. PubMed

Gao B, Sekido Y, Maximov A, Saad M, Forgacs E, Latif F, Wei MH, Lerman M, Lee JH, Perez-Reyes E, Bezprozvanny I and Minna JD. (2000). *J. Biol. Chem.*, **275**, 12237–12242. Article PubMed

Gross A, McDonnell JM and Korsmeyer SJ. (1999). *Genes Dev.*, **13**, 1899–1911. PubMed

Hobom M, Dai S, Marais E, Lacinova L, Hofmann F and Klugbauer N. (2000). *Eur. J. Neurosci.*, **12**, 1217–1226.

Hofmann F, Lacinova L and Klugbauer N. (1999). *Rev. Physiol. Biochem. Pharmacol.*, **139**, 33–87.

Hurley JH, Cahill AL, Currie KP and Fox AP. (2000). *Proc. Natl. Acad. Sci. USA*, **97**, 9293–9298. Article PubMed

Ji L, Fang B, Yen N, Fong K, Minna JD and Roth JA. (1999). *Cancer Res.*, **59**, 3333–3339. PubMed

Kao JP, Harootunian AT and Tsien RY. (1989). *J. Biol. Chem.*, **264**, 8179–8184. PubMed

Klugbauer N, Lacinova L, Marais E, Hobom M and Hofmann F. (1999). *J. Neurosci.*, **19**, 684–691.

Kochegarov AA, Beylina SI, Matveeva NB, Leontieva GA and Zinchenko VP. (2001). *Comparative Biochem. Physiol.* **128**(Part A), 279–288.

Kroemer G and Reed JC. (2000). *Nat. Med.*, **6**, 513–519. Article PubMed

Lacinova L, Klugbauer N and Hofmann F. (2000). *Gen. Physiol. Biophys.*, **19**, 121–136.

Lam M, Dubyak G, Chen L, Nunez G, Miesfeld RL and Distelhorst CW. (1994). *Proc. Natl. Acad. Sci. USA*, **91**, 6569–6573. PubMed

Lemasters JJ, Nieminen AL, Qian T, Trost LC, Elmore SP, Nishimura Y, Crowe RA, Cascio WE, Bradham CA, Brenner DA and Herman B. (1998). *Biochim. Biophys. Acta.*, **1366**, 177–196. Article PubMed

Lerman MI and Minna JD. (2000). *Cancer Res.*, **60**, 6116–6133. PubMed

Marais E, Klugbauer N and Hofmann F. (2001). *Mol. Pharmacol.*, **59**, 1243–1248.

Martinou JC and Green DR. (2001). *Nat. Rev. Mol. Cell Biol.*, **2**, 63–67. Article PubMed

Nishizaki M, Meyn RE, Levy LB, Atkinson EN, White RA, Roth JA and Ji L. (2001). *Clin. Cancer Res.*, **7**, 2887–2897.

Raveh T and Kimchi A. (2001). *Exp. Cell Res.*, **264**, 185–192.

Reed JC and Kroemer G. (2000). *Cell Death Differ.*, **7**, 1145. Article PubMed

Rutter GA and Rizzuto R. (2000). *Trends Biochem. Sci.*, **25**, 215–221.

Singer D, Biel M, Lotan I, Flockerzi V, Hofmann F and Dascal N. (1991). *Science*, **253**, 1553–1557. PubMed

Toyota M, Ho C, Ohe-Toyota M, Baylin SB and Issa JP. (1999). *Cancer Res.*, **59**, 4535–4541.

Ueki T, Toyota M, Sohn T, Yeo CJ, Issa JP, Hruban RH and Goggins M. (2000). *Cancer Res.*, **60**, 1835–1839. PubMed

Varadi G, Strobeck M, Koch S, Caglioti L, Zucchi C and Palyi G. (1999). *Crit. Rev. Biochem. Mol. Biol.*, **34**, 181–214.

Vieira HL, Haouzi D, El Hamel C, Jacotot E, Belzacq AS, Brenner C and Kroemer G. (2000). *Cell Death Differ.*, **7**, 1146–1154.

von Ahsen O, Waterhouse NJ, Kuwana T, Newmeyer DD and Green DR. (2000). *Cell Death Differ.*, **7**, 1192–1199.

Walker D and De Waard M. (1998). *Trends Neurosci.*, **21**, 148–154. Article PubMed

Wang HG, Pathan N, Ethell IM, Krajewski S, Yamaguchi Y, Shibasaki F, McKeon F, Bobo T, Franke TF and Reed JC. (1999a). *Science*, **284**, 339–343. Article PubMed

Wang M, Offord J, Oxender DL and Su TZ. (1999b). *Biochem. J.*, **342**, 313–320.

Zhu L, Ling S, Yu XD, Venkatesh LK, Subramanian T, Chinnadurai G and Kuo TH. (1999). *J. Biol. Chem.*, **274**, 33267–33273. Article PubMed

Zhu LP, Yu XD, Ling S, Brown RA and Kuo TH. (2000). *Cell Calcium*, **28**, 107–117.

Zochbauer-Muller S, Fong KM, Virmani AK, Geradts J, Gazdar AF and Minna JD. (2001). *Cancer Res.*, **61**, 249–255. PubMed

Figures

Figure 1 Adenoviral vector-mediated ectopic expression of CACNA2D2 gene inhibited NSCLC cell growth *in vitro*. (**a**) Expression of the CACNA2D2 gene in Ad-CACNA2D2 (CACN)-transduced NSCLC cells by RT–PCR analysis. Total RNAs were prepared from H1299, A549, H460, and H358 cells transduced by the Ad-CACNA2D2 vector for 48 h at MOIs of 1000 and 2500 vp/c, respectively, and the RNA prepared from cells transfected with a CACNA2D2-expressing plasmid DNA (pLJ58) was used as a positive control. The RNA samples were treated with DNAse prior to the RT reaction. (**b**) Western blot analysis of expression of CACNA2D2 protein. The crude protein lysates were prepared from NSCLC cells treated in the same way as described for RNA sample preparation in **a**. The rabbit anti-CACNA2D2 polyclonal antibodies were used for blotting. (**c**) XTT assay shows the effect of ectopic expression of CACNA2D2 on tumor cell viability. Cells from NSCLC cell lines A549, H460, H1299, and H358 were tranduced with Ad-CACNA2D2 vectors (CACN) at varied MOIs: 2500 for A549, 4000 for H460, 1000 for H1299, and 2000 vp/c for H358 cells. Untreated (PBS), Ad-EV (EV) treated, and Ad-LacZ(LacZ)-treated cells were used as negative controls and Adp53(p53)-treated cells as a positive control, at the same MOIs as CACN-treated cells for each cell line. Cell viability was calculated relative to that of untreated (PBS) controls. Differences were significant in the CACN-transduced cells compared to the untreated (PBS) control cells (P=0.021 in H1299, P<0.0001 in H358, H460, and A549 cells) and to the Ad-LacZ-transduced cells (P<0.0001 in H358, H460, and A549 cells) after 5 days of transduction. Differences between CACN-treated cells and controls were not significant in the H1299 cell line. (**d**) Effects of intratumoral administration of CACN on growth of human lung cancer H460 subcutaneous tumors in *nu/nu* mice. Results were reported as the mean±s.d. in five to 10 mice for each treatment group. Tumor volumes were normalized by the percentage increase of tumor sizes after treatment relative to those at the beginning of the treatment in each group. Mean tumor volumes±s.e. from these experiments are shown. The differences of the tumor volumes in the CACN-treated mice versus the PBS- and Ad-LacZ-treated controls were significant (P<0.0001 and 0.015, respectively)

Figure 2 Apoptosis is induced by adenoviral vector-mediated expression of CACNA2D2 *in vitro*. NSCLC cell lines A549 (**a**), H460 (**b**), H1299 (**c**), and H358 (**d**) were tranduced with Ad-CACNA2D2 vectors (CACN) at varied MOIs for each line as shown in Figure 1. Untreated (PBS), Ad-EV (EV)-treated, and Ad-LacZ (LacZ)-treated cells were used as negative controls and Ad-p53(p53)-treated as a positive control. The percentage of apoptosis (TUNEL-positive) in cells transduced for 2 or 5 days, respectively, was determined by FACS analysis. Induction of apoptosis was significant in CACN-treated A549, H460, and H358 cells compared to those in PBS-treated (P=0.0004, 0.0321, and 0.0003, respectively) and to those in Ad-LacZ-treated (P=0.021, 0.048, and 0.027, respectively) controls 5 days after transduction. Differences in induction of apoptosis were not significant (P>0.05) between CACN-treated cells and controls in A549, H460, and H358 cell lines at 48 h post-transduction and in H1299 at both 48 and 120 h post-transduction

Figure 3 Ectopic expression of CACNA2D2 increased the level of the intracellular free calcium. (**a**) Fluorescence image analysis of free cytosolic Ca^{2+} in Ad-CACNA2D2 (CACN)-transduced H460 and A549 cells by Fluo 3-AM staining. Images of the CACN-treated H460 cells at an MOI of 4000 vp/c (**c**) and A549 cells (**g**) at an MOI of 2500 vp/c, untreated (PBS) (**a** and **e**) and Adp53 (p53)-treated cells (**b** and **f**), and ionomycin-treated control cells (**d** and **h**) at 48 h post-treatment are

shown. (b) Free Ca^{2+}-specific fluorescence emission was quantified by FACS analysis with Fluo 3-AM staining. Cells were treated as described in panel. (a) The differences of free intracellular Ca^{2+} are expressed semiquantitatively through the differences in relative fluorescence. The increase in free cytosolic Ca^{2+} was significant in the CACN-treated H460 ($P=0.015$ and 0.032) and A549 cells ($P=0.001$ and 0.002), but not significant in H1299 cells ($P=0.785$ and 0.865) compared with the increase seen with untreated (PBS) and p53-treated controls

Figure 4 Ectopic expression of CACNA2D2 reduced the mitochondria membrane potential. (a) Changes in the mitochondria membrane potential in Ad-CACNA2D2-transduced A549 cells are revealed by FACS analysis with JC-1 staining. A549 cells were transduced with adenoviral vectors for 6, 24, 48, and 72 h at an MOI of 2500 vp/c. Fluorescence emission of red at 590 nm (indicating high membrane potential and aggregation of JC-1 dye) and green at 530 nm (indicating the collapse of membrane potential and the monomer of JC-1 dye) were measured by FACS. CACN (n, o, p, q)- and p53 (j, k, l, m)-transduced cells showed mitochondria membrane depolarization as evidenced by the fluorescence emission shift to the longer wavelength of green. PBS (a, b, c, d)- and LacZ (e, f, g, h)-transduced cells did not show a marked shift to the right. (b) Relative green fluorescence was higher in CACN-transduced A549, H460, and H1299 cells than in untreated (PBS) control cell. The decrease of the mitochondria membrane potential or depolarization is significant in the CACN-transduced A549 cells ($P=0.002$) and H460 ($P=0.005$) but not in H1299 cells after 48 h of transduction or in the untreated (PBS) control cells

Figure 5 Western blotting was used to analyse cyt c release from mitochondria to cytosol in Ad-CACNA2D2-transduced cells. (a) Western blot of cyt c in CACN-transduced A549 and H460 cells. Cells were transduced with adenoviral vectors at an MOI of 2500 vp/c for A549 and MOI of 4000 vp/c for H460 for 48 h, and untreated (PBS) (lanes 1 and 4) and Ad-LacZ (LacZ)-transduced (lanes 2 and 5) cells were used as controls. Immunoblotting for cyt c was performed in fractionated lysates of mitochondria (lanes 1–6) and cytosol (lanes 7–12). Immunoblots of COX IV (I) were used as a mitochondria enzyme marker and β-actin as an internal loading control. (b) Time course of cyt c release in Ad-CACNA2D2-transduced A549 cells. (c) Immunofluorescence image analysis of the subcellular rearrangement of mitochondria and translocation of cyt c in Ad-CACNA2D2-transduced A549 cells. Mitochondria were probed with an FITC-labeled cyt c antibody (green) and the nucleus was counterstained with PI (red). (d) Timetable of induction of apoptosis in Ad-CACNA2D2-transduced A459 cells by FACS analysis with PI staining for DNA content. The percentage of induction of apoptosis was indicated by the increase of the $SubG_0$-G_1 cell populations (shown by a bar in each plot)

Figure 6 Downstream caspase 3 and PARP are activated by ectopic expression of the CACNA2D2 gene. (a) Western blot analysis of caspase 3. The whole cell lysate was prepared from Ad-CACNA2D2 (CACN)-transduced H460 cells (lanes 1–3) at an MOI of 4000 vp/c and A549 (lanes 5 and 6) cells at an MOI of 2500 vp/c after 72 h of transduction, and untreated (PBS) and Ad-LacZ (LacZ)- or Ad-p53 (p53)-transduced cells were used as controls. The cleaved procaspase 3 was indicated by an arrow. (b) Western blot analysis of PARP. Cells were transduced by Ad-CACNA2D2 (CACN) at the same MOI as described in a for each cell line. The cleaved PARP is indicated by the immunoblotting complexes of about 85 kDa. β-actin was used as an internal loading control

Persistent Transgene Expression Following Intravenous Administration of a Liposomal Complex: Role of Interleukin-10-Mediated Immune Suppression

Isao Ito,* Tomoyuki Saeki,† Imran Mohuiddin, Yuji Saito,†
Cynthia D. Branch, Ara Vaporciyan, Jack A. Roth, and Rajagopal Ramesh‡

*Department of Thoracic and Cardiovascular Surgery, The University of Texas M. D. Anderson Cancer Center, Houston,
TX 77030, USA*

*Current address: Department of Surgery, Tokai University School of Medicine, Ooiso Hospital, Kanagawa, Japan.
†Current address: Department of Surgery, Jikei University School of Medicine, Tokyo, Japan.

‡To whom correspondence and reprint requests should be addressed at the Department of Thoracic and Cardiovascular Surgery,
The University of Texas M. D. Anderson Cancer Center, 1515 Holcombe Boulevard, Box 445,
Houston, TX 77030, USA. Fax: (713) 794-4901. E-mail: rramesh@mdanderson.org.*

Studies conducted in non-tumor-bearing, immunocompetent mice have shown that intravenous administration of liposome–DNA complex elicits an inflammatory response that results in a failure to sustain adequate transgene expression. In the present study, however, we investigated the effects of a cationic liposomal DOTAP:cholesterol (DOTAP:Chol)–DNA complex on cytokine production and transgene expression in both experimental lung tumor-bearing (TB) mice and non-tumor-bearing (NTB) syngeneic mice and nude mice. Intravenous injection of DOTAP:Chol–luciferase (*luc*) DNA complex resulted in tumor necrosis factor-α levels that were 50% lower and interleukin-10 levels that were 50–60% higher in TB mice than in NTB mice. Furthermore, a significant increase in luc expression ($P = 0.001$) that persisted for 7 days was observed in TB mice. In contrast, luc expression decreased significantly from day 1 to day 2 in NTB mice. Also, luc expression was two- to threefold higher in TB mice that were given multiple injections of DOTAP:Chol-*luc* complex than in mice who received a single injection. In contrast, luc expression was significantly suppressed following multiple injections in NTB mice ($P = 0.01$). Further analysis revealed IL-10 protein expression by the tumor cells in TB mice. Injection of anti-IL-10 antibody in TB mice resulted in a significant decrease in luc expression ($P = 0.01$) compared with that in mice injected with a control antibody. Based on these findings, we conclude that transgene expression persists in TB mice and is partly mediated by IL-10. Additionally, multiple injections of liposome–DNA complex can increase transgene expression in TB mice. These findings have clinical applications in the treatment of cancer.

Key Words: gene therapy, liposome, IL-10, cancer, cytokines, inflammation, lung,
gene expression

INTRODUCTION

The development of efficient nonviral vectors that can deliver therapeutic genes when injected systemically will provide novel therapeutic options for the treatment of disseminated cancers. However, recent studies have demonstrated that liposomal vectors elicit an inflammatory response when injected systemically resulting in toxicity [1–7]. Induction of inflammatory responses due to the presence of immunostimulatory CpG sequences in plasmid DNA has been reported previously [8–12].

Associated with the inflammatory response is the production of proinflammatory cytokines (tumor necrosis factor- (TNF-α), interleukin-1 (IL-1), IL-6), which in turn have been shown to inhibit transgene expression [9,13]. Failure to achieve sustained transgene expression following repeated injections has also been attributed to the production of these proinflammatory cytokines [13]. Furthermore, a 3- to 4-day interval between injections was shown to be necessary to achieve sustained gene expression [14]. This need for injections at intervals has

been attributed to the cells' "refractory" state [14]. Thus, the inability to increase transgene expression following repeated injections has been a major obstacle in the development of therapeutic applications of liposomes. Likewise, reducing the number of CpG sequences in the plasmid DNA has been shown to reduce the inflammatory response and increase transgene expression [15]. These results, however, were obtained from studies of non-tumor-bearing (NTB), immunocompetent animals.

In contrast to these reports, we recently demonstrated effective gene transfer to experimental lung tumors in mice following intravenous injections of extruded DOTAP:cholesterol (DOTAP:Chol)–DNA:liposome complex [16]. In that study, although animals were treated with repeated injections, the relative effectiveness of multiple treatments was not studied. However, the major difference between the results of our study and those of others is that we conducted experiments in tumor-bearing (TB) animals, while others studied NTB animals. It is therefore possible that the pathophysiological condition of the animal may influence transgene expression following intravenous administration of the liposome:DNA complex.

Several preclinical and clinical studies have demonstrated functional alterations of immune cells (macrophages, neutrophils, and T cells) resulting in immune suppression in lung cancer [17–21]. These alterations have been attributed to several factors, including the production of immunosuppressive factors by tumor cells [22–25] and alterations in the immune cell receptors [26]. On the basis of these reports, we speculated that TB and NTB animals might respond differently to liposome:DNA complexes administered intravenously.

In the present study, we investigated the effects of intravenous administration of DOTAP:Chol–DNA complex on the cytokine profile and transgene expression of lung TB and NTB immunocompetent mice and nude mice.

RESULTS

Cytokine Expression Following Intravenous Injection of DOTAP:Chol–luciferase (luc) DNA Complex

Prior to the start of the experiment, we established lung tumors by injecting 1×10^6 UV2237m or A549 cells intravenously via the tail vein into female C3H and nude mice, respectively. Ten to fifteen days after injection of tumor cells, we treated the animals with DOTAP:Chol-luc complex. Note that at this time the tumors are well established in the lungs and can be detected histologically (data not shown). Animals receiving no treatment served as controls. In a separate but parallel set of experiments, NTB animals were also untreated or treated with DOTAP:Chol-luc complex.

We analyzed serum samples from NTB and lung TB C3H mice injected with DOTAP:Chol-luc DNA complex

for cytokine levels at regular time intervals. TNF-α, IL-1α, interferon-γ (IFN-γ), and IL-10 were produced by TB and NTB mice, with maximum peak levels observed in both groups at 2 h for TNF-α and at 6 h for IFN-γ (Fig. 1A). We observed maximum levels of IL-10 expression at 12 and 24 h in both groups. However, TNF-α levels were 50% lower in TB mice than in NTB mice. In contrast, IL-10 levels were 50–60% higher in TB mice (Fig. 1A). The expression of cytokines was time dependent over the 24-h postinjection period. IL-1α levels did not differ significantly in animals from the two groups. Cytokine levels except those of IL-1α were not detected in control animals that were not treated, were treated with naked plasmid DNA, or were treated with an empty liposome (data not shown).

To examine whether a similar phenomenon occurred in other tumor models we also determined serum cytokine levels in A549 lung TB nude mice and compared them to NTB nude mice (Fig. 1B). Both TB and NTB nude mice produced TNF-α, IL-1α, IFN-γ, and IL-10. The time courses for production of these cytokines were identical to those observed in C3H mice described above, with maximum production occurring at 2 h for TNF-α and at 6 h for IFN-γ. Similarly, we observed maximum levels of IL-10 expression at 12 and 24 h in TB and NTB mice. However, the levels of the cytokine produced in nude mice differed from the levels produced in C3H mice (Figs. 1A and 1B). Furthermore, TNF-α levels were moderately reduced in TB nude mice compared to NTB mice. The difference in the reduction of TNF-α levels in TB C3H mice and TB nude mice can be attributed to strain difference. However, other possibilities may exist and need additional investigation. In TB C3H mice we observed a significant increase in IL-1α at 12 h compared to NTB mice. This increase in IL-1α levels is not clear and needs additional investigation. These results demonstrate that increased IL-10 is produced in TB mice compared to NTB mice following injection of DOTAP:Chol–DNA complex.

Transgene Expression Persists in Tumor-Bearing Mice Following a Single Intravenous Injection of DOTAP:Chol-luc DNA Complex

To determine transgene expression in vivo, we injected lung TB and NTB C3H mice intravenously via the tail vein with DOTAP:Chol-luc DNA complex and removed their lungs at different times and analyzed them for luc activity. We observed luc expression in both TB and NTB mice, with maximal gene expression occurring 24 h after treatment in both groups (Fig. 2A). However, luc expression in NTB mice had decreased by 48 h after treatment and reached baseline levels by 72 h; luc expression remained at baseline through day 7. In contrast, levels of luc activity remained significantly higher than baseline ($P = 0.01$) in TB animals through
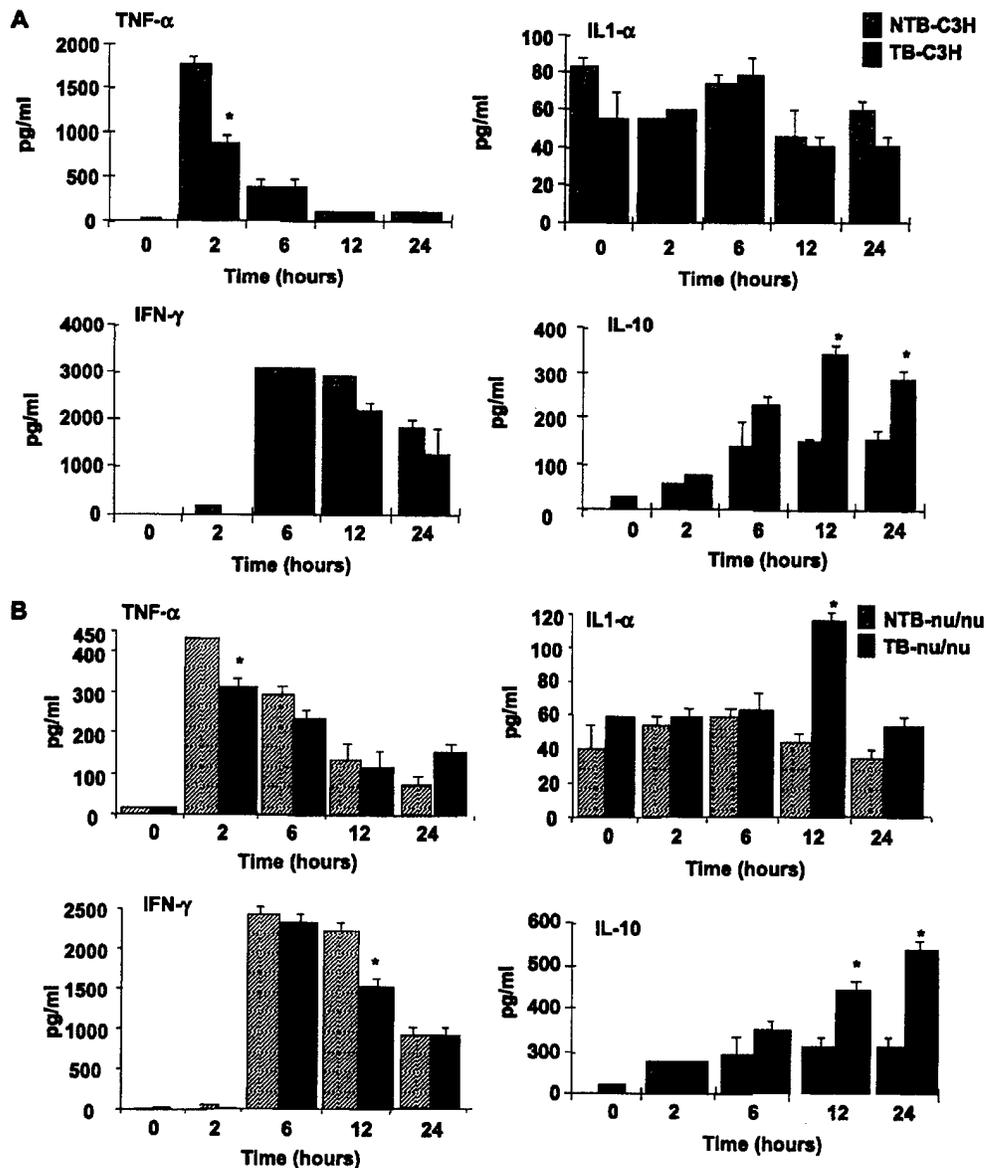
FIG. 1. Cytokine profile following systemic injection of DOTAP:Chol-*luc* DNA complex. Serum was collected from lung TB and NTB mice at 0, 2, 6, 12, and 24 h after injection of DOTAP:Chol-*luc* DNA complex (50 μg) and was assayed for cytokines (TNF-α, IL-1α, IFN-γ, IL-10) using ELISA. Untreated TB and NTB animals served as controls from each group. (A) Cytokine profile in UV2337m TB and NTB mice. (B) Cytokine profile in A549 lung TB and NTB mice. Data represent the average cytokine levels in four animals per group per time point.

day 7. However, a trend in decline (50%) of luc expression was observed on day 7 compared to day 1 in TB animals.

We performed an analysis of transgene expression in A549 lung TB and NTB nude mice. We observed increased luc expression at 24 h in both groups after treatment (Fig. 2B). However, significant levels of luc expression persisted in TB mice until day 7 compared to NTB mice. Although luc expression in NTB mice did not reach baseline levels as observed in C3H mice, luc expression was significantly reduced by day 3 compared to day 1. These results demonstrate that persistent trans-
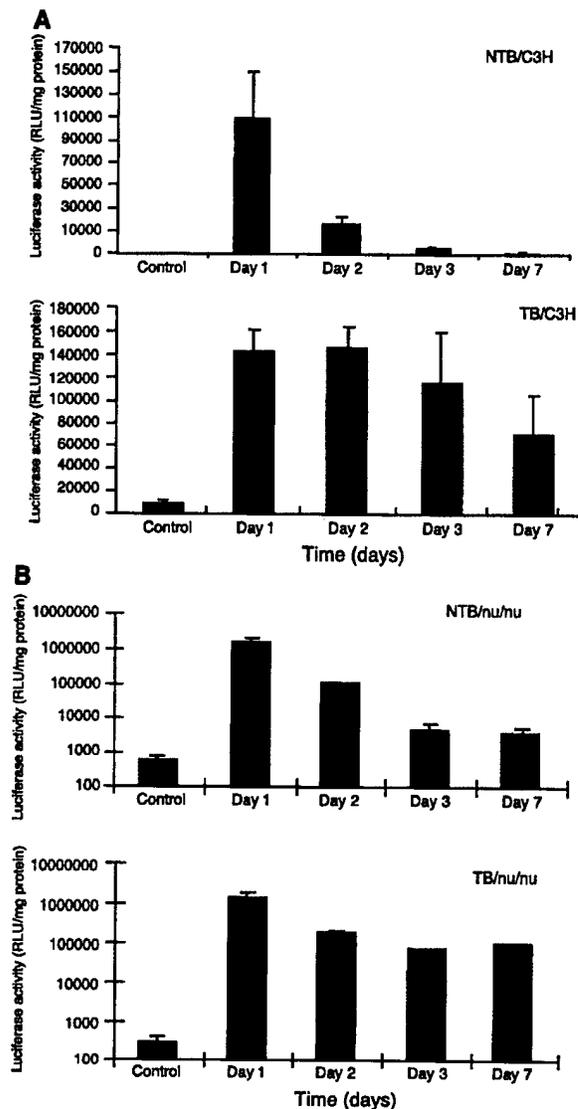
FIG. 2. Persistent transgene expression occurs in TB animals. (A) UV2237M TB and NTB C3H mice and (B) A549 TB and NTB nude mice were injected with DOTAP:Chol-*luc* DNA complex via the tail vein. Their lungs were resected on days 1, 2, 3, and 7 after treatment and analyzed for luc expression. Luc activity is expressed as relative light units (RLU) per milligram of total protein. Each time point represents the average luc activity in four animals. Bars represent standard deviation.

gene expression occurs in TB mice compared to NTB mice.

Repeated Injections of DOTAP:Chol-*luc* DNA Complex Result in Increased Transgene Expression

We next evaluated the effects of repeated injections on transgene expression in both lung TB and NTB C3H mice

and nude mice. We injected the animals via the tail vein with the DOTAP:Chol-*luc* DNA complex either one time or daily for 3 consecutive days. We analyzed lungs for luc activity 48 h after injection. In C3H mice luc expression was observed in both TB and NTB mice. In TB C3H mice, however, luc expression was twofold greater ($P = 0.001$) in mice treated three times than in mice treated once (Fig. 3A). In contrast, NTB mice treated three times expressed significantly lower levels of luc than did those treated only once ($P = 0.01$). Similarly, analysis of luc expression in TB nude mice and NTB nude mice demonstrated expression of luc expression (Fig. 3B). TB nude mice that received three treatments demonstrated threefold increase in luc expression compared to mice treated once ($P = 0.001$). In contrast, NTB mice that received three treatments showed decreased luc expression compared to mice receiving a single treatment. Thus, expression of luc in TB mice receiving multiple treatments was higher than in TB mice receiving a single treatment. Furthermore, luc expression in TB mice receiving multiple treatments was higher than in NTB mice that received multiple treatments. These results demonstrate that repeated injections of DOTAP:Chol–DNA complex in TB mice results in increased transgene expression and are in agreement with our previous results [16].

Lung Tumor Cells Express IL-10

To determine whether tumor cells contributed to the production of IL-10, we stained lungs from UV2237m TB and NTB mice for murine IL-10. TB lungs, especially tumor cells, stained intensely for IL-10 (Fig. 4). We also observed staining of infiltrating lymphocytes in the lung tumor sections. In contrast, NTB lung cells showed very little IL-10 expression. We also observed IL-10 protein expression in human lung tumor cell lines and in clinical specimens from patients diagnosed with lung cancer (data not shown). To determine further the levels of IL-10 produced by UV2237m tumor cells, we analyzed cell culture supernatants for IL-10 production by ELISA. The level of IL-10 produced by murine tumor cells was approximately 30 pg/ml (data not shown). These results demonstrate that tumor cells in addition to lymphocytes produce IL-10.

Alveolar Macrophages from Lung TB Mice Are Less Responsive to Stimulation

Since we had observed IL-10 production by lung TB mice, we examined the suppressive effects of IL-10 on alveolar macrophages by macrophage activation assay. We plated alveolar macrophages isolated from lung TB and NTB C3H mice in 96-well plates and stimulated them with phorbol myristic acetate (PMA). We measured stimulation of macrophages by addition of 2',7'-dicholorofluorescein diacetate. Macrophages from NTB mice showed significantly more activation ($P = 0.001$) than those from TB mice (Fig. 5A). Furthermore, a significant reduction
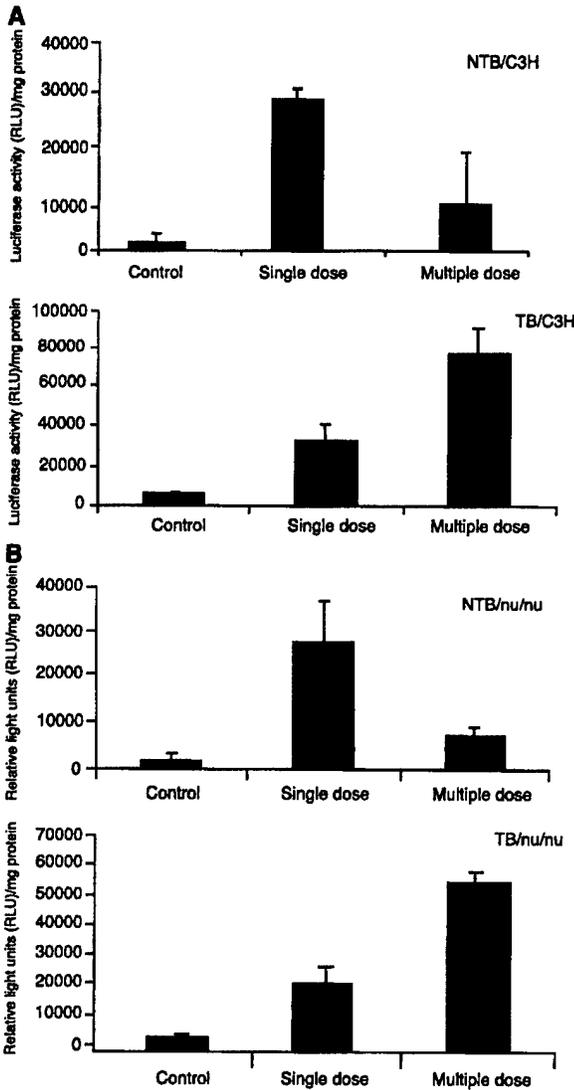
A

B

FIG. 3. Multiple treatments resulted in increased transgene expression. TB and NTB C3H or nude mice injected either once or three times with DOTAP:Chol-*luc* DNA complex (50 μg DNA/dose) via a tail vein were assayed for luc activity. (A) A twofold increase in luc activity was observed in TB C3H mice receiving three treatments compared with those receiving one treatment. In contrast, luc activity in NTB C3H mice receiving three treatments was significantly lower that in those receiving one treatment. (B) Luc activity in TB nude mice receiving three treatments showed two- to threefold increase in luc expression compared with those receiving one treatment. In contrast, luc activity in NTB nude mice receiving three treatments was significantly lower than in those receiving one treatment. Luc activity is expressed as RLU per milligram of total protein. Bars represent standard deviation.

(P = 0.01) in TNF-α production by alveolar macrophages from TB mice was observed when the macrophages were treated with LPS (Fig. 5B). In contrast, macrophages from

NTB animals produced higher levels of TNF-α when treated with LPS.

Neutralization of IL-10 in TB Animals Results in Decreased Transgene Expression

To determine the effects of IL-10 on transgene expression *in vivo*, we injected TB animals with a mouse IL-10 neutralizing antibody 24 h prior to injection of DOTAP:-Chol-*luc* DNA complex. Analysis of the lungs 48 h after liposome–DNA complex injection showed a significant reduction in luc expression ($P \leq 0.01$) compared with that in TB animals that were not treated with the neutralizing IL-10 antibody (DOTAP:Chol-*luc* complex
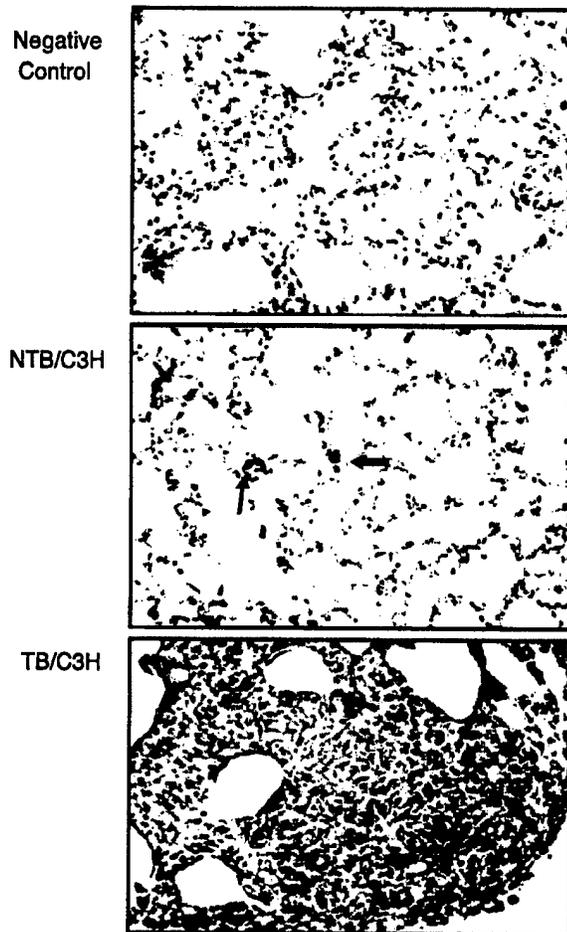
FIG. 4. UV2237M tumor cells produce IL-10. UV2237m TB and NTB lung tissue sections were immunohistochemically stained for mouse IL-10. IL-10 was detected in lung tissue sections as indicated by the intense brown cytoplasmic staining. Staining for IL-10 in NTB lung tissue sections was weak. Tissue sections stained only with secondary antibody served as negative controls. Arrows indicate cells staining positive for IL-10.

322

only) and in animals that were treated with a control isotypic antibody (Fig. 6). Luc expression was also significantly lower in animals that received the control IgG antibody than in animals that did not receive any
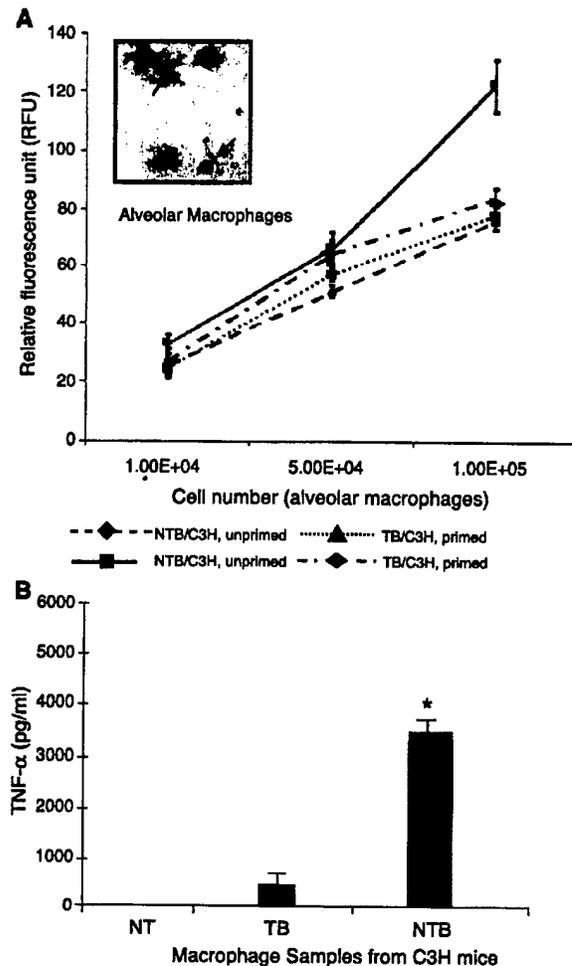
A

B

FIG. 5. Alveolar macrophages (AM) from TB mice are less responsive to PMA stimulation. (A) Alveolar macrophages from TB and TNB C3H mice were plated in 96-well plates at various cell densities and incubated overnight at 37°C. Cells were exposed to PMA (1 μg/ml) for 1 h. After 1 h, 2′,7′ dichlorofluorescein diacetate was added and incubated for 30 min. Macrophage stimulation was detected by measuring the fluorescence intensity at 530 nm in a spectrofluorometer. AM from TNB animals responded to PMA stimulation significantly compared to those from TB animals. AM not exposed to PMA served as controls. Values shown are the means of quadruplicate wells. Bars represent standard error. (B) Alveolar macrophages from TB and TNB C3H mice were treated with LPS (1 μg/ml) for 24 h and the culture medium was assayed for murine TNF-α. A significant amount of TNF-α protein was detectable in the medium from AM harvested from NTB mice compared to that from TB mice. AM not exposed to LPS served as negative control (NT). Positive control included was provided in the kit. Data are represented as the means of quadruplicate wells. Bars represent standard error.
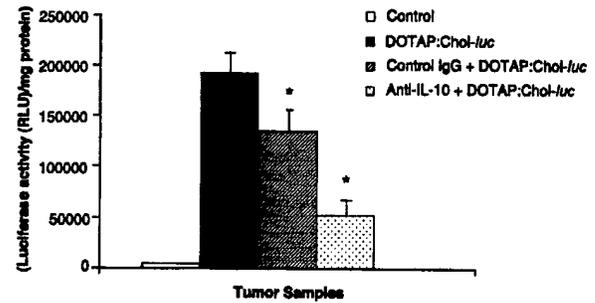
FIG. 6. Neutralization of IL-10 in TB mice results in decreased transgene expression. Lung tumors were established in C3H mice by injecting UV2237m cells (1 × 10⁶cells/well) via the tail vein. Three weeks later, animals were divided into three groups and treated as follows: group 1 received no treatment, group 2 received an intraperitoneal (ip) injection of isotypic control IgG antibody (20 μg), and group 3 received an ip injection of neutralizing anti-IL-10 antibody (20 μg). Twenty-four hours later, animals from all three groups were treated with DOTAP:Chol-*luc* DNA complex via the tail vein. Animals that did not receive any treatment served as negative controls. Animals were euthanized 48 h after injection, and their lungs were removed and analyzed for luc activity. Luc expression was significantly less in animals from group 3 than in those from groups 1 and 2. A significant reduction in luc activity was also observed in group 2 compared with group 1, indicating nonspecific inhibition. Luc activity is expressed as RLU per milligram of total protein. Bars represent standard error.

antibody treatment, indicating nonspecific inhibition of gene expression.

DISCUSSION

The present study demonstrated for the first time that transgene expression persists in TB animals but not in NTB animals. Although persistent transgene expression was demonstrated in TB animals *in vivo*, the cell types that primarily express the transgene were not investigated in the present study. However, we have recently demonstrated that tumor cells primarily express the transgene at higher levels compared to surrounding normal tissues, both *in vitro* and *in vivo* [27]. Based on our previous observation we can speculate that persistent transgene expression primarily occurs in tumor cells. However, expression can also persist in other cell types that are present within the tumor microenvironment.

The underlying mechanism for the prolonged transgene expression was next examined. It is possible that inflammatory cytokines (TNF-α, IL-1α), which have been previously shown to inhibit transgene expression, may be altered in TB animals or that the immune cells (macrophages, neutrophils, T cells) that produce the inflammatory cytokines are functionally altered in TB animals [17–25]. To understand the mechanism involved, we measured cytokine expression levels in TB and NTB animals after intravenous administration of a liposome–DNA complex. TNF-α, IL-1α, IFN-γ, and IL-10 expression was observed in both TB animals and NTB animals.

However, TNF-α levels were 50% lower in TB animals. The role of TNF-α as a proinflammatory cytokine and its primary source, alveolar macrophages, are well known [26,28]. It appears that the alveolar macrophages may be functionally suppressed by soluble factors released by the in situ tumor [29,30]. As a result, production of TNF-α and other cytokines triggered by TNF-α may also be reduced, thereby allowing persistent transgene expression. The observation that IL-10 levels were higher in TB animals supports this hypothesis. The inhibitory effects of IL-10 on macrophages and TNF-α production are well documented [29–34]. Similarly, IL-10 expression by tumor cells has been previously demonstrated [35–39]. Based on these reports we next determined the source of IL-10. Immunohistochemical analysis of TB lung tissue sections demonstrated intense cytoplasmic staining for IL-10 in UV2237m tumor cells. Additionally, in vitro assay demonstrated IL-10 production by tumor cells albeit at low levels. The difference in in vitro and in vivo IL-10 levels can be due to several reasons that include difference in tumor cell number, cell type (tumor cells, epithelial cells, mononuclear cells, etc.), and in situ tumor conditions. In support of this are the findings that IL-10 staining was also observed in infiltrating lymphocytes. Additionally, IL-10 expression was also observed in the surrounding normal tissues that comprised fibroblast and epithelial cells. In contrast, IL-10 expression was observed to be minimal in NTB lung tissue sections.

IL-10 is a Th$_2$-type cytokine that acts as an immunosuppressor under a variety of conditions and is primarily produced by macrophages and T cells [36,37]. Production of IL-10 and its effects on immune cells have been shown in a variety of human cancers [39–43]. In fact, it has been shown that IL-10 production by tumor cells suppresses the immune functions of macrophages and T cells, thereby promoting tumor growth [44–49]. Furthermore, when present in the tumor microenvironment, macrophages can produce IL-10 in an autocrine fashion, resulting in functional inactivation [36,37]. Based on these findings, we examined the effect of exogenous IL-10 on transgene expression in alveolar macrophages from TB and NTB animals, as well as the effect of PMA on macrophage stimulation as a measure of function. Transgene expression was significantly higher in alveolar macrophages from NTB animals compared with those from TB animals. However, in the presence of IL-10, transgene expression was significantly suppressed in macrophages from NTB animals (data not shown). This observation suggests two possibilities: the transgene expression was transcriptionally suppressed or the macrophages were functionally inactivated, resulting in a decreased inflammatory response. We believe that functional inactivation is a more likely mechanism since alveolar macrophages from TB animals, when exposed to PMA, were not stimulated. In contrast, macrophages from NTB animals, when exposed to

PMA, were observed to undergo significant stimulation. Furthermore, a reduction in TNF-α production was observed in alveolar macrophages from TB animals compared with those from NTB animals.

The difference in the alveolar macrophage function may partly explain the observed increase in transgene expression in TB mice receiving repeated treatments compared to NTB mice. Although persistent and increased transgene expression has been demonstrated in TB mice it is not clear whether this is a local effect or a systemic effect. Preliminary studies from our laboratory indicate that this is primarily a local effect that is influenced by the tumor microenvironment. Analysis of transgene expression in mice bearing subcutaneous tumors demonstrated an increase in transgene expression over time when the mice were injected with a single dose of DOTAP:Chol-luc DNA complex. However, analysis of the normal tumor-free lungs from these subcutaneous tumor-bearing mice demonstrated a decrease in transgene expression over time (data not shown). We are currently conducting additional studies in the laboratory to delineate the local versus systemic effect.

Finally, the effect of IL-10 on transgene expression was demonstrated by in vivo neutralization experiments conducted in TB animals. Treating animals with a neutralizing anti-IL-10 antibody prior to injection of the liposome–DNA complex resulted in an approximately 50% reduction in luc expression compared with animals that did not receive the neutralizing antibody and animals that received an isotypic control antibody. These results indicate that blocking IL-10 activity might restore the inflammatory response, thereby resulting in decreased transgene expression levels. Based on these results, we would like to propose the following hypothesis: Tumor cells in addition to infiltrating inflammatory cells produce IL-10, which acts in an autocrine fashion to promote its growth and produce more IL-10 and in paracrine fashion to suppress the functions of immune cells (macrophages, monocytes, T cells) present in the tumor microenvironment or stimulate them to produce more IL-10 (Fig. 7). Intravenous injection of liposome–DNA complex in TB animals thus results in a diminished inflammatory response, resulting in persistent and enhanced transgene expression following repeated multiple treatments and in therapeutic effect. A note of caution in that apart from IL-10 other immunosuppressive factors produced by the tumor cells may also play a role in the observed persistent transgene expression. We are currently investigating these possibilities in the laboratory.

In conclusion, this study demonstrates for the first time that a diminished inflammatory response, partly mediated by IL-10, leads to persistent gene expression in lung TB animals.. This phenomenon allows multiple treatments, resulting in enhanced transgene expression and therapeutic efficacy. Thus, repeated delivery of ther-
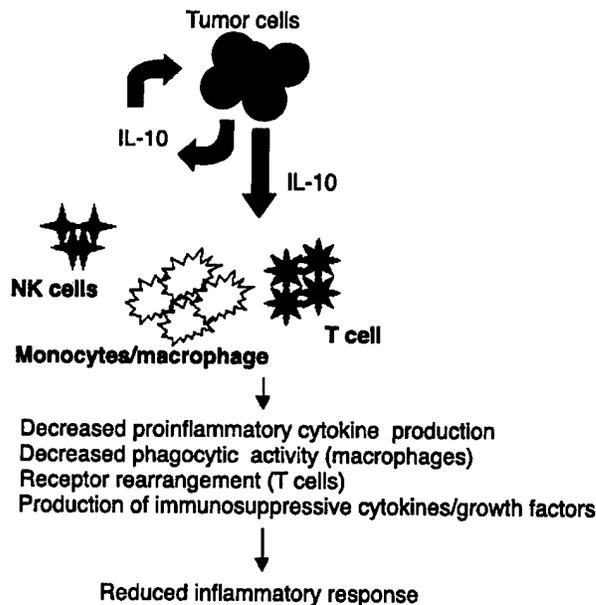
FIG. 7. Schematic representation of IL-10 production by tumor cells and its effects on immune cells and inflammatory response. Tumor cells produce IL-10, which acts in an autocrine manner to promote growth and production of more IL-10 and in a paracrine fashion to suppress the functions of immune cells (macrophages, T cells) present in the tumor milieu by decreasing phagocytic activity and proinflammatory cytokine production (IL-1, TNF-α, IL-6) and rearranging receptors. Intravenous injection of liposome–DNA complex in TB animals thus results in a diminished inflammatory response, resulting in persistent and enhanced transgene expression after repeated treatments and in a therapeutic effect.

apeutic genes encapsulated in a liposome is feasible for lung cancer treatment.

MATERIALS AND METHODS

Materials. All lipids (DOTAP, cholesterol) were purchased from Avanti Polar Lipids (Alabaster, AL, USA). RPMI 1640 medium and fetal bovine serum were purchased from Invitrogen (New York, NY, USA). Polyclonal goat anti-human IL-10 antibody and anti-mouse IL-10 monoclonal antibody were obtained from Pharmingen (San Diego, CA, USA). Anti-IL-10 neutralizing antibody was purchased from Biosource International (Camarillo, CA, USA) and isotypic IgG antibody was purchased from Sigma Chemicals (St. Louis, MO, USA).

Cell lines and animals. Murine fibrosarcoma cells (UV2237) obtained from Dr. Isaiah Fidler, M. D. Anderson Cancer Center, were maintained in RPMI 1640 medium. Human A549 lung cancer cells were obtained from American Tissue Culture Collection (Rockville, MD, USA) and maintained in Hams/F12 medium. Cells were regularly passaged and tested for the presence of mycoplasma. Four- to six-week-old female C3H/Ncr mice (National Cancer Institute, Frederick, MD, USA) and athymic nude mice (Charles River Laboratories, Wilmington, DE, USA) used in the study were maintained in a pathogen-free environment and handled according to institutional guidelines established for animal care and use.

Purification of plasmids. Growth and purification of plasmids used in the study have been described previously [16].

Synthesis, preparation, and particle size analysis of liposome:DNA complexes. The synthesis of 20 mM DOTAP:Chol, the preparation of liposome:DNA complexes, and the determination of mean particle sizes in freshly prepared liposome:DNA complexes have been described previously [16,50].

Cytokine profiles in TB and NTB mice. Experimental lung tumors were established by injecting 1×10^6 UV2237m and A549 tumor cells into C3H/Ncr mice and nude mice, respectively. Tumor cells were injected via the tail vein. Ten to fifteen days after tumor cell injection animals were given a single intravenous injection of DOTAP:Chol-*luc* DNA complex (50 µg DNA) via the tail vein. Cytokine profiles were determined in these lung TB mice and compared with those in NTB mice after treatment. Serum samples were collected from the animals at 0, 2, 6, 12, and 24 h after injection; the samples were stored at −80°C and analyzed for cytokines using murine cytokine ELISA kits (R&D Systems, Inc., Minneapolis, MN, USA). Assays were performed in quadruplicate according to the manufacturer's guidelines.

Luciferase expression in TB and NTB animals. Lung TB and NTB C3H mice and nude mice were injected with a single dose of DOTAP:Chol-*luc* DNA:liposome complex (50 µg DNA) via the tail vein. On days 1, 2, 3, and 7 after injection, the animals were euthanized using CO_2 inhalation, and their lungs were resected. The lungs were snap-frozen in liquid nitrogen and analyzed for luc expression as described previously [50]. Luc was expressed as relative light units (RLU) per milligram of protein. Four animals were analyzed at each of the time points. The experiments were performed twice, and the results reported were the average means of the two experiments.

In vivo luc expression following single and multiple treatments with DOTAP:Chol-luc DNA complex. UV2237m lung TB ($n = 15$) and NTB ($n = 15$) C3H mice and A549 lung TB ($n = 15$) and NTB ($n = 15$) nude mice were divided into three groups each. Five TB and five NTB mice were treated with intravenous injections of DOTAP:Chol-*luc* DNA complex once, and five more from each group were treated daily for 3 days. Five TB mice and five NTB mice did not receive any treatment and served as controls. The mice were euthanized by CO_2 inhalation 48 h after treatment, and their lungs were resected. Total protein was extracted from the lung tissues by homogenizing the tissue in lysis buffer and assaying for luc activity as described above (RLU/mg of protein). Each experiment was performed at least three times and the results reported were the means of the three experiments.

Immunohistochemical analysis. UV2237m lung tumors removed from C3H/Ncr mice were fixed in 10% buffered formalin before being embedded in paraffin and cut into 4-µm sections. Sections were stained for murine IL-10 expression as previously described [16]. Briefly, tissue sections were treated with 0.3% H_2O_2 in methanol for 30 min to block endogenous peroxidase activity and subsequently incubated with normal goat serum for 30 min at room temperature. Following incubation, slides were treated with goat polyclonal anti-IL-10 antibody for 60 min. After 30 min more of incubation with an appropriate secondary antibody (provided with the ABC kit; Vector Laboratories, Burlingame, CA, USA), IL-10 protein was detected in tissues using diaminobenzidine enhanced with the avidin–biotin reaction ABC kit. The slides were then counterstained with hematoxylin and mounted with Aqua-Mount (Lerner Laboratories, Pittsburgh, PA, USA).

Alveolar macrophage activation assay. Alveolar macrophages from TB and NTB C3H mice were acquired as previously described [27,51]. Briefly, the mice were euthanized using CO_2 inhalation, and an incision was made in the region of the trachea. Once the trachea was exposed, a 21-gauge needle was inserted, and 10 ml of sterile Hanks' balanced salt solution (HBSS) was infused into the lungs with a 10-ml syringe. After the lungs were flushed with HBSS, the remaining liquid was aspirated into a sterile Falcon centrifuge tube placed on ice. The procedure was repeated three to four times. Cells were centrifuged at 1000 rpm for 10 min, washed

thrice, and seeded in six-well plates. An aliquot of the cell preparation was subjected to cytopathological analysis, and more than 90% of the cells were identified as macrophages. Alveolar macrophages thus isolated were used for activation assay. Briefly, alveolar macrophages from TB and NTB C3H mice were plated in 96-well plates at varying cell densities (1×10^4, 5×10^4, and 5×10^5 cells/well) and incubated overnight at 37°C. The next day, PMA was added (1 μg/ml) to the wells and incubated. One hour after incubation with PMA, 2',7'-dicholorofluorescein diacetate (DCFH-DA; Sigma Chemicals) was added to the wells. DCFH-DA is a substrate that is converted into a fluorescent 2',7'-dicholorofluorescein product by intracellular oxidants produced by alveolar macrophages [52]. The amount of fluorescence produced is directly proportional to the macrophage response (activation) to PMA. This test is routinely used to measure alveolar macrophage response to various stress inducers [53,54]. Plates were incubated in the dark for 30 min, after which the plates were read in a spectrofluorometer at 485 nm excitation and 530 nm emissions. Values were obtained, and the results reported were the average of quadruplicates for each sample.

In a separate but parallel set of experiments, alveolar macrophages from TB and NTB C3H mice were plated in 96-well plates and incubated overnight. The next day, cells were treated with LPS (1 μg/ml; Sigma Chemicals) and culture supernatants assayed for TNF-α production using a murine TNF-α ELISA kit (R&D Systems). Untreated cells served as negative controls. Positive control was provided in the kit.

In vivo neutralization experiments with anti-IL-10 antibody. UV2237m lung TB C3H mice ($n = 15$) were divided into three groups and treated as follows: group 1 ($n = 5$) received no treatment, group 2 ($n = 5$) received a single intraperitoneal injection of control isotypic IgG antibody (20 μg); and group 3 ($n = 5$) received a single intraperitoneal injection of murine anti-IL-10 neutralizing antibody (20 μg). Twenty-four hours later, mice from all three groups were injected with DOTAP:Chol-*luc* DNA complex (50 μg DNA) via the tail vein. An additional group of animals ($n = 5$) that did not receive any treatment served as negative control for these experiments. The mice were euthanized 48 h after treatment with DOTAP:Chol-*luc*, and their lungs were resected and analyzed for luc activity as described above. Experiments were performed twice and results reported were the averages of two separate experiments.

Statistical analysis. The statistical significance of the experimental results was calculated using ANOVA. A P value <0.05 was considered significant.

REFERENCES

1. Whitmore, M., et al. (1999). LPD lipopolyplex initiates a potent cytokine response and inhibits tumor growth. *Gene Ther.* 6: 1867–1875.
2. Huang, L., and Li, S. (1997). Liposomal gene delivery—a complex package. *Nat. Biotechnol.* 15: 620–621.
3. Li, S., et al. (1999). Effect of immune response on gene transfer to the lung via systemic administration of cationic lipidic vectors. *Am. J. Physiol.* 276: L796–L804.
4. Freimark, B. D., et al. (1998). Cationic lipids enhance cytokine and cell influx levels in the lung following administration of plasmid–cationic lipid complexes. *J. Immunol.* 160: 4580–4586.
5. Whitmore, M., et al. (1999). LPD lipopolyplex initiates a potent cytokine response and inhibits tumor growth. *Gene Ther.* 6: 1867–1875.
6. Dow, S. W., et al. (1999). Lipid–DNA complexes induce potent activation of innate immune responses and antitumor activity when administered intravenously. *J. Immunol.* 163: 1552–1561.
7. Scheule, R. K. J., et al. (1997). Basis of pulmonary toxicity associated with cationic lipid-mediated gene transfer to the mammalian lung. *Hum. Gene Ther.* 8: 689–707.
8. Tousignant, J. D., et al. (2003). DNA sequences in cationic lipid:pDNA-mediated systemic toxicities. *Hum. Gene Ther.* 14: 203–214.
9. Tan, Y., et al. (1999). The inhibitory role of CpG immunostimulatory motifs in cationic lipid vector mediated transgene expression in vivo. *Hum. Gene Ther.* 10: 2153–2161.
10. Yew, N. S., et al. (2000). Reduced inflammatory response to plasmid DNA vectors by elimination and inhibition of immunostimulatory CpG motifs. *Mol. Ther.* 1: 255–262.
11. Schwartz, D. A., et al. (1997). Cpg motifs in bacterial DNA cause inflammation in the lower respiratory tract. *J. Clin. Invest.* 100: 68–73.
12. McLachlan, G., et al. (2000). Bacterial DNA is implicated in the inflammatory response to delivery of DNA/DOTAP to mouse lungs. *Gene Ther.* 7: 384–392.
13. Qin, L., et al. (1997). Promoter attenuation in gene therapy: interferon-gamma and tumor necrosis factor alpha inhibit transgene expression. *Hum. Gene Ther.* 8: 2019–2029.
14. Li, S., et al. (1998). Characterization of cationic lipid–protamine–DNA (LPD) complexes for intravenous gene delivery. *Gene Ther.* 5: 930–997.
15. Yew, N. S., et al. (2002). Cpg-depleted plasmid DNA vectors with enhanced safety and long-term gene expression in vivo. *Mol. Ther.* 5: 731–738.
16. Ramesh, R., et al. (2001). Successful treatment of primary and disseminated human lung cancers by systemic delivery of tumor suppressor genes using an improved liposome vector. *Mol. Ther.* 3: 337–350.
17. Kuda, T., Yasumoto, K., Yano, T., Nakahashi, H., Sugimachi, K., and Nomoto, K. (1987). Role of antitumor activity of alveolar macrophages in lung cancer patients. *Cancer Res.* 47: 2199–2202.
18. Sotomayor, E. M., et al. (1993). Impaired activation of tumoricidal function in macrophages from mammary tumor bearers: the role of IFN-γ. *Int. J. Oncol.* 3: 719–727.
19. Sotomayor, E. M., et al. (1995). Decreased macrophage mediated cytotoxicity in mammary tumor bearing mice is related to alterations in nitric oxide production and/or release. *Int. J. Cancer* 60: 660–667.
20. Mazzoccoli, G., et al. (1999). Lymphocyte subpopulations anomalies in lung cancer patients and relationship to the stage of disease. *In Vivo* 13: 205–209.
21. Koutsami, M. K., Gorgoulis, V. G., Kastrinakis, N. G., Asimacopoulos, P. J., and Kittas, C. (2002). Prognostic factors in non-small cell lung carcinoma. *Anticancer Res.* 22: 347–374.
22. Sotomayor, E. M., et al. (1991). Role of tumor-derived cytokines on the immune system of mice bearing a mammary adenocarcinoma. *J. Immunol.* 147: 2816–2823.
23. Lopez, D. M., et al. (1996). Cytokine production by lymphoreticular cells from mammary tumor bearing mice: the role of tumor-derived factors. *Anticancer Res.* 16: 3923–3930.
24. Lopez, D. M., et al. (1991). Modulation of the immune system by mammary tumor derived factors. *Cancer Invest.* 9: 643–653.
25. Ghosh, P., et al. (1995). Gradual loss of T-helper 1 populations in spleen of mice during progressive tumor growth. *J. Natl. Cancer Inst.* 87: 1478–1483.
26. Beutler, B., and Cerami, A. (1989). The biology of cachectin/TNF-α as primary mediator of host response. *Annu. Rev. Immunol.* 7: 625.
27. Ito, I., et al. (2003). Increased uptake of liposomal–DNA complexes by lung metastases following intravenous administration. *Mol. Ther.* 7: 409–418.
28. Vassali, P. (1992). The pathophysiology of tumor necrosis factor. *Annu. Rev. Immunol.* 10: 411.
29. Fiorentino, D. F., Zlotnik, A., Mossman, T., Howard, M., and O'Garra, A. (1991). IL-10 inhibits cytokine production by activated macrophages. *J. Immunol.* 147: 3815.
30. Alleva, D. G., Burger, C. J., and Elgert, K. D. (1994). Tumor-induced regulation of suppressor macrophage nitric oxide and TNF-α production: role of tumor-derived IL-10, TGF-β, and prostaglandin E_2. *J. Immunol.* 153: 1674.
31. Kambayashi, T., Alexander, H. R., Fong, M., and Strassman, G. (1995). Potential involvement of IL-10 in suppressing tumor-associated macrophages. *J. Immunol.* 154: 3383–3390.
32. Bogdan, C. Y., Vodovotz, Y., and Nathan, C. (1991). Macrophage deactivation by interleukin-10. *J. Exp. Med.* 174: 1549.
33. de Waal Malefyt, R., Abrams, J., Bennet, B., Figdor, C., and deVries, J. E. (1991). Interleukin-10 inhibits cytokine synthesis by human monocytes: an autoregulatory role for IL-10 production by monocytes. *J. Exp. Med.* 174: 1209.
34. Strassman, G., Koota, V., Finkelman, F., Fong, M., and Kambayashi, T. (1994). Evidence for the involvement of interleukin 10 in the differential deactivation of murine peritoneal macrophages by prostaglandin E2. *J. Exp. Med.* 180: 2365.
35. Gastl, G. A., et al. (1993). Interleukin 10 production by human carcinoma cell lines and its relation to interleukin 6 expression. *Int. J. Cancer.* 55: 96.
36. Howard, M., and O'Garra, A. (1992). Biological properties of interleukin 10. *Immunol. Today* 13: 198.

37. Moore, K. W., et al. (1993). Interleukin-10. Annu. Rev. Immunol 11: 165–190.

38. Loercher, A. E., et al. (1999). Identification of an IL-10 producing HLA DR negative monocyte subset in the malignant ascites of patients with ovarian carcinoma that inhibits cytokine protein expression and proliferation of autologous T cells. J. Immunol. 163: 6251–6260.

39. Gotlieb, W. H., et al. (1992). Presence of interleukin-10 (IL-10) in the ascites of patients with ovarian and other intra-abdominal cancers. Cytokine 4: 385–390.

40. de Waal Malefyt, R., et al. (1991). IL-10 and viral IL-10 strongly reduce antigen-specific human T cell proliferation by diminishing the antigen-presenting capacity of monocytes via downregulation of class II MHC expression. J. Exp. Med. 174: 915–924.

41. Fiorentino, D. F., et al. (1991). L-10 acts on the antigen-presenting cells to inhibit cytokine production by Th1 cells. J. Immunol. 146: 3444–3451.

42. Ding, L., and Shevach, E. M. (1992). IL-10 inhibits mitogen-induced T cell proliferation by selectively inhibiting macrophage costimulatory function. J. Immunol. 148: 3133–3139.

43. Bogdan, C., Vodovotz, Y., and Nathan, C. (1991). Macrophage deactivation by interleukin-10. J. Exp. Med. 174: 1549–1555.

44. Armstrong, L., Jordan, N., and Miller, A. (1996). Interleukin-10 (IL-10) regulation of tumor necrosis factor alpha (TNF-alpha) from human alveolar macrophages and peripheral blood monocytes. Thorax 51: 143–149.

45. Ralph, P., et al. (1992). IL-10, T lymphocyte inhibitor of human blood cell production of IL-1 and tumor necrosis factor. J. Immunol. 148: 808–814.

46. de Waal Malefyt, R., Yssel, H., and de Vries, J. E. (1993). Direct effects of IL-10 on subsets of human CD4⁺ T cell clones and resting T cells. J. Immunol. 150: 4754–4765.

47. Yue, F. Y., et al. (1997). Interleukin-10 is a growth factor for human melanoma cells and downregulates HLA class-I, HLA class-II and ICAM-1 molecules. Int. J. Cancer 71: 630–637.

48. Lu, Z. Y., et al. (1995). Interleukin-10 is a proliferation factor but not differentiation factor for human myeloma cells. Blood 85: 2521–2527.

49. Masood, R., et al. (1995). Interleukin-10 is an autocrine growth factor for acquired immunodeficiency syndrome-related B-cell lymphoma. Blood 85: 3423–3430.

50. Templeton, N. S., et al. (1997). Improved DNA:liposome complexes for increased systemic delivery and gene expression. Nat. Biotechnol. 15: 647–652.

51. Moxley, M. A., Baird, T. L., and Corbett, J. A. (2000). Adoptive transfer of acute lung injury. Am. J. Physiol. Lung Cell Mol. Physiol. 279: 985–993.

52. Wan, X. S., Zhou, Z., and Kennedy, A. R. (2003). Adaptation of the dichlorofluorescein assay for detection of radiation-induced oxidative stress in cultured cells. Radiat. Res. 160: 622–630.

53. Goldsmith, C. A., Imrich, A., Danaee, H., Ning, Y. Y., and Kobzik, L. (1998). Analysis of air pollution particulate-mediated oxidant stress in alveolar macrophages. J. Toxicol. Environ. Health A 54: 529–545.

54. Tsai, J. J., Kao, M. H., and Han, S. H. (1999). The respiratory burst activity of activated eosinophils in atopic asthmatics. Int. Arch. Allergy Immunol. 119: 38–44.

Expression of Several Genes in the Human Chromosome 3p21.3 Homozygous Deletion Region by an Adenovirus Vector Results in Tumor Suppressor Activities *in Vitro* and *in Vivo*[1]

Lin Ji,[2] Masahiko Nishizaki, Boning Gao, David Burbee, Masashi Kondo, Craig Kamibayashi, Kai Xu, Nancy Yen, E. Neely Atkinson, Bingliang Fang, Michael I. Lerman, Jack A. Roth, and John D. Minna

Section of Thoracic Molecular Oncology, Departments of Thoracic and Cardiovascular Surgery [L. J., M. N., K. X., N. Y., B. F., J. A. R.] and Biomathematics [E. N. A.], The University of Texas M. D. Anderson Cancer Center, Houston, Texas 77030; Department of Internal Medicine and Pharmacology, Hamon Center for Therapeutic Oncology Research, University of Texas Southwestern Medical Center, Dallas, Texas 75390 [B. G., D. B., M. K., C. K., J. D. M.]; and Laboratory of Immunobiology, National Cancer Institute, Frederick Cancer Research and Development Center, Frederick, Maryland 21702 [M. I. L.]

ABSTRACT

A group of candidate tumor suppressor genes (designated *CACNA2D2, PL6, 101F6, NPRL2, BLU, RASSF1, FUS1, HYAL2,* and *HYAL1*) has been identified in a 120-kb critical tumor homozygous deletion region (found in lung and breast cancers) of human chromosome 3p21.3. We studied the effects of six of these 3p21.3 genes (*101F6, NPRL2, BLU, FUS1, HYAL2,* and *HYAL1*) on tumor cell proliferation and apoptosis in human lung cancer cells by recombinant adenovirus-mediated gene transfer *in vitro* and *in vivo*. We found that forced expression of wild-type *FUS1, 101F6,* and *NPRL2* genes significantly inhibited tumor cell growth by induction of apoptosis and alteration of cell cycle processes in 3p21.3 120-kb region-deficient (homozygous) H1299 and A549 cells but not in the 3p21.3 120-kb region-heterozygous H358 and the normal human bronchial epithelial cells. Intratumoral injection of Ad-101F6, Ad-FUS1, Ad-NPRL2, and Ad-HYAL2 vectors or systemic administration of protamine-complexed vectors significantly suppressed growth of H1299 and A549 tumor xenografts and inhibited A549 experimental lung metastases in *nu/nu* mice. Together, our results, coupled with other studies demonstrating a tumor suppressor role for the *RASSF1A* isoform, suggest that multiple contiguous genes in the 3p21.3 120-kb chromosomal region may exhibit tumor suppressor activity *in vitro* and *in vivo*.

INTRODUCTION

Lung cancers develop after a multistage process involving a variety of genetic and epigenetic changes in dominant oncogenes and TSGs[3] (1, 2). Several of these changes can be found in smoking damaged respiratory epithelium in preneoplastic lesions, normal appearing epithelium, and in persons even before lung cancer develops (3–6). In these and related studies, allelic loss of chromosome region 3p (particularly 3p21.3) was found to be a frequent and early event in the development of several cancers, including lung and breast cancers (4–9). Several *3p* genes have been extensively studied and include *FHIT* at 3p14.2, *RARB* at 3p24, and *VHL* at 3p25 (summarize for lung cancer in Ref. 1). These results directed an intensive TSG search of the 3p21.3 region for one or more genes that could function as "gatekeepers" in the molecular pathogenesis of lung cancer, as well as several other human cancers.

Identification of nested 3p21.3 homozygous deletions in small cell lung cancers and a breast cancer line directed positional cloning efforts to a 630-kb region, which was narrowed subsequently to a 120-kb subregion by a breast cancer homozygous deletion (10, 11). This defined 3p21.3 region undergoes allele loss in ~80% of primary lung cancers and ~40% of preneoplastic or normal epithelial samples of smoking-damaged lung, marking it as one of the first sites to be involved (6). In addition, patients whose peripheral blood lymphocytes showed greater damage in this 3p21.3 region after *in vitro* treatment with the carcinogen benzo-a-pyrene diol epoxide had an increased risk of having lung cancer, suggesting the potential for genetic polymorphisms in this region predisposing to lung cancer development (12). The 630-kb region contains ≥25 genes, whereas 9 genes are located in or on the border of the 120-kb 3p21.3 region (10). This group of potential TSGs includes *CACNA2D2* (GenBank no. AF040709), *PL6* (U09584), *101F6* (AF040704), *NPRL2* (AF040707), *FUS1* (AF055479), *BLU* (U70880), *RASSF1* (AF040703, RASSF1C and AF102770, RASSF1A), *HYAL2* (U09577), and *HYAL1* (U03056). The *RASSF1A* isoform of the *RASSF1* gene has been studied extensively for promoter methylation in a variety of tumors, including lung and breast cancer, found to be frequently epigenetically inactivated in these tumors, and shows the ability to suppress lung cancer malignant growth (13, 14). The *FUS1* gene was also found to suppress the growth of NSCLCs *in vitro* (15). However, there have been no detailed tests comparing the activity of several of the genes in this small region or in testing their effect on lung cancer xenografts (local tumors or metastases) *in vivo*. At the start of the search for a 3p21.3 TSG, everyone expected that one gene would be found that frequently suffered mutations. However, from detailed studies of the genes in the region, that was not the case (10). In addition, the possibility of haploinsufficiency needed to be considered. Thus, it was important to further define the tumor suppressing capability of these genes both *in vitro* and *in vivo*. Such identification, which is the focus of the current report, would target the gene(s) for development as new tools for the early detection, monitoring of prevention efforts, prognosis, and therapy of lung and other cancers.

In this study, we used recombinant adenoviruses to introduce WT 3p21.3 genes into NSCLC tumor cell lines or tumor xenografts, where 3p21.3 120-kb region genes are either heterozygous or homozygous to characterize their potential tumor suppressing function *in vitro* and *in vivo*. We demonstrate that introduction of individual WT 3p21.3 genes by recombinant adenoviral vector-mediated transfer into lung cancer cells with loss of heterozygosity at the 3p21.3 120-kb region inhibited tumor cell growth and induced apoptosis *in vitro*. Moreover, intratumoral injection of recombinant adenoviral vectors containing WT 3p21.3 genes significantly suppressed growth of human NSCLC xenografts, whereas systemic administration of protamine-complexed

[2] To whom requests for reprints should be addressed, at Department of Thoracic and Cardiovascular Surgery, Box 445, The University of Texas M. D. Anderson Cancer Center, 1515 Holcombe Boulevard, Houston, TX 77030. Phone: (713) 745-4530; Fax: (713) 794-4901; E-mail: lji@mail.mdanderson.org.

[3] The abbreviations used are: TSG, tumor suppressor gene; NSCLC, non-small cell lung cancer; TUNEL, terminal deoxynucleotidyl transferase-mediated nick end labeling; WT, wild type; HBEC, human bronchial epithelial cell; GFP, green fluorescence protein; pfu, plaque-forming unit(s); vp, viral particle; FACS, fluorescence-activated cell sorter; MOI, multiplicities of infection.

adenoviral vectors of 3p21.3 genes efficiently inhibited development of experimental metastases of lung cancer cells in xenograft mouse models. Together, our results strongly suggest that multiple contiguous genes in the 3p21.3 chromosomal region may function as TSGs *in vitro* and *in vivo*.

MATERIALS AND METHODS

Cell Lines and Cell Culture. Four human NSCLC cell lines with varied 3p21.3 and *p53* gene status, A549 (homozygous for multiple 3p21.3 region markers and WT *p53*), NCI-H1299 (homozygous for multiple 3p21.3 region markers and homozygous deletion of *p53*), NCI-H358 (retained heterozygosity of multiple 3p21.3 region markers and homozygous deletion of *p53*), and NCI-H460 (homozygous for multiple 3p21.3 region markers and WT *p53*), and a normal HBEC line, were used for *in vitro* and *in vivo* experiments. The multiple 3p21.3 polymorphic markers that were used for typing the lung cancer lines are located in the 630-kb homozygous deletion region in which the 120-kb region containing the six genes studied in this report reside and have been described previously (16). The homozygosity of multiple markers is consistent with loss of heterozygosity in this region. In this report, lung cancer cell lines with such homozygosity are referred to as "3p21.3-deficient" cells. The A549 line was maintained in Ham's F12 medium supplemented with 10% FCS. The H1299, H358, and H460 lines were maintained in RPMI 1640 supplemented with 10% FCS and 5% glutamine. Normal HBECs were obtained from Clonetics, Inc. (Walkersville, MD) and cultured in the medium supplied by the manufacturer according to the instructions provided.

Construction of Recombinant Ad-3p21.3 Gene Vectors. The recombinant Ad-3ps were constructed using our recently developed ligation-mediated plasmid adenovirus vector construction system, named herein pAd-RAP and pAd-RAP-Shuttle (detailed structures of plasmids will be provided on request). The 3p21.3 genes were assembled as a mammalian expression cassette that is driven by a cytomegalovirus promoter and tailed with Bovine Growth Hormone poly(A) signal sequence. The resulting Ad-3p vectors were named Ad-101F6, Ad-NPRL2, Ad-BLU, Ad-RASSF1C, Ad-FUS1, Ad-HYAL1, and Ad-HYAL2. Sequences of 3p21.3 genes in the viral vectors were confirmed by automated DNA sequencing. A vector expressing GFP gene (Ad-GFP), and a vector carrying the β-galactosidase gene *LacZ* (Ad-LacZ), were used to monitor efficiency of transduction by the viral vectors and as nonspecific transgene expression controls. Ad-EV, an E1-deleted empty vector, was used as a negative control. Ad-p53, a vector containing the WT *p53* gene, was used as a positive tumor suppressor control. Viral titers were determined by both absorbance measurement (*i.e.*, vp/ml) and plaque assay (*i.e.*, pfu/ml).

Cell Viability Assay. Inhibition of tumor cell growth by treatment with various Ad-3p vectors was analyzed by quantitatively determining cell viability using an improved 2,3-bis[2-methoxy-4-nitro-5-sulfophenyl]-2H-tetrazolium-5-carboxanilide inner salt (XTT) assay (Roche Molecular Biochemicals, Indianapolis, IN; Ref. 17) as described previously (18). Percentage of cell viability was calculated in terms of the absorbency of treated cells relative to the absorbency of untreated control cells. Experiments were repeated at least three times with quadruplicate samples for each treatment in each individual experiment.

Analysis of Apoptosis and Cell Cycle Kinetics. Induction of apoptosis in tumor cells treated by various Ad-3p vectors was analyzed by flow cytometry (FACS) using TUNEL reaction with FITC-labeled dUTP (Roche Molecular Biochemicals, Mannheim, Germany). Cells were processed for FACS analysis for apoptosis and cell cycle kinetics as described previously (19).

Animal Studies. All animals were maintained, and animal experiments were performed under NIH and institutional guidelines established for the Animal Core Facility at the University of Texas M. D. Anderson Cancer Center. Procedures for A549 and H1299 s.c. tumor inoculations in *nu/nu* mice were described previously (19). When average tumor size reaches ~0.5 cm in diameter, mice were injected intratumorally three times within a week with various Ad-3p and control vectors at a dose of 3×10^{10} pfu (3×10^{12} vp)/tumor in a volume of 0.2 ml. Differences in tumor volumes between treatment groups were analyzed with a mixed model ANOVA using the Statistica software (StatSoft, Inc., Tulsa, OK). A difference was considered to be statistically significant when $P < 0.05$.

An experimental A549 lung metastasis model was used to study the effects of 3p21.3 genes on development of metastases. Briefly, *nu/nu* mice were inoculated with A549 cells ($1-2 \times 10^6$) in 200 μl of PBS via tail vein injection. Pulmonary experimental metastatic tumor colonies were formed 7–10 days after inoculation. Then, protamine-complexed Ad-3p (P-Ad3p) vectors or control complexes were administered systemically to animals by i.v. injection for three times within a week at each a dose of $2-5 \times 10^{10}$ vp/200–500 μg of protamine in a total volume of 200 μl/animal. The P-Ad complexes are prepared by mixing an equal volume of the adenoviral vector (1×10^{10} vp) and the protamine sulfate (100 μg; Fujisawa USA, Inc., Deerfield, IL) in room temperature for 15 min and then bringing it to a total volume of 200 μl with PBS. Two weeks after the last injection, the animals were euthanized, and their lung metastatic tumors were stained with India ink. Tumor colonies on lung surfaces were counted under a dissecting microscope without knowledge of the treatment groups, and the lung tissues were sectioned for further pathologic and immunohistochemical analysis.

RESULTS

Effects of Forced Expression of 3p Genes on Tumor Cell Growth. To test the hypothesis that one or more of the 3p genes function as tumor suppressors *in vitro*, we performed a series of experiments to study the effects of expression of the 3p21.3 genes on cell proliferation in several types of Ad-3p-transduced human NSCLC and normal HBEC cells. Cells from each line were transduced *in vitro* by Ad-101F6, Ad-FUS1, Ad-NPRL2, Ad-BLU, Ad-RASSF1C, Ad-HYAL2, and Ad-HYAL1 vectors at various MOIs in units of vp/c; cells were also treated with PBS, Ad-EV, Ad-LacZ, or Ad-p53 as mock, negative, nonspecific, or positive controls, respectively. The ratio of vp/ml:pfu/ml in our adenoviral preparations is ~100:1. The transduction efficiency was determined by examining GFP-expressing cells in the Ad-GFP-transduced cell population under a fluorescence microscope and was found to be >80% at the highest MOI applied for each cell line.

Cell proliferation was analyzed by using the XTT assay to determine the number of viable cells at 1, 2, 3, and 5 days after transduction (only data for day 5 at various MOIs are shown; Fig. 1). In all cases, the viability of transduced cells was compared with that of untransduced (PBS treated) control cells (whose viability was set at 100%). As can be seen in Fig. 1, cell viability was reduced significantly in Ad-101F6-, Ad-Fus1-, and Ad-NPRL2-transduced A549 and H460 cells, which show homozygosity for multiple 3p21.3 markers and contain WT *p53*, and H1299 cells, which exhibit 3p21.3 homozygosity but also have a homozygous deletion of p53. A modest reduction of cell viability was shown in Ad-RASSF1C-transduced H1299 cells (data not shown). However, no significant effect on growth was observed in any of these cells transduced with Ad-HYAL1, Ad-HYAL2, Ad-BLU, Ad-EV, or Ad-LacZ. These results suggest that exogenous expression of some but not all WT 3p21.3 genes can inhibit 3p-deficient tumor cell growth *in vitro*.

To clarify the specificity of the observed inhibitory effects on tumor cell growth and examine the potential cytotoxicity of the exogenously expressed 3p21.3 genes on normal cells, we analyzed the effects of these 3p21.3 genes on cell proliferation in 3p21.3 heterozygous H358 cells and normal HBECs (Fig. 1). As shown in Fig. 1, HBECs transduced with all Ad-3p genes at MOIs that generated >80% transduction efficiency had reductions in cell number after 5 days of transduction of <10%, whereas H358 cells transduced with the same vectors had losses of <20% when compared with the untransduced control cells. Similar levels of losses of cell numbers were observed in H358 and HBEC cells transduced with control vectors Ad-EV and Ad-LacZ. As a positive control, H358 cells, which are homozygously deleted for *p53*, showed reduced cell numbers when transduced with the Ad-p53 vector. These results, coupled with the lack of effect with Ad-LacZ, Ad-HYAL2, Ad-HYAL1, Ad-RASSF1C, and Ad-BLU,
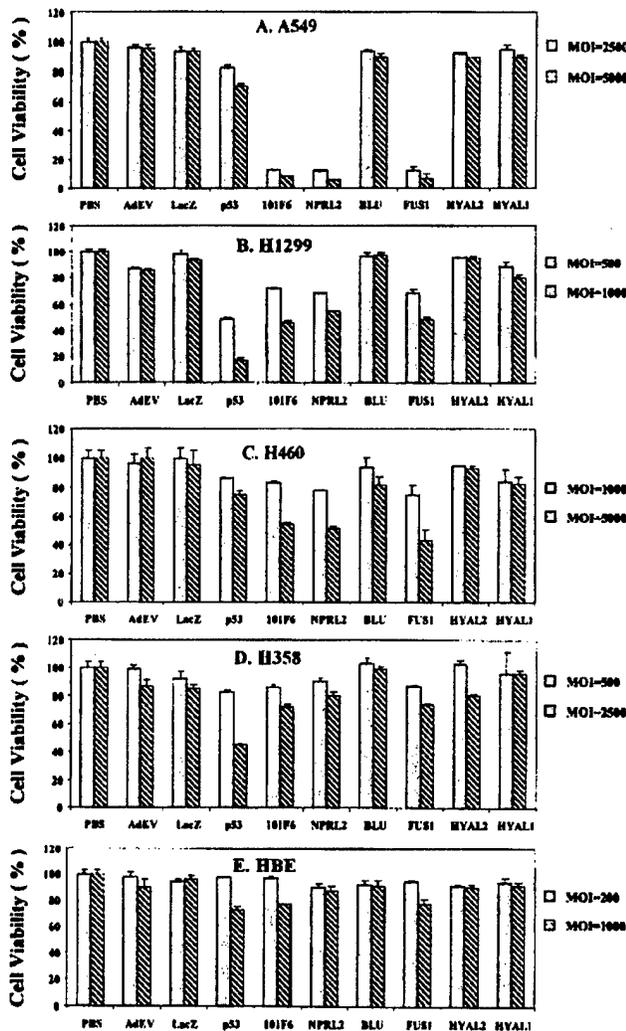
Fig. 1. Effects of exogenous expression of 3p21.3 genes on tumor cell growth in Ad-3p-transduced human lung cancer cells and normal bronchial epithelial cells. Cells were transduced with adenoviral vectors of 3p21.3 genes *101F6, NPRL2, BLU, FUS1, HAYL2,* and *HYAL1,* control genes *LacZ* and *p53,* and empty vector, Ad-EV, at various MOIs (vp/c) as indicated, and PBS alone was used as a mock control. The cell viability was expressed as the percentage of viable adenoviral vector-transduced cells in relation to PBS-treated control cells (100%). *Bars,* SDs of the mean in at least three individual experiments. Treatments were given in quadruplicate for each experiment. The significance of the difference in cell viability between vector-treated cells and the Ad-EV-, Ad-LacZ-, or PBS-treated controls was analyzed by two-sided Student's t test. $P < 0.05$ was taken as significant. The differences between the cell viability of the Ad-EV- and Ad-LacZ-transduced cells *versus* PBS-treated controls were not significant ($P = 0.25$–0.95 from different time points and cell lines). The differences between the cell viability of the Ad-101F6-, Ad-Fus1-, and Ad-NPRL2-transduced cells *versus* the Ad-EV- and Ad-LacZ-transduced cells or PBS-treated controls at the same MOI were significant in A549, H1299, and in H460 at both 3 and 5 days post-transduction ($P \le 0.0001$–0.005) but not significant in H358 and HBEC cell lines at both 3 and 5 days post-transduction ($P \ge 0.10$–0.95, from different time points and cell lines), respectively. The effects of Ad-BLU, Ad-HYAL2, and Ad-HYAL1 on cell viability were not significant in all cell lines ($P > 0.45$), compared with those of Ad-EV and Ad-LacZ.

demonstrate the specificity of the tumor suppressing function of 3p21.3 genes *FUS1, NPRL2,* and *101F6* in 3p-deficient tumor cells and indicate that no generalized cytotoxicity was associated with exogenous expression of these WT 3p21.3 120-kb region genes.

Expression of 3p21.3 genes in Ad-3p-transduced H1299 and normal HBEC cells was verified by quantitative real-time reverse transcription-PCR. Known concentrations of human Raji total RNA and a TaqMan probe for *glyceraldehyde-3-phosphate dehy-*

drogenase cDNA were used to make a standard curve as an internal control. The increase in levels of transcripts of exogenously expressed 3p21.3 genes relative to those of endogenously expressed mRNAs in HBEC is $\sim$10–15-, 30–50-, and 50–80-fold at an MOI of 100, 500, and 1000 vp/cell, respectively (data not shown). The levels of expression in transduced H1299 cells were similar to those in HBEC (data not shown). In addition, there was an association between increased levels of expression of these 3p21.3 genes and increased MOIs of the corresponding Ad-3p vectors transduced in both H1299 and HBEC cells. The expression of FUS1 and 101F6 proteins after transfection was detected by Western blot analysis using available polyclonal antibodies raised against the oligopeptides derived from their deduced amino acid sequences (data not shown).

Induction of Apoptosis by 3p Genes in Ad-3p-transduced Tumor Cells. The ability of exogenously expressed 3p21.3 genes to induce apoptosis in the Ad-3p-transduced H1299, A549, H460, H358, and HBEC cells was analyzed by FACS using the TUNEL reaction (Fig. 2). Induction of apoptosis was detected in Ad-101F6-, Ad-FUS1-, and Ad-NPRL2-transduced A549 (Fig. 2A), H1299 (Fig. 2B), and H460 (Fig. 2C) cells but not in H358 (Fig. 2D) and HBEC (Fig. 2E) cells. The apoptotic cell populations increased with increased duration of transduction; >15–20, 40–65, and 75% of cells were apoptotic 5 days after transduction with Ad-101F6, Ad-FUS1, and Ad-NPRL2 in the transduced H1299, A549, and H460 cells, respectively, whereas only $\sim$7 and 10% of cells treated with PBS alone and transduced with Ad-EV vector, respectively, were TUNEL positive after the same time interval. The levels of apoptosis induction by Ad-101F6, Ad-FUS1, and Ad-NPRL2 were quantitatively greater in A549 and H460 cell lines with WT *p53* genes (Fig. 2, A and C) than that in H1299 cell line deleted for *p53* gene (Fig. 2B). Levels of apoptosis in A549 and H460 cells were comparable with those induced by Ad-p53 in *p53*-deficient H1299 and H358 cells (Fig. 2, B and D). However, no significant induction of apoptosis was observed in any tumor cell line transduced by Ad-BLU, Ad-RASSF1, Ad-HYAL2, and Ad-HYAL1 (Fig. 2). The levels and time of induction of apoptosis in cells transduced by these Ad-3p vectors correlated with those of reduction of cell numbers in cells treated with the same vectors (Fig. 1), suggesting that suppression of tumor cell growth by these 3p21.3 genes is mediated directly or indirectly through a mechanism of apoptosis.

Suppression of Tumor Growth by Intratumoral Injection of Ad-3p Vectors. To determine whether the observed inhibitory effects of these 3p21.3 genes on tumor cell proliferation *in vitro* could be demonstrated on tumor growth *in vivo*, we evaluated the efficacy of 3p21.3 genes in suppressing tumor growth by direct intratumoral injection of Ad-3p21.3 gene vectors, along with PBS and Ad-EV, Ad-LacZ, and Ad-p53 vectors as controls, into A549 or H1299 tumor xenografts in *nu/nu* mice (Fig. 3). The growth of tumors was recorded from the first injection until 23 days after the last injection. Tumor volumes were normalized by calculating the percentage increase in tumor volume after treatment relative to volume at the beginning of treatment in each group. In both A549 (Fig. 3A) and H1299 (Fig. 3B) tumor models, all of the tumors treated with Ad-101F6, Ad-FUS1, or Ad-NPRL2 showed significantly suppressed growth ($P < 0.001$), compared with mouse groups treated with Ad-LacZ or Ad-EV controls, whereas no significant effect was observed in Ad-HYAL1-, Ad-BLU (data not shown)-, and Ad-HYAL2 (data not shown)-treated tumors. Moreover, a significantly stronger inhibition of tumor growth was shown in A549 tumors treated with Ad-101F6 and Ad-NPRL2 vectors than in tumors treated with the Ad-p53 vector (Fig. 3A).
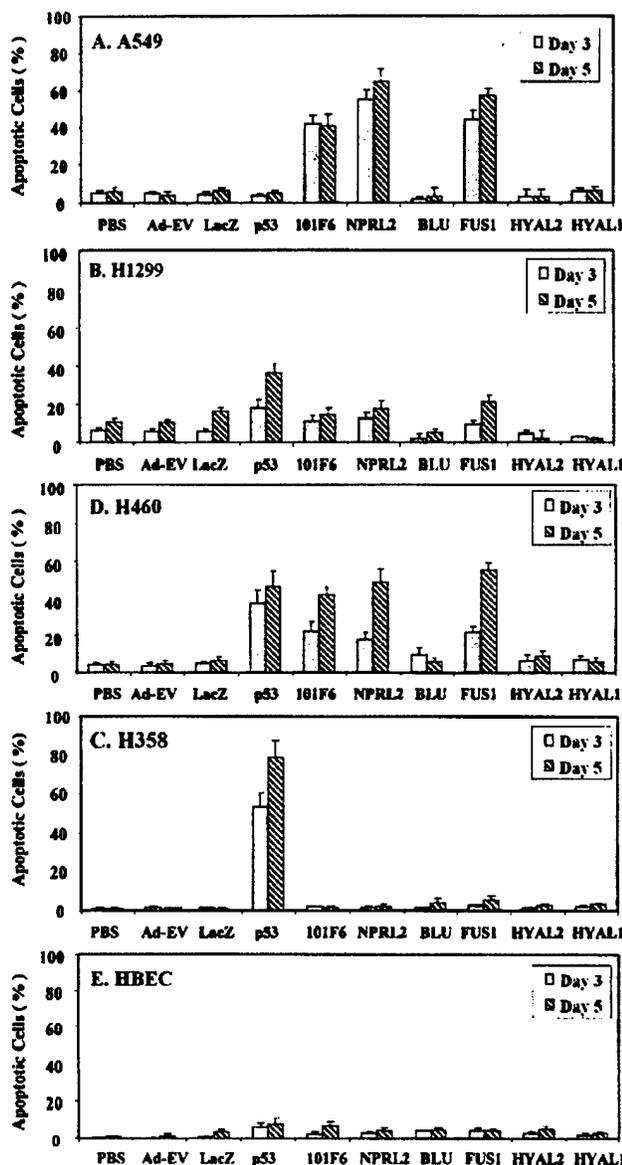
Fig. 2. Induction of apoptosis by exogenous expression of 3p21.3 genes in Ad-3p-transduced human NSCLC cells and normal HBECs. Apoptosis was analyzed by FACS, using TUNEL reaction with FITC-labeled dUTP. Cells were transduced with adenoviral vectors of 3p21.3 genes at an MOI (vp/c) of 5000 for A549 (*A*), 1000 for H1299 (*B*), 5000 for H460 (*C*), 2500 for H358 (*D*), and 1000 for HBEC (*E*), respectively, and PBS, Ad-EV, and p53 were used as controls. Cells were harvested and analyzed for apoptosis at the indicated days post-transduction. The rate of apoptosis is expressed as the percentage of FITC-labeled cells in the total cell population. *Bars*, SDs of the mean in two or three repeated experiments with triplicate treatments and TUNEL reactions for each experiment. The significance of the difference in apoptosis between vector-treated cells and the Ad-EV-, Ad-LacZ-, or PBS-treated controls was analyzed by two-sided Student's *t* test. $P < 0.05$ was considered significant. The differences between the apoptosis induced by the Ad-EV- and Ad-LacZ-transduced cells *versus* PBS-treated controls were not significant ($P = 0.925–0.675$ from different time points and cell lines). The differences between the apoptosis induced in the Ad-101F6-, Ad-FUS1-, and Ad-NPRL2-transduced cells *versus* the Ad-EV-, Ad-LacZ-, or PBS-treated controls were significant in A549 and H460 cells at both 3 and 5 days post-transduction ($P \le 0.0001–0.005$) and significant *versus* the Ad-EV- and PBS-treated cells in H1299 at 5 days post-transduction ($P \le 0.02$) but not significant in H358 and HBEC cell lines at both 3 and 5 days post-transduction at all time points ($P \ge 0.85–0.95$), respectively. Induction of apoptosis in Ad-p53-transduced H358 cells was significant at all time points compared with all other treatments ($P < 0.0001$). Induction of apoptosis in cells treated with Ad-BLU, Ad-HYAL2, and Ad-HYAL1 was not significant compared with those treated with PBS, Ad-EV, or Ad-LacZ, in all cell lines at all time points ($P > 0.85$).

Inhibition of Development of Experimental Lung Metastases by Protamine-Adenovirus Complex-mediated 3p21.3 Gene Transfer.

A novel formulation using protamine/adenovirus complexes (designated P-Ad) for enhanced systemic delivery of recombinant adenovirus *in vivo* was developed to further explore the potential of 3p21.3 genes in suppressing systemic metastases. An experimental A549 metastatic human lung cancer model (established by i.v. injection of tumor cells) was used to study the effects of 3p21.3 gene transfer on the development of lung metastases in *nu/nu* mice (Fig. 4). The adenoviral 3p21.3 gene vectors were complexed to protamine and delivered via i.v. injection. The development of A549 pulmonary metastases was inhibited significantly, and the numbers of metastatic tumor colonies found on the surfaces of lungs from mice inoculated with A549 cells were reduced by >80% in animals treated with P-Ad-101F6, P-Ad-FUS1, P-Ad-NPRL2, or P-Ad-HYAL2 (70% reduction), compared with those in control treatment groups (Fig. 4). However, no significant reduction of metastatic colony formation was observed in animals treated with P-Ad-HYAL1 and P-Ad-BLU. These data are consistent with results obtained from Ad-3p-treated s.c. tumor xenografts, further supporting the roles of these 3p21.3 genes in suppression of tumor growth and inhibition of tumor progression *in vivo*. Finally, we noted no systemic toxicity to the mice given the systemic injection of PAd-3p complexes.

DISCUSSION

In this study, we used recombinant adenoviral vectors to introduce individual WT 3p21.3 genes into 3p-deficient tumor xenograft or tumor cell lines. The ectopic expression of WT 3p21.3 genes *101F6*, *FUS1*, and *NPRL2* effectively inhibited the growth of 3p-deficient NSCLC A549, H1299, and H460 cells *in vitro* but had no effect on the growth of H358 cells (which remains heterozygous for multiple polymorphic markers in the 3p21.3 650-kb homozygous deletion region) or on the growth of normal HBECs, suggesting the specificity of the exogenous WT 3p21.3 genes in inhibiting tumor cell growth. These findings also indicate the possibility that exogenous expression of 3p21.3 genes will be safe as cancer gene therapy agents because they caused no generalized cytotoxicity to normal cells or in mice treated systemically. The tumor suppressing effects of some TSGs under normal physiological conditions are generally mediated by increased levels of TSG expression in response to the oncogenic and environmental stimuli. These include *p53*, *WAF1*, *BAX*, and *BAK* (20), *e.g.*, expression of both endogenous WT *p53* gene and protein increased 6–8-fold after heat treatment of myeloblastic leukemia cells and DNA-binding activity of p53 increased >17-fold after γ-irradiation of human glioblastoma cells (21, 22). The level of 3p21.3 gene expression by the adenoviral vector-mediated 3p21.3 gene transfer in normal HBEC cells was increased ~10–15-fold (data not shown) and is close to the elevated levels of TSG expression induced by environmental stimuli under physiological conditions shown by that of p53.

In most cases, there is loss of heterozygosity at the 3p21.2 locus with no mutations detected in the remaining allele. However, haploinsufficiency can be associated with abrogation of tumor suppressor activity, *e.g.*, the *p27* gene is haploinsufficient for tumor suppression with tumor suppressor activity critically dependent on the absolute level of p27 protein expression (23). Elevated p27 expression inhibits cell cycle progression and promotes apoptosis in human glioma, colon, NSCLC, and mantle cell lymphoma, suggesting that p27 acts as a rheostat rather than as an on/off switch tumor suppressor in suppressing neoplasia (24). Similar to *p27*, some of the 3p21.3 genes are possibly inactivated by haploinsufficincy (10), and the modulation of protein expression may play an important role for their tumor suppressor activities. Furthermore, the overexpression of these 3p21.3

Fig. 3. Effects of intratumoral administration of adenoviral vectors of 3p21.3 genes on growth of human lung cancer A549 (A) and H1299 (B) s.c. tumors in *nu/nu* mice. When the tumor reached 5–10 mm in diameter at ~2 weeks after tumor inoculation, the tumor was injected with individual adenoviral vectors of 3p21.3 genes *101F6*, *NPRL2*, *FUS1*, and *HYAL1* or control vectors Ad-EV and p53, at a dose of 5×10^{10} vp/tumor each in 200 μl of PBS for three times within a week, respectively, and PBS alone was used as a mock control. Results were reported as the mean ± SD in 5–10 mice for each treatment group. Tumor volumes were normalized by the percentage increase of tumor sizes after treatment relative to those at the beginning of the treatment in each group. Mean tumor volumes ±SE from these experiments are shown. ANOVA was performed to determine statistical significance between each treatment group using Statistica software (Stat-Soft, Inc.), and $P \leq 0.05$ was considered significant. The differences of the tumor volumes in the Ad-101F6-, Ad-FUS1-, and Ad-NPRL2-treated mice *versus* in the Ad-EV-treated mouse controls were statistically significant in both A549 and H1299 tumor models ($P < 0.0001$) after 5 days from the last injection but not significant in Ad-HYAL1 ($P > 0.05$ in both A549 and H1299 tumor models).
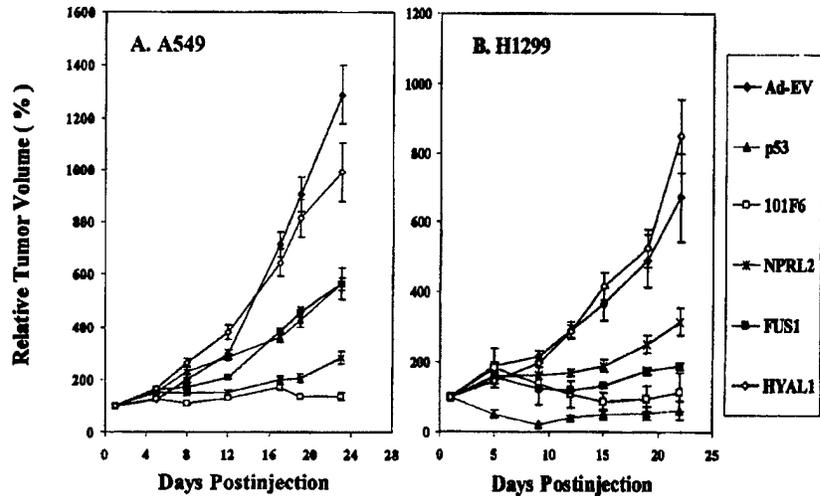
genes at higher MOIs may be pharmaceutically appropriate for enhancing their function as cancer therapeutics and may be necessary for proper TSG function to overcome degradation pathways and inactive pathways in the cancer cell. The selectivity of the vectors with respect to growth inhibition and induction of the specific pathway of apoptosis in cancer compared with normal cells further supports their physiological role.

Inhibition of cell proliferation and induction of cell death by activated TSGs, such as *retinoblastoma* (*Rb*) and *p53*, are attributed primarily to these genes' ability to mediate cell cycle arrest and apoptosis (25–27). Because apoptosis is a genetically programmed cellular response to environmental stresses or stimuli, inactivation of TSGs involved in the apoptotic pathways could result in deregulated cell proliferation and tumorigenesis. To elucidate the mechanism governing the inhibition of NSCLC cell growth by 3p21.3 genes, we
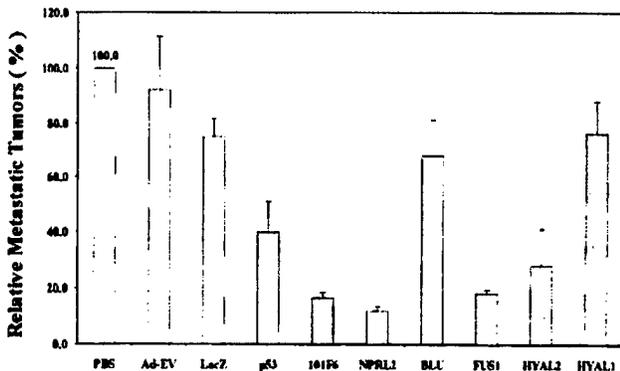

Fig. 4. Effect of systemic administration of protamine-Ad-3p complexes on development of A549 experimental lung metastases in *nu/nu* mice. All animals were i.v. injected with various protamine-adenoviral vector complexes every other 2 days for three times each at a dose of 3×10^{10} vp plus 300 μg of protamine in a total volume of 200 μl/animal, and PBS alone was used as a mock control. Each treatment group consisted of 5–10 animals. Lungs were harvested 2 weeks after the last injection, and metastastic colonies on the surfaces of lung were counted without knowledge of the treatment groups. Development of metastases was represented as the percentages of metastatic colonies formed in protamine-adenovirus complex-treated groups in relation to those in the PBS-treated group (as 100%). Bars, SE. Nonparametric *t* test (Wald-Wolfowitz Runs Test) was performed to determine statistical significance between each treatment group using Statistica software (StatSoft, Inc.), and $P \leq 0.05$ was considered significant. A significant inhibition of development of metastases was observed in mice treated with P-Ad-101F6 ($P = 0.002$), P-Ad-NPRL2 ($P = 0.001$), P-Ad-FUS1 ($P = 0.002$), and P-Ad-HYAL2 ($P = 0.014$), respectively, compared with mice treated with PBS, P-Ad-EV, or P-Ad-LacZ but no significant inhibition in mice treated with P-Ad-BLU ($P = 0.818$) or P-Ad-HYAL1 ($P = 0.904$).

studied the effects of exogenously expressed 3p21.3 genes on apoptosis mediated by adenoviral vector transduction. Introduction of WT 3p21.3 genes *101F6*, *FUS1*, and *NPRL2* into the 3p-deficeint A549, H1299, and H460 cells induced apoptosis. However, this was not a generalized feature of 3p21.3 gene overexpression, as the *HYAL2*, *HYAL1*, and *BLU* genes from this same 120-kb region did not induce a significant increase in apoptosis in the same lung cancer cells. The time and the magnitude of the induction of apoptosis by these 3p21.3 genes were also well correlated with those of the inhibition of growth observed *in vitro*. These observations suggest that the tumor suppressing function mediated by the 3p21.3 genes is through induction of apoptosis.

To demonstrate whether the observed inhibitory effects of these 3p21.3 genes on tumor cell growth *in vitro* could be reproduced *in vivo*, we evaluated the efficacy of 3p21.3 genes in suppressing tumor growth by directly injecting Ad-3p vectors into A549 or H1299 tumor xenografts in *nu/nu* mice. Growth of both A549 and H1299 tumors was suppressed significantly by treatments with Ad-101F6, Ad-FUS1, and Ad-NPRL2. Furthermore, we explored the tumor suppressing potential of 3p21.3 genes in inhibiting experimental metastases *in vivo* by systemic administration of protamine-Ad-3p complexes. The novel protamine-Ad-3p complexes developed as part of this study allowed us to deliver 3p21.3 genes efficiently to the lung by systemic injection. The development of metastases was inhibited effectively by the protamine-adenovirus complex-mediated transfer of the *101F6*, *FUS1*, *HYAL2*, and *NPRL2* genes. These *in vivo* data are consistent with the *in vitro* data, further supporting the roles of 3p21.3 genes as TSGs.

Two of the 3p21.3 genes, *HYAL1* and *RASSF1C*, showed neither tumor suppressor activity *in vitro* nor *in vivo* nor apoptosis-inducing activity *in vitro* in all cell lines tested. Recently, one splicing isoform of one of the genes, *RASSF1A*, has been shown to undergo epigenetic inactivation by promoter region hypermethylation acquired in tumors. This isoform, but not the expressed *RASSF1C* isoform, also exhibits functional tumor suppressing activity. Consistent with these results, we also found no significant effects on growth of NSCLC cells and induction of apoptosis in these NSCLC cells *in vitro* and *in vivo* in our experiments using the Ad-RASSF1C vector (data not shown). The results with *RASSF1A* indicate that it will be important to study all of the genes in the region for loss of expression via tumor-acquired promoter hypermethylation. Alternatively, with 3p allele loss, haplo-insufficiency of one or more of these 3p21.3 genes may play a role in tumorigenesis. On the basis of the evidence that multiple contiguous

3p21.3 genes, including *101F6, NPRL2, RASSF1A,* and *FUS1,* exhibited varied degrees of tumor suppressing activity, we propose that genes in this 3p21.3 120-kb region act together as part of a tumor suppressor region to suppress tumor growth through their functional activation of tumor suppressing pathways. Likewise, their inactivation may contribute directly to the development of cancer because of haploinsufficiency, loss of expression, or rarely mutations. In summary, we have demonstrated here for the first time that introduction of several WT 3p21.3 genes (*101F6, NPRL2,* and *FUS1*) contiguously located within a 120-kb region by recombinant adenoviral vector-mediated gene transfer into 3p-deficient tumor xenografts and tumor cell lines efficiently suppressed tumor cell growth and metastases and induced apoptosis *in vitro* and *in vivo.* These results suggest the role of these genes as TSGs. A better understanding of the biological function of genes in this region may result in the development of new strategies for the prevention, early detection, diagnosis, and treatment for lung cancer and other human cancers.

REFERENCES

1. Zochbauer-Muller, S., Gazdar, A. F., and Minna, J. D. Molecular pathogenesis of lung cancer. Ann. Rev. Physiol., *64:* 681–708, 2002.
2. Fong, K., Sekido, Y., and Minna, J. D. The molecular basis of lung carcinogenesis. *In:* W. B. Coleman and G. Tsongalis (eds.), The Molecular Basis of Human Cancer, pp. 379–405. Totowa, NJ: Humana Press, 2001.
3. Park, I. W., Wistuba, I. I., Maitra, A., Milchgrub, S., Virmani, A. K., Minna, J. D., and Gazdar, A. F. Multiple clonal abnormalities in the bronchial epithelium of patients with lung cancer. J. Natl. Cancer Inst. (Bethesda), *91:* 1863–1868, 1999.
4. Wistuba, I. I., Lam, S., Behrens, C., Virmani, A. K., Fong, K. M., LeRiche, J., Samet, J. M., Srivastava, S., Minna, J. D., and Gazdar, A. F. Molecular damage in the bronchial epithelium of current and former smokers. J. Natl. Cancer Inst. (Bethesda), *89:* 1366–1373, 1997.
5. Wistuba, I. I., Berry, J., Behrens, C., Maitra, A., Shivapurkar, N., Milchgrub, S., Mackay, B., Minna, J. D., and Gazdar, A. F. Molecular changes in the bronchial epithelium of patients with small cell lung cancer. Clin. Cancer Res., *6:* 2604–2610, 2000.
6. Wistuba, I. I., Behrens, C., Virmani, A. K., Mele, G., Milchgrub, S., Girard, L., Fondon, J. W., Garner, H. R., McKay, B., Latif, F., Lerman, M. I., Lam, S., Gazdar, A. F., and Minna, J. D. High resolution chromosome 3p allelotyping of human lung cancer and preneoplastic/preinvasive bronchial epithelium reveals multiple, discontinuous sites of 3p allele loss and three regions of frequent breakpoints. Cancer Res., *60:* 1949–1960, 2000.
7. Girard, L., Zochbauer-Muller, S., Virmani, A. K., Gazdar, A. F., and Minna, J. D. Genome-wide allelotyping of lung cancer identifies new regions of allelic loss, differences between small cell lung cancer and non-small cell lung cancer, and loci clustering. Cancer Res., *60:* 4894–4906, 2000.
8. Maitra, A., Wistuba, I. I., Washington, C., Virmani, A. K., Ashfaq, R., Milchgrub, S., Gazdar, A. F., and Minna, J. D. High-resolution chromosome 3p allelotyping of breast carcinomas and precursor lesions demonstrates frequent loss of heterozygosity and a discontinuous pattern of allele loss. Am. J. Pathol., *159:* 119–130, 2001.

9. Wistuba, I. I., Behrens, C., Milchgrub, S., Bryant, D., Hung, J., Minna, J. D., and Gazdar, A. F. Sequential molecular abnormalities are involved in the multistage development of squamous cell lung carcinoma. Oncogene, *18:* 643–650, 1999.
10. Lerman, M. I., and Minna, J. D. The 630-kb lung cancer homozygous deletion region on human chromosome 3p21.3: identification and evaluation of the resident candidate tumor suppressor genes. Cancer Res., *60:* 6116–6133, 2000.
11. Sekido, Y., Ahmadian, M., Wistuba, I. I., Latif, F., Bader, S., Wei, M. H., Duh, F. M., Gazdar, A. F., Lerman, M. I., and Minna, J. D. Cloning of a breast cancer homozygous deletion junction narrows the region of search for a 3p21.3 tumor suppressor gene. Oncogene, *16:* 3151–3157, 1998.
12. Wu, X., Zhao, Y., Honn, S. E., Tomlinson, G. E., Minna, J. D., Hong, W. K., and Spitz, M. R. Benzo[a]pyrene diol epoxide-induced 3p21.3 aberrations and genetic predisposition to lung cancer. Cancer Res., *58:* 1605–1608, 1998.
13. Burbee, D. G., Forgacs, E., Zochbauer-Muller, S., Shivakumar, L., Fong, K., Gao, B., Randle, D., Kondo, M., Virmani, A., Bader, S., Sekido, Y., Latif, F., Milchgrub, S., Toyooka, S., Gazdar, A. F., Lerman, M. I., Zabarovsky, E., White, M., and Minna, J. D. Epigenetic inactivation of RASSF1A in lung and breast cancers and malignant phenotype suppression. J. Natl. Cancer Inst. (Bethesda), *93:* 691–699, 2001.
14. Dammann, R., Li, C., Yoon, J. H., Chin, P. L., Bates, S., and Pfeifer, G. P. Epigenetic inactivation of a RAS association domain family protein from the lung tumour suppressor locus 3p21.3. Nat. Genet., *25:* 315–319, 2000.
15. Kondo, M., Ji, L., Kamibayashi, C., Tomizawa, Y., Randle, D., Sekido, Y., Yakota, J., Kashuba, V., Zabarovsky, E., Kuzmin, I., Lerman, M., Roth, J. A., and Minna, J. D. Overexpression of candidate tumor suppressor gene FUS1 isolated from the 3p21.3 homozygous deletion region leads to G1 arrest and growth inhibition of lung cancer cells. Oncogene, *20:* 6258–6262, 2001.
16. Fondon, J. W., Mele, G. M., Brezinschek, R. I., Cummings, D., Pande, A., Wren, J., O'Brien, K. M., Kupfer, K. C., Wei, M. H., Lerman, M., Minna, J. D., and Garner, H. R. Computerized polymorphic marker identification: experimental validation and a predicted human polymorphism catalog. Proc. Natl. Acad. Sci. USA, *95:* 7514–7519, 1998.
17. Roehm, N. W., Rodgers, G. H., Hatfield, S. M., and Glasebrook, A. L. An improved colorimetric assay for cell proliferation and viability utilizing the tetrazolium salt XTT. J. Immunol. Methods, *142:* 257–265, 1991.
18. Nishizaki M., Meyn R. E., Atkinson E. N., White R. A., Roth, J. A., and Ji, L. Synergistic inhibition of human lung cancer cell growth by adenovirus-mediated wild-type *p53* gene transfer in combination with docetaxel and radiation therapeutics *in vitro* and *in vivo.* Clin. Cancer Res., *7:* 2683–2689, 2001.
19. Ji, L., Fang, B., Yen, N., Fong, K., Minna, J. D., and Roth, J. A. Induction of apoptosis and inhibition of tumorigenicity and tumor growth by adenovirus vector-mediated fragile histidine triad (FHIT) gene overexpression. Cancer Res., *59:* 3333–3339, 1999.
20. Bishay, K., Ory, K., Lebeau, J., Levalois, C., Olivier, M. F., and Chevillard, S. DNA damage-related gene expression as biomarkers to assess cellular response after γ irradiation of a human lymphoblastoid cell line. Oncogene, *19:* 916–923, 2000.
21. Kastan, M. B., Radin, A. I., Kuerbitz, S. J., Onyekwere, O., Wolkow, C. A., Civin, C. I., Stone, K. D., Woo, T., Ravindranath, Y., and Craig, R. W. Levels of p53 protein increase with maturation in human hematopoietic cells. Cancer Res., *51:* 4279–4286, 1991.
22. Ohnishi, T., Wang, X., Ohnishi, K., Matsumoto, H., and Takahashi, A. p53-dependent induction of WAF1 by heat treatment in human glioblastoma cells. J. Biol. Chem., *271:* 14510–14513, 1996.
23. Fero, M. L., Randel, E., Gurley, K. E., Roberts, J. M., and Kemp, C. J. The murine gene *p27Kip1* is haplo-insufficient for tumour suppression. Nature (Lond.), *396:* 177–180, 1998.
24. Kemp, C. J., Sun, S., and Gurley, K. E. p53 induction and apoptosis in response to radio- and chemotherapy *in vivo* is tumor-type-dependent. Cancer Res., *61:* 327–332, 2001.
25. Evan, G., and Littlewood, T. A matter of life and cell death. Science (Wash. DC), *281:* 1317–1322, 1998.
26. Levine, A. J. p53, the cellular gatekeeper for growth and division. Cell, *88:* 323–331, 1997.
27. Vousden, K. H. p53: death star. Cell, *103:* 691–694, 2000.

Abstract Number: 1053

Synergistic Inhibition of Tumor Cell Growth by CACNA2D2 and p53 via Activation of DAPK Pathway in Lung Cancer

Giovanni L. Carboni, Jianhua Shao, Kai Xu, Boning Gao, Masahiko Nishizaki, Ralph A. Schmid, John D. Minna, Jack A. Roth, Lin Ji. University Hospital Bern, Division of General Thoracic Surgery, Berne, Switzerland; UT MD Anderson Cancer Center, Dept. of Thoracic and Cardiovascular Surgery, Houston, TX; UT Southwestern Medical Center, Dallas, TX.

The Ca^{2+}-channel subunit gene CACNA2D2 (CACN) is located in the human chromosome 3p21.3 homozygous deletion region. We previously showed that enforced expression of wild-type (wt)-CACN by the recombinant adenoviral vector-mediated transfer in CACN-deficient NSCLC cells significantly inhibited cell growth and induced apoptosis in vitro and in vivo. We also observed that the wt-p53-expressing NSCLC cells appeared more sensitive to Ad-CACN-mediated growth inhibition and apoptosis induction, suggesting a possible p53-dependent mechanism for the CACN-mediated function. To explore the molecular mechanism behind the apparent interaction between CACN and p53, we evaluated the combined effect of the Ad-CACN and Ad-p53-mediated gene co-transfer on tumor cell growth and apoptosis and analyzed the potential downstream signaling pathways mediated by these tumor suppressors in NSCLC cells. A significant synergistic inhibition of tumor cell growth was observed in Ad-CACN and Ad-p53-cotransduced H358 and H1299 (p53 null) cells (p = 0.035 and p = 0.046, respectively) by isobologram modeling and statistical analysis. A similar synergistic effect on induction of apoptosis was also observed, as shown by the significant increase of apoptotic cell populations, 26.3% (p = 0.03) in H358 and 20.3 % (p = 0.06) in H1299 cotransduced by Ad-CACN and Ad-p53, respectively, compared to the either vector treatment alone. To analyze the effect of CACN on endogenous p53 expression, we performed Western-blot analysis in Ad-CACN-transduced A549 and H460 (p53 wt) cells and found that the ectopic expression of CACN enhanced p53 protein expression, possible due to p53 stabilization, in both cells but with a less degree of increase in H460. Furthermore, we explored the possibility of the involvement of the death associated protein kinase (DAPK), a Ca^{2+}/Calmodulin activated protein kinase that has been shown to induce apoptosis in a p53-dependent mechanism. We found that exogenous CACN expression induces phosphorylation of DAPK in A549 and H358. The H460 cells are deficient of both gene and protein expression due to promoter methylation, as confirmed by methylation-specific PCR, Western blot and RT-PCR analysis. Treatment with the methyltransferase inhibitor 5-Aza-2'-deoxycytidine (AZA) restored DAPK protein expression in H460. Combination treatment with Ad-CACN and AZA synergistically suppressed H460 cell growth and efficiently induced p53 stabilization. Based on these observations, we conclude that exogenous co-expression of CACN and p53 synergistically inhibits tumor cell growth in NSCLC cells and the observed synergy might result from the p53 stabilization through the CACN-mediated DAPK activation and phosphorylation.

Presenter: Giovanni L. Carboni

Affiliation: University Hospital Bern, Division of General Thoracic Surgery, Berne, Switzerland. Email: giovanni.carboni@dkf4.unibe.ch

Abstract Number: 5901

Overexpression of FHIT inhibits tumor cell invasion and metastases via inactivation of the Rho-PKC-Ezrin signaling pathway in human pancreatic cancer.

Masahiko Nishizaki, Jiichiro Sasaki, Giovanni Carboni, Jack A. Roth, Lin Ji. M.D.Anderson Cancer Center, Houston, TX.

Genetic alterations and deficient expression of FHIT tumor suppressor gene has been found in more than 70% of human pancreatic cancers, suggesting its important role in development of pancreatic cancer. In this study, we used a human pancreatic cancer cell line SUIT-2 and its sub lines SCP-9 and SVP-10 to evaluate the effects of FHIT on pancreatic tumor growth, progression, and metastasis in vitro and in vivo. These unique cell lines were derived from the liver metastases of a pancreatic cancer patient and can produce spontaneous metastasis to lung and regional lymph nodes from the primary s.c. xenografts in nude mice, with an increased metastatic potential in an order of SVP-10->SCP-9>SUIT-2. We found that enforced FHIT expression significantly inhibited tumor cell growth, induced apoptosis, and blocked tumor cell migration and invasion in these FHIT-deficient pancreatic cancer cells by adenoviral vector-mediated gene transfer in vitro. Overexpression of FHIT also significantly suppressed the aggressive growth of SVP-10 tumor xenografts by intratumoral injection and inhibited tumor progression and metastasis in both the SVP-10-derived experimental and the spontaneous lung metastases in nude mice by systemic administration of the protamine-complexed Ad-FHIT (P-Ad-FHIT) vectors, compared to untreated or P-Ad-LacZ-treated controls. To understand the molecular mechanism behind the observed FHIT-mediated inhibition of tumor progression and metastasis, we analyzed activities of several major down stream components involving in tumor invasion and metastasis. We confirmed that the highly-metastatic variant SCP-9 and SVP-10 cells expressed a significantly higher level of endogenous Ezrin protein compared to their low-potential parental SUIT-2 cells and found that overexpression of FHIT significantly suppressed the endogenous Ezrin protein expression and phosphorylation and inhibited its binding to actin. The PKCa-Ezrin element is one of the key downstream signaling components in the Ras/Rho GTPase pathway, which function as molecular switches regulating many essential cellular processes including cytoskeletal organization, actin dynamics, cell-cycle progression, mitogenesis, and cell migration. We also observed that Fhit protein could associate with PKCa and, thus, may prevent PKCa from interacting with Ezrin and inhibit its phosphorylation as shown in immunoprecipitation-Western blots. Moreover, we found that PKCa kinase activity itself was significantly inhibited by Fhit activity. These findings suggest that one of the molecular mechanism in FHIT-mediated inbition of tumor cell growth, invation and metastasis might be through the inactivation of the Rho-PKC- Ezrin signaling pathway in pancreatic cancer.

Presenter: Jiichiro Sasaki

Affiliation: M.D.Anderson Cancer Center, Houston, TX . Email: jiichirou@hotmail.com

Abstract Number: 397

Myristoylation of Fus1 protein is required for Fus1-mediated tumor suppressing activities in human lung cancer.

Futoshi Uno, Jiichiro Sasaki, Masahiko Nishizaki, Giovanni Carboni, Kai Xu, John D. Minna, Jack A. Roth, Lin Ji. The University of Texas M.D. Anderson Cancer Center, Houston, TX; The University of Texas Southwestern Medical Center, Dallas, TX.

FUS1 is a novel 3p21.3 candidate tumor suppressor gene which is inactivated in primary lung cancers by a combination of allele loss, rare mutations, and frequent deficiency of protein expression. Re-expression of wild-type (wt)-Fus1 in Fus1-deficient non-small cell lung cancer (NSCLC) cells inhibits tumor cell growth and induced apoptosis in vitro and in vivo. A motif-based profile scanning analysis revealed a potential myristoylation site at the N-terminus of Fus1 protein sequence. Using surface-enhanced laser desorption and ionization-Mass (SELDI-MS) spectrometry analysis on a Fus1-antibody-captured ProteinChip array (ACPA), we identified wt-Fus1 as a myristoylated protein, which was further confirmed by Western-blot and immunoprecipitation analysis of H3-myristate-labeled Fus1 protein. We evaluated Fus1 protein expression and posttranslational modification using ACPA with SELDI-MS in primary uncultured NSCLCs and non-involved lung tissues using Laser Capture Micro-dissection to separate tumor from normal cells. Only myristoylated protein species were detected in normal lung cells but both unmyristoylated and myristoylated Fus1 protein were detected in tumor cells. N-myristoyl-proteins play essential roles in diverse biological functions, such as regulating cellular structure, directing protein intracellular localization, and mediating protein-protein and protein-substrate interactions. Thus, We tested whether myristoylation was required for tumor suppressing activity by transfecting expression plasmid vectors containing wt-FUS1 or a myristoylation-deficient mutant (Myr-mut-FUS1) made by site-directed mutagenesis. By immuno-fluorescence imaging analysis, Myr-mut-Fus1 compared to wt-Fus1 dramatically lost its characteristic intracellular membrane localization in transfected H1299 cells. We then analyzed the effects of the wt-FUS1 and Myr-mut-FUS1 expression on tumor cell-induced clonogenicity in vitro, on the growth of NSCLC NCI-H1299 subcutaneous tumor xenografts, and on the development of NSCLC A549 lung metastases in nude mice by intratumoral injection or systemic administration of FUS1-Lipoplexes. Myr-mut-FUS1 compared to wt-FUS1 exhibited significant loss of the ability to inhibit clonogenicity in vitro and suppress xenograft subcutaneous tumor and lung metastasis growth in H1299 tumor-bearing animals. We conclude that posttranslational myristoylation is required for Fus1 tumor suppressing activity and that loss of both protein expression and myristoylation occur in primary human lung cancers.

Presenter: Futoshi Uno

Affiliation: The University of Texas M.D. Anderson Cancer Center, Houston, TX . Email: funo@mdanderson.org

Abstract Number: 4639

The anti-inflammatory drug naproxen protects mice from lipoplex-mediated toxicity.

Began Gopalan, Lin Ji, Isao Ito, Yuji Saito, Cynthia D. Branch, Kai Xu, Clifton Stephens, John D. Minna, Jack A. Roth, Rajagopal Ramesh. M.D. Anderson Cancer Center, Houston, TX; U.T. Southwestern Medical Center, Dallas, TX.

High doses of liposome-DNA complexes (lipoplexes) injected intravenously (i.v.) cause toxicity and mortality in mice. The underlying mechanism is not well characterized and has been attributed to CpG motifs and impurities in the plasmid DNA preparation. We have recently shown cures in a mouse disseminated human lung cancer xenograft model using DOTAP:cholesterol (DOTAP:Chol) liposomes delivering therapeutic genes (*p53, FHIT, Fus1*). In an attempt to abrogate high dose toxicity, we tested the protective effects of Naproxen, a widely used anti-inflammatory drug, on lipoplex induced toxicity. Preliminary studies demonstrated i.v. injection of DOTAP: Chol-*Fus1* complex in immunocompetent C3H mice resulted in a dose-dependent morbidity and mortality. The MTD was observed to be <50 µg of DNA with 100% mortality occurring at 100 µg of DNA. Based on these observations we conducted experiments to test the protective effects of Naproxen on DOTAP:Chol-*Fus1* induced toxicity. C3H animals were either treated with clinical grade Naproxen (15 mg/Kg; n=15) orally or were not treated (control; n=15). 2-h later DOTAP:Chol-Fus1 complex (100 µg) was injected i.v. and monitored for morbidity and mortality. Control animals demonstrated 100% mortality within 48 h after lipoplex injection. In contrast, Naproxen treated animals were protected (100%) from the lipoplex-mediated mortality and showed no signs of morbidity or mortality for more than 30 days. Naproxen protection in mice appears to be mediated by a reduced inflammatory response as evidenced by decreased IL-1α, TNF, IFN-γ and IL-6 levels at 2, 4, 6 and 15hr after treatment. Decrease in serum cytokine levels correlated with reduced NFκB and COX-2 expression. Furthermore, analysis for Fus1 transgene expression in the lungs demonstrated no significant difference between Naproxen treated and untreated mice. These findings suggest that Naproxen exerts its anti-inflammatory activity in part by suppressing inflammatory cytokine production that is mediated by activation of NF-κ B and COX-2 gene expression. We conclude that Naproxen treatment prior to intravenous administration of lipoplex facilitates delivery of therapeutic genes at higher concentrations and may be incorporated in therapeutic protocols.

Presenter: Began Gopalan

Affiliation: M.D. Anderson Cancer Center, Houston, TX . Email: bgopalan@mail.mdanderson.org

Abstract Number: 1232

Discovery of specific cellular regulatory pathway mediated by the tumor suppressor gene FHIT in NSCLC cells by gene and protein expression profiling

Lin Ji, Kai Xu, Masahiko Nishizaki, Jiichiro Sasaki, Uno Futoshi, Luc Girard, Harold Garner, John D. Minna, Jack A. Roth. M.D. Anderson Cancer Center, Houston, TX; UT Southwestern Medical Center, Dallas, TX.

Tumor suppressor genes (TSGs) play an important role in human cancer development and their activities modulate biological networks involving many genes, signaling pathways, and cellular processes. High-throughput systems that can provide a global view of cellular function are necessary to gain a comprehensive understanding of such a complex system. In this study, we used complementary gene and protein expression profiling with DNA Microarray and ProteinChip array technology to quantitatively monitor cellular changes in gene and protein expression mediated by FHIT tumor suppressing activity in non-small cell lung carcinoma (NSCLC) cells. We performed gene expression profiling analysis using Affymetrix HG-U133A GeneChips in Ad-FHIT-transduced NSCLC cells compared with those of PBS-treated mock and empty vector (Ad-EV) or Ad-LacZ-treated negative controls. The gene expression data were analyzed by a perfect-match model-based analysis with the dChip program and integrated to extract statistically significant ($P \leq 0.05$) expression indexes that are up or down-regulated compared to controls. A hierarchal clustering analysis of the gene expression profiles among various treatment groups and cell lines identified about 200 differentially expressed genes in Ad-FHIT-transduced cells. Simultaneously, we performed a protein expression profiling analysis using a ProteinChip array-based surface enhanced laser desorption/ionization-Mass (SELDI-MS) spectrometry to quantitatively analyze cellular changes in protein expression. About 40 differentially expressed proteins mediated by FHIT tumor suppressing activities were identified by a serial analysis of protein lysate micro-fractionation, expression profiling on ProteinChip, and SDS-PAGE separation, in-gel trypsin digestion, peptide mass resolution by SELDI-MS, and computer-based peptide mapping. More than 70% of these differentially expressed proteins identified on ProteinChip arrays were also correspondingly found as differentially expressed mRNAs in DNA microarray analysis. A comparative analysis of the gene and protein expression profiling revealed several specific cellular targets and signaling pathways modulated by FHIT activity. For example, the expression of proteins in the Ras/Rho GTPase super-family, including Ran, Rab, Rac, Rap, and Ral, were significantly down regulated, and this was confirmed by Western blot analysis. Our findings demonstrated the great potential of using the complementary gene and protein expression technology as powerful tools for identification of specific cellular targets and signaling pathways mediated by TSGs.

Presenter: Lin Ji

Affiliation: M.D. Anderson Cancer Center, Houston, TX . Email: lji@mdanderson.org

Abstract Number: 6177

IGFBP-3 and the farnesyl transferase inhibitor SCH66336 act synergistically to induce apoptosis in non-small cell lung cancer (NSCLC) cells

Yoon S. Chang, Fadlo R. Khuri, Khaled A. Hassan, Sandra A. Wiehle, Lin Ji, Reuben Lotan, Kyung-Hee Chun, Waun K. Hong, Richard Cristiano, Ho-Young Lee. UT M. D. Anderson Cancer Center, Houston, TX; Winship Cancer Institute, Atlanta, GA.

n">

Insulin-like growth factor (IGF) binding protein (IGFBP)-3 inhibits the mitogenic and anti-apoptotic actions of IGFs. Previous studies have shown that IGFBP-3 can induce apoptosis in certain NSCLC cells. However, the therapeutic efficacy of IGFBP-3 may be antagonized in many NSCLC tumors, which have an activated Ras pathway as a result of *ras* mutations and/or overexpression of growth factor receptors. This preclinical study evaluated the hypothesis that SCH66336, a farnesyl transferase inhibitor (FTI) designed to prevent the membrane localization of Ras acts synergisiticaly with IGFBP-3 in NSCLC cells. In addition, the mechanisms that mediate the growth inhibitory effects of IGFBP-3 and SCH66336 in NSCLC cells were investigated. We found that the combination of adenovirus expressing IGFBP-3 (Ad5CMV-BP3) and SCH66336 produced synergistic anti-proliferative effects over a range of clinically achievable concentrations in NSCLC cell lines and caused a significant reduction in NSCLC xenograft tumor growth by inducing apoptosis. The combination was more effective in down-regulating the anti-apoptotic Bcl-xL than either agent alone. IGFBP-3 protein level was up-regulated by SCH66336-mediated stabilization, which resulted in potentiation of apoptosis as well. Surprisingly, SCH66336 caused the down-regulation of pro-survival Akt and thus phosphorylation of Akt and its substrate. This effect was markedly increased by combination of SCH66336 with Ad5CMV-BP3. Adenoviruses expressing PTEN inhibited the activation of Akt in parallel with an increase in IGFBP-3 protein. These findings suggest that the anticancer effects of IGFBP-3 in NSCLC may be enhanced when it is combined with therapeutic approaches targeting Ras as well as Akt.

Presenter: Ho-Young Lee

Affiliation: UT M. D. Anderson Cancer Center, Houston, TX . Email: hlee@mdanderson.org